Electronic Supplementary Material (ESI) for Materials Advances.

SUPPORTING INFORMATION

LaMer's 1950 Model of Particle Formation: A Review and Critical Analysis of Its Classical Nucleation and Fluctuation Theory Basis, of Competing Models and Mechanisms for Phase-Changes and Particle Formation, and then of Its Application to Silver Halide, Semiconductor, Metal, and Metal-Oxide Nanoparticles

Christopher B. Whitehead,[a] Saim Özkar,[b] Richard G. Finke*,[a]

[a] Department of Chemistry, Colorado State University, Fort Collins, CO 80523, USA

[b] Department of Chemistry, Middle East Technical University, 06800 Ankara, Turkey

Abbreviations:
AES = atomic emission spectroscopy
AFM = atomic force microscopy
DLS = dynamic light scattering
DXAFS = dispersive X-ray absorption fine structure
EDX/EDS = electron-dispersive X-ray spectroscopy
EXAFS = extended X-ray absorption fine structure
FE-SEM = field-emission scanning electron microscopy
FE-TEM = field-emission transmission electron microscopy
FT-IR = Fourier-transform infrared spectroscopy
GATR = grazing angle attenuated total reflectance
GLC = gas-liquid chromatography
HAADF-STEM = high-angle annular dark-field scanning transmission electron microscopy
HR-TEM = high resolution transmission electron microscopy
ICP = inductively coupled plasma
LSA = laser scattering analysis
MALDI–TOF = matrix-assisted laser desorption/ionization time-of-flight
MS = mass spectrometry
NMR = nuclear magnetic resonance spectroscopy
OES = optical emission spectrometry
PCS = photon correlation spectroscopy
QXAFS = quick X-ray absorption fine structure
SAED = selected area electron diffraction
SAR = specific absorption rate
SAXS = small-angle X-ray scattering
SEM = scanning electron microscopy
SQUID = superconducting quantum interference device
STEM = scanning transmission electron microscopy
TGA = thermogravimetric analysis
TEM = transmission electron microscopy
UV-vis = UV-visible spectroscopy
XAFS = X-ray absorption fine structure
XANES = X-ray absorption near-edge structure
XPS = X-ray photoelectron spectroscopy
XRD = X-ray diffraction

Abbreviations of Mechanisms/Models:
AE = Avrami-Erofe'ev
CNT = Classical Nucleation Theory
FW = Finke-Watzky

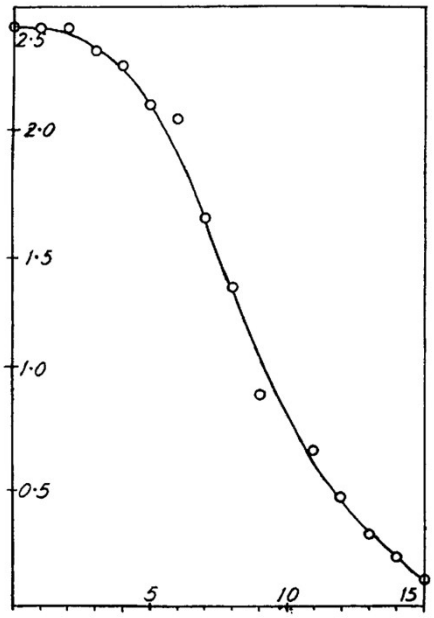

Figure S1. (Fig. 11 from Ref. 1) Concentration of Au(III) as a function of time during the reduction of auric acid by sodium citrate at 49 °C. The presence of an induction period is evidence against instantaneous nucleation, and by extension the 1950 model. Reproduced with permission from ref 1. Copyright 1951 Royal Society of Chemistry.

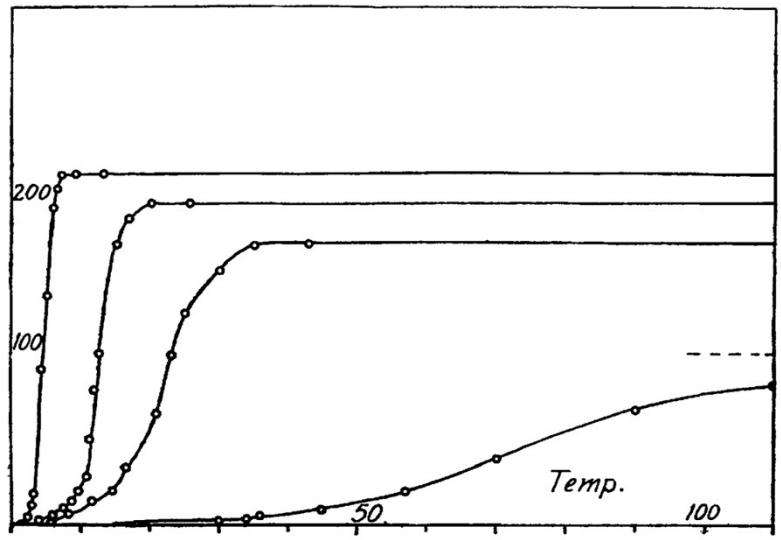

Figure S2. (Fig. 15 from Ref. 1) The "nucleation curves" (from left to right) at 49.5, 39.0, 30.0, and 15.4 °C with the y-axis being "Particles per unit volume" and x-axis being "Time (min)". The data were obtained via nephelometry. The shortening of the induction period of each curve as temperature increases indicates the dependence of the nucleation on rate temperature, a fact that cannot be accounted for by the 1950 model because of its assumption of an "instantaneous" (hence, not increasable) rate of nucleation. Reproduced with permission from ref 1. Copyright 1951 Royal Society of Chemistry.

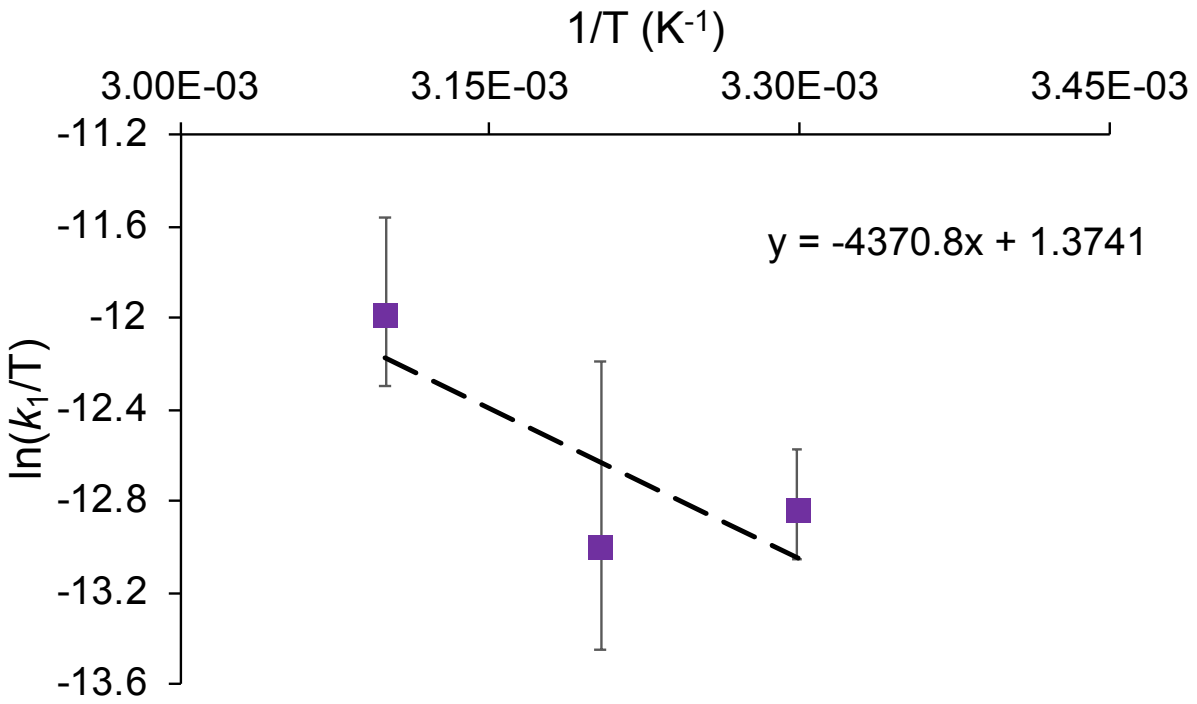

Figure S3. Eyring plot of the data presented in Table 1 of the main text for reduction of chloroaurate(III) by sodium citrate at three different temperatures. The data were fit using the Finke-Watzky 2-step mechanism. The resulting, crude activation parameters are: $\Delta H^{\ddagger} = 8.9 \pm 2.1$ kcal mol^{-1} and $\Delta S^{\ddagger} = 3.4 \pm 6.5$ e.u.

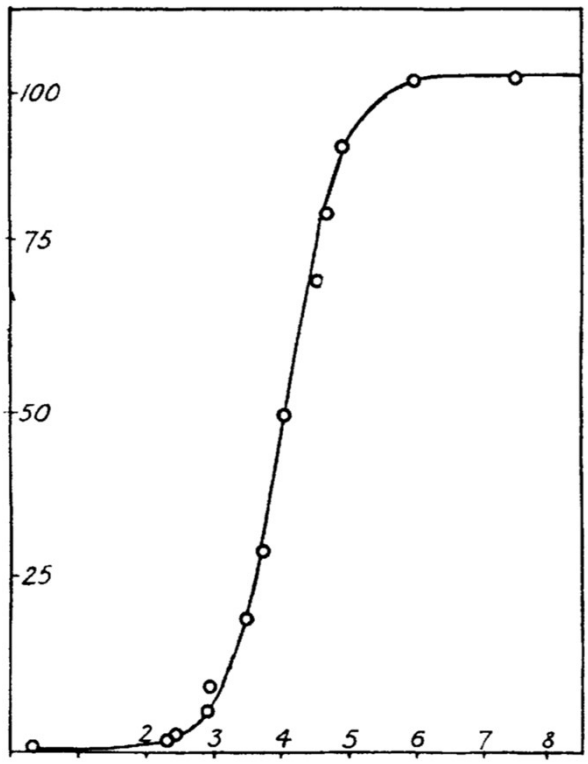

Figure S4. (Fig. 8 from Ref. 1) Plot of the number of gold nanoparticles per unit volume versus time (in seconds) during gold sol formation from a sodium citrate and tetrachloroauric acid mixture with the addition of hydroxylamine at 49 °C. Circles represents the experimental points measured using a nephelometer. Reproduced with permission from ref 1**.** Copyright 1951 Royal Society of Chemistry.

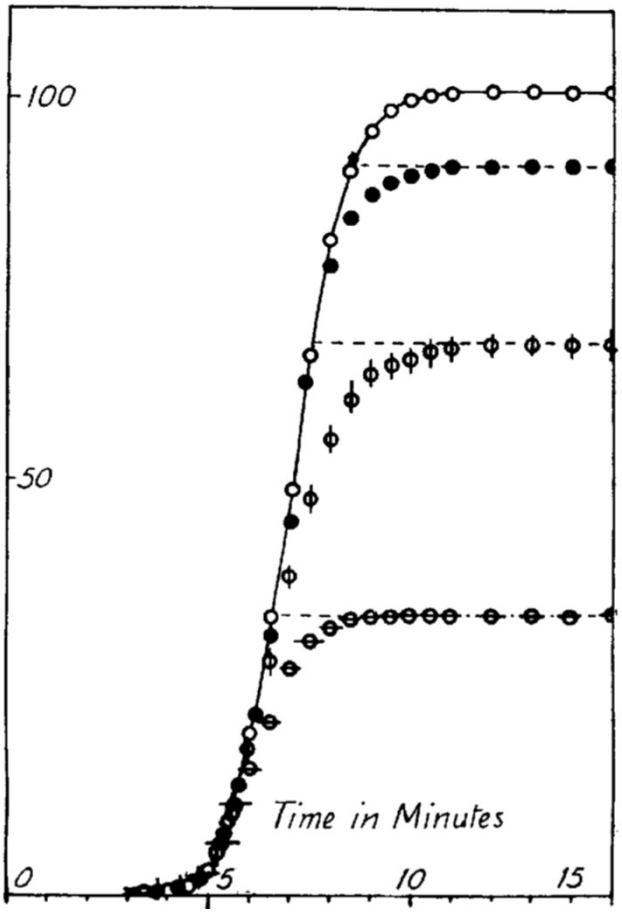

Figure S5. (Fig. 10 from Ref. 1) Plots of the number of gold nanoparticles per unit volume versus time (in minutes) of gold sol formation from a sodium citrate and tetrachloroauric acid mixture. Empty circles represent nanoparticles obtained after complete development without adding hydroxylamine. Thetas, phis, and filled circles represent nanoparticles obtained after addition of hydroxylamine at later and later times. Reproduced with permission from ref 1**.** Copyright 1951 Royal Society of Chemistry.

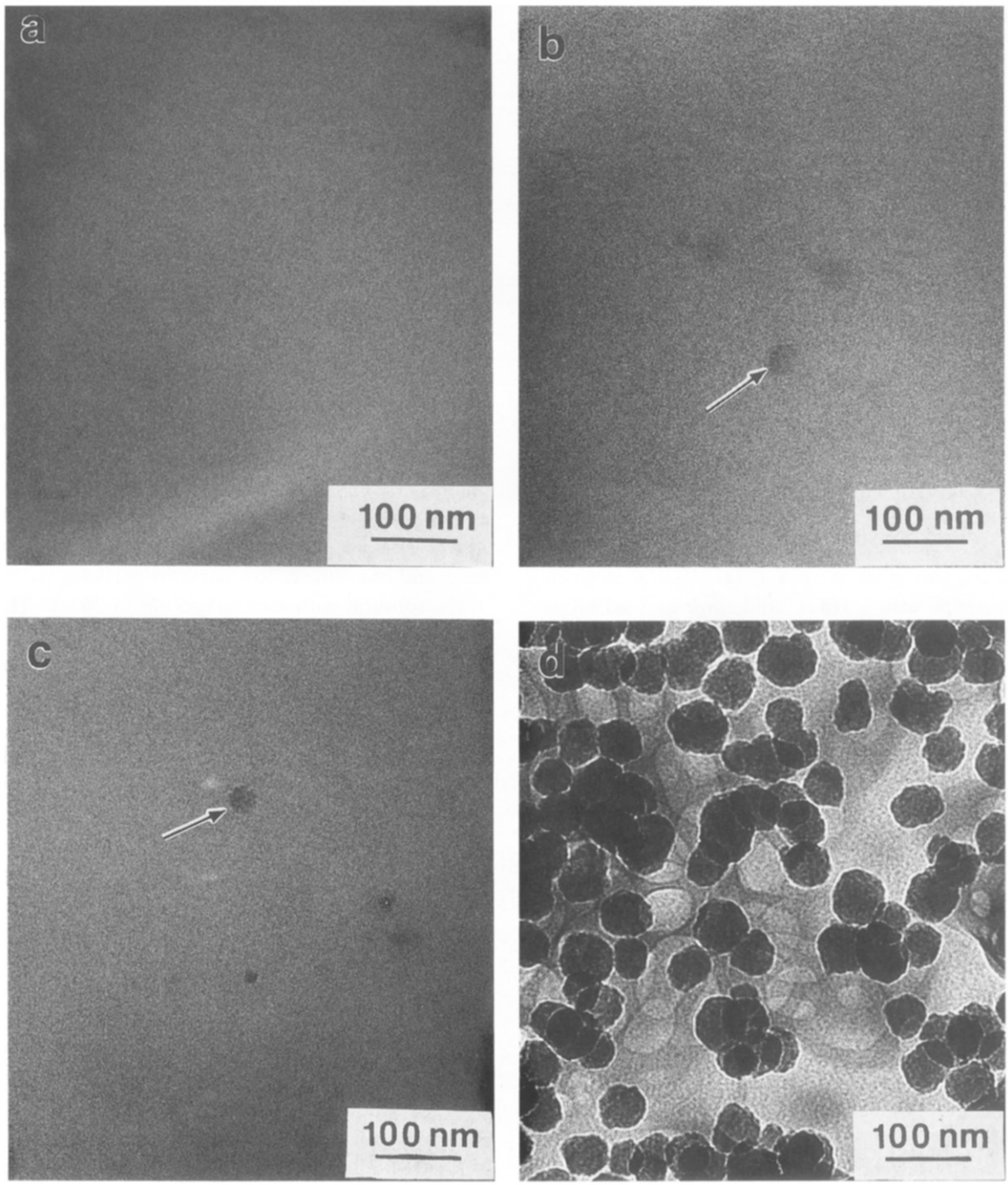

Figure S6. (Fig. 1 from Ref. 2) "Growth sequence observed by cryo-TEM for particles prepared from a solution of 0.17 M tetraethoxysilane (TEOS), 1.0 M H_2O, and 1.0 M NH_3 in *n*-propanol. (a) Sample frozen 6 min into the reaction, no particles are visible; (b) sample frozen 16 min into reaction, arrow indicates a low density particle; the average particle size, 26 nm; (c) sample frozen 24 min into reaction, arrow indicates high density of particle; average size, 20 nm; (d) sample frozen 66 min into the reaction; the average particle size, 48 nm."[2] Reproduced with permission from ref 2. Copyright 1992 Elsevier.

(a)

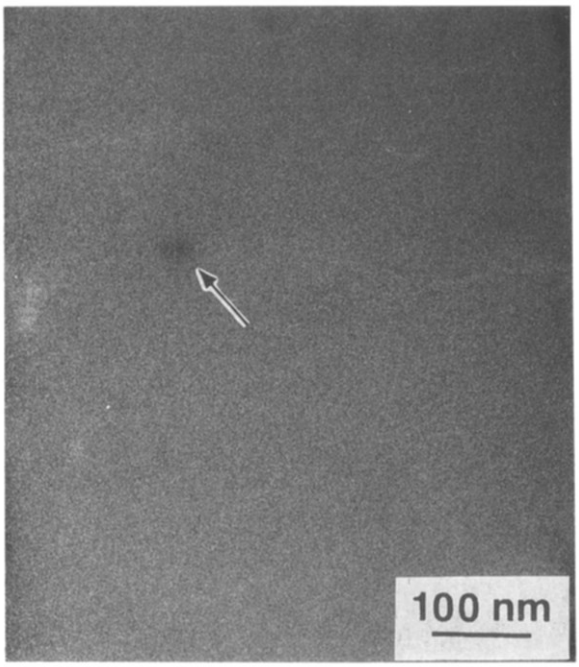

(b)

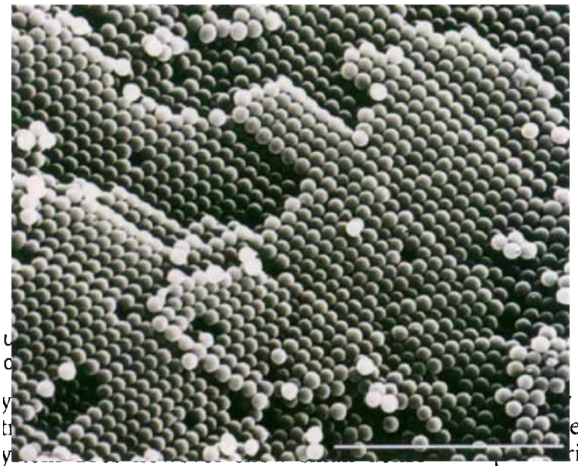

Figure S7. (a) (Fig. 3 from Ref. 2) Cryo-TEM micrograph of particle growing from reaction solution containing 0.17 M tetraethoxysilane (TEOS), 2.0 M H_2O and 1.0 M NH_3. "Sample frozen at 75 s into reaction which took 240 s to show turbidity, arrow indicates low density particle."[2] Reproduced with permission.[2] Copyright 1992 Elsevier. (b) (Figure from Ref. 3) TEM image of "submicrometer silica spheres formed by the Stöber process. Scale bar, 10 μm."[3] Reproduced with permission from ref 3. Copyright 1994 Nature Publishing Group.

Table S1 Summary of literature on the formation of silver halide nanoparticles relating to the 1950 model.

Entry	Title	System	Evidence & Insights	Comments and/or Relevance to the 1950 Model	Ref.
1	Association phenomena. I. The growth of particles of silver chloride and the higher-order Tyndall effect	Silver chloride sols were produced from solutions of silver nitrate and ammonium chloride in ethanol and water. Tyndall light scattering was conducted using white light and measurements collected using a Zeiss Spectrometer (without its prism).	The authors observe that "the time of appearance of the higher order Tyndall effect was roughly inversely proportional to the concentration [of silver]."[4] Particles were observed, via color bands, to be fairly uniform with some particles growing larger and precipitated from solution. The stability of the particles increased by either the dilution of the solution increased or by increasing the amount of chloride ion present.	The authors note "the formation of precipitates by the reaction of two ionic species is generally so rapid that it is often described as happening instantaneously. However, it is definitely a process, or series of processes, that are time-dependent although the rate at which they occur may be very great."[4] This paper serves as an excellent example of critical, thoughtful science being conducted with light scattering. Here, the authors have recognized the limitations of their investigation and theoretically explored all possible components of the mechanism.	4
2	The preparation of monodisperse silver bromide and silver iodide sols	Silver iodide and silver bromide sols were prepared in water. The exact silver and halide reagents used were not reported by the authors. Silver halide sols were analyzed spectroscopically with higher-order Tyndall spectra (HOTS) and electron microscopy.	The sols prepared in this study exhibited HOTS. The electron microscopy results show an average sol diameter of ca. 0.3-0.4 microns. Not surprisingly, the silver bromide sols with excess bromide ions have the lowest polydispersity and brightest HOTS.	This 1961 study applies the 1950 model to their system and claim their silver bromide system is "in agreement with La Mer's hypothesis."[5] The authors note that the appearance of HOTS "does not necessarily mean that the sols are completely monodisperse, but it is usually a criterion that they are nearly so. This is confirmed by the present work."[5] The author's data do not support this claim of monodispersity nor the application of the 1950 model, in our opinion.	5
3	Precipitation of Silver Chloride from Homogeneous Solution 1. - Particle Size and Shape Characterization	Silver nitrate and allyl chloride were combined in water to produce silver chloride sols. Characterization was performed "by conductance measurements, electron microscopy, electrophoresis",[6] and higher order Tyndall spectra (HOTS).	The authors report the appearance of HOTS during the growth stage. Furthermore, they report that growth of the particles is too small to detect, then it is autocatalytic, before slowing at the end of the reaction (as can be seen in Fig. 4). Importantly, the authors recognize that nucleation has a time dependence and *is not* instantaneous.	The author explicitly state that "the La Mer theory of monodisperse sol formation does not apply to this system, and factors other than time spent in the critical region seem to be important."[6] The authors of this 1968 paper insightfully postulate heterogeneous nucleation. Further analysis and repetition of this classic work seems warranted, such as the interpretation of time when the deviation from linear conductance starts or the extrapolation of the fraction of AgCl precipitation versus time plot to zero. Of note is that the authors analyzed their data via multiple alternative	6

				hypotheses.	
4	The Theory of the Nucleation of Monodisperse Particles in Open Systems and Its Application to AgBr Systems	The theoretical basis for the nucleation of monodisperse particles is presented, which is then followed by an experimental investigation of the formation of AgBr colloids. Silver bromide particles are prepared from 1:1 molar equivalents of $AgNO_3$ and KBr in a pH 5.0 aqueous gelatin. The particles were analyzed with a Karl Zeiss TGZ particle analyzer and an electron microscope.	The author used a theory "based on a nucleation model where stable nuclei as origins of the product particles are produced through a kind of Ostwald ripening from stationary unstable nuclei that are in a quasi-steady state of balance between the generation of their embryos by instantaneous reaction of the introduced reactants and either dissolution or growth."[7] For the experimental work on AgBr, the particle size is observed to grow fast and then slow as the particle reaches its final size. The author claims "the reduction of particle number always observed following its peak is another direct proof of Ostwald ripening."[7]	Despite consideration of an instantaneous formation of embryos of a definite mean size, it is assumed that nucleation and growth processes in the open system proceeds by a kind of Ostwald ripening. This and the reduction of the number of nuclei during the growth process stand in stark contrast to the 1950 model. Furthermore, the author's claim 'to prove' several aspects of their theory and experimental research, rather than attempt to disprove or *even test* any other alternative hypotheses,[144] an improper scientific method.	7
5	Mechanism of Formation of Silver Halide Ultrafine Particles in Reverse Micellar Systems	Silver halide particles were prepared from injecting aqueous solutions of silver nitrate and sodium bromide, chloride, or iodide into the reverse micellar system of sodium bis(2-ethylhexyl) sulfosuccinate (AOT) and isooctane. Preparations were done at various ratios of water to AOT. Particle formation was monitored using UV-vis spectroscopy.	For AgBr particles, the diameter increases from 4.5 nm to 10 nm depending on the water concentration. The authors report "the kinetics of coagulation of AgBr particles can be expressed by first-order kinetics with respect to the concentration of micellar droplets containing two or more particles."[8] The AgI particles were observed to "grow larger than [the] reverse micelles in low water content solution and tend to form visible particles."[8] In analyzing the kinetics of particle formation, the authors assume the particles are spherical and monodispersed.	This early study of the formation of silver halide nanoparticles inside reverse micelles of AOT is important due to its attempt at investigating the kinetics and formation mechanism. However, the authors do overstate what they know and try to apply models that are illogical. Unfortunately, they do not have enough data to advance knowledge of the formation mechanism.	8
6	Spontaneous nucleation of monodisperse silver halide particles from homogeneous gelatin solution I: silver chloride	Silver chloride particles were formed from a gelatin solution containing $AgNO_3$, KCl, and KOH. The reaction was initiated by adding diethyl sulfate (DES) and lowering of the pH by hydrolysis of DES. Silver ion concentration was monitored using a Ag ion specific electrode. Particles were characterized by TEM.	The final particle density is determined only by the supply rate of Ag^+ ion and the volumetric growth rate during the nucleation stage. The duration of nucleation is found to be independent of the supply rate of Ag^+ ions. The authors claim that "the theory of the nucleation process of monodisperse particles based on a mass balance in the consumption of increasing solute by generation and growth of stable nuclei has been formulated and verified by experiment from the proportional relationship between the rate of increasing concentration of solute and the final particle density."[9]	The authors claim "the LaMer diagram as a fundamental principle of formation of monodispersed particles has actually been demonstrated by experiment."[9] The authors claim they have created the LaMer diagram with the degree of supersaturation as the y-axis. Here, they have fundamental changed the diagram axes and then claim they are equivalent. Furthermore, they later claim Ostwald ripening is involved, which is not possible under the 1950 model. Of note, the reported TEM micrograph claims to present uniform AgCl particles, yet the particles do not appear to be visually uniform. No particle size-distribution is reported.	9
7	Spontaneous nucleation of monodisperse silver halide particles from homogeneous	The preparation of AgBr particles is done in the same manner as the above (Entry 6)[9] by the same primary	The authors report the proposed "nucleation mechanism of AgBr system is basically the same as in the AgCl system[9] of Part I."[10]	The 1950 model is again accepted by the authors as fact. The suggestion that Ostwald ripening is involved in the	10

	gelatin solution II: silver bromide	author, Sugimoto. The only experimental difference is the use of KBr instead of KCl.	Spontaneous nucleation is assumed to yield nuclei in certain number, these nuclei are then postulated to undergo growth by consuming the solute.	nucleation process contradicts the 1950 model.	
8	Synthesis of Inorganic and Organic Nanoparticles in Microemulsions	AgCl and AgBr nanoparticles were formed from mixing microemulsions of silver nitrate and potassium chloride/bromide. Microemulsions were prepared from mixtures of bis(2-ethylhexyl)sodium sulfosuccinate (AOT), heptane, and water. The particles are characterized by ^{1}H NMR.	The authors used ^{1}H NMR to quantify the amount of water in the different environments of the emulsion system. The authors claim the size for AgBr particles increases with increased $AgNO_3$ concentration. For AgCl particles, the particle size remains constant when the concentration of chloride increases because the growth is governed by the interaction of AgCl with the surfactant. Meanwhile, studying the formation of mixed bromochloro silver salts shows the faster nucleating AgBr stays in the core while the better stabilized AgCl grows at the surface.	Two models are tested by the authors. First, the LaMer diagram, and second, a model of "the thermodynamic stabilization of the particles"[11] by the surfactant. The authors claim the formation of the AgBr particles is explained by the LaMer diagram. However, the authors do note, for AgBr particles, that the 1950 model "does not take into account the stabilization of the particles by the surfactant."[11] Meanwhile, the authors say the 1950 model does not work well for AgCl particles.	11
9	Growth Mechanism of AgCl Nanoparticles in a Reverse Micelle System	Silver chloride particles were formed from aqueous solutions of $AgNO_3$ and KCl in a closed reverse micelle system of NP-6 surfactant in cyclohexane. TEM was used to characterize the resulting AgCl particles.	The authors show the particle size versus time with "the zero point of the aging time"[12] starting at the average particle size of 6.4 nm. They found the particles eventually grow to be larger than 8 nm, "much greater than the mean size of the water pools of the reverse micelles (1.51 nm)."[12]	The authors claim the AgCl nanoparticles "grow through Ostwald ripening, and not by the coagulation process."[12]	12
10	Relationship between Supersaturation Ratio and Supply Rate of Solute in the Growth Process of Monodisperse Colloidal Particles and Application to AgBr Systems	Cubic and octahedral silver bromide seed particles were prepared in gelatin solutions at 50 °C from $AgNO_3$ and KBr using the controlled double-jet technique. Supersaturation was measured using Ag^+ and Br^- ion-selective electrodes.	The authors find solubility "is one of the important factors in both nucleation and growth processes of fine particles."[13] Exact measurement of the solubility (C_0) and *D* (diffusion coefficient) were found to have some ambiguity when attempting precise analyses. However, "the present study does not provide the explanations for the pBr dependence of the growth-limiting step experimentally."[13]	During the formation, the supersaturation ratio increases to a plateau and then remains constant during the growth of AgBr particles, compelling evidence *against* burst nucleation. Needed is the control experiment where the preparation is done without seeds. Of note, the authors observe "high coverage of adsorbed Br^- ions may retard incorporation of the constituent ions in a crystal lattice."[13] The suggestion of ligand coverage slowing growth is mentioned throughout the literature for decades. A recent paper by Karim et al.[106] fits experimental data and provides compelling kinetics-based evidence for a ligand effect in nanoparticle formation (in that case for a Pd nanoparticle formation reaction).	13
11	Underlying mechanisms in size control of uniform nanoparticles	The author of this paper reviews the various advances in the field of silver halide nanoparticles, primarily those	The author remarks that, based on classical nucleation theories and the 1950 model, an equation for the nucleation process was derived. It was based on 3	The proposed model and derived equation were done on the basis of classical nucleation theories, and specifically the	148

		of the author's own papers. Specifically, the author covers "the underlying mechanisms of size control in some unique processes chosen from them, such as hydrolysis-induced precipitation of AgCl nanoparticles, double-jet precipitation of AgCl nanoparticles in a reverse micelle system to resolve the mechanism of particle formation in general reverse micelle systems, and a gel-sol process for the formation of nanoparticles of anatase TiO_2."[148]	assumptions: (i) "mass balance between the supply rate of solute and its consumption rate"[148]; (ii) "supply rate of solute in independent of subsequent precipitation events"[148]; (iii) "nucleation rate is controlled only by the growth of the preformed nuclei at a fixed supply rate of solute."[148] Of note, if any one of these assumptions is violated, the equation cannot be applied to the system in question. Hence, the author of this paper is adamant a researcher must determine whether or not a given nucleation theory is appropriate for the system in question.	1950 model. Unfortunately, this does not make sense, as the 1950 model claims an instantaneous ('burst') of nucleation, whereas the author here describes a nucleation time period. It is our understanding the author here is using the 1950 model as a qualitative model that separates nucleation and growth in time, which they try and replicate in their quantitative derivation. However, for the systems analyzed within, particle size control was only explained in terms of separate of nucleation and growth and not in terms of ligand coverage modulating growth rate. *We recommend caution when reading this review*.	
12	Silver chlorobromide nanocubes with significantly improved uniformity: synthesis and assembly into photonic crystals	In ethylene glycol, NaCl and KBr were combined in varying ratios with PVP. Under N_2 at 60 °C, ethylene glycol solutions of $AgNO_3$ were added at 1 mL/min. The reaction kinetics were monitored using synchrotron XRD. Ex situ characterization was done with XRD, SEM, and a custom-built visible/near-IR microscope. The resulting product studies was a silver chlorobromide nanoparticle ($AgCl_xBr_{1-x}$, $0 < x < 1$).	The authors report "the size of the nanocubes is tunable by varying a number of parameters, including the molar ratio of Cl^- to Br^- ions, the injection rate of Ag^+ ions, and the reaction temperature. The real-time formation of colloidal $AgCl_xBr_{1-x}$ nanocubes was monitored by *in situ* high-energy synchrotron X-ray diffraction."[15] "The time-resolved results reveal that a fast injection rate of Ag^+ ions is critical for the formation of $AgCl_xBr_{1-x}$ nanocubes with a highly pure, face-centered cubic crystalline phase."[15]	Although it was not clearly indicated in the paper, by careful reading of the paper one can extract four solid lines of evidence against the 1950 model: (i) Observation of a bimodal distribution for the binary AgCl nanocubes, a bimodal distribution being inconsistent with the 1950 model. (ii) Observation of an induction period and sigmoidal kinetic data, which is inconsistent with the 1950 model. (iii) Observation of the growth of XRD pattern of only one phase from the beginning on until the end of reaction—that is, lack of an initial burst phase. And (iv) the sequential formation of two ternary silver halide nanocubes with fixed, but different, compositions at a lower injection rate of 0.2 mL/min, something outside of the range of observations explainable by the 1950 model. Unfortunately, despite the evidence that indicates non-LaMer behavior, the paper uses the 1950 model in a "words only" way to try to rationalize their results—their outstanding, in-situ, high-energy synchrotron XRD data that, therefore, merits a reinvestigation and reanalysis (see also Özkar, S.; Finke, R. G. *J. Phys. Chem.*	15

				C **2017**, *121*, 27643-27654).[14]	
13	Evaluating the mechanism of nucleation and growth of silver nanoparticles in a polymer member under continuous precursor supply: tuning of multiple to single nucleation pathway.	Silver nanoparticles were prepared from aqueous solutions of silver nitrate and trisodium citrate at 60 °C, 80 °C, and 92 °C. Particles were formed on Nafion-117 membranes, immersed in the solution for specific periods of time. Membranes were immediately transferred to an aqueous solution of $NaNO_3$ to quench the reaction and stop particle growth. The silver monomer concentration was monitored in real-time by using a ^{110m}Ag radiotracer. Nanoparticle characterization was done using SAXS and TEM.	The authors claim "the mechanism of nucleation and growth during formation of AgNPs in a Nafion-117 membrane by a nanoconfinement driven silver citrate reduction route, has been successfully probed for the first time using a radiolabeling technique accompanied by [SAXS] experiments."[16] The authors claim multiple nucleation events take place that lead to polydispersity and non-uniform growth kinetics. The authors present a 'tuned' experiment they find 'better controls' the size, whereby they let the reaction run for 5 minutes before removing the membrane from the silver citrate solution and placing it in a 10x dilute silver citrate solution (at room temperature).	The 1950 model has been described and applied to this system. However, there are several issues that arise from this study. First, the effect of ligands on the nanoparticle growth has not been considered nor discussed. In similar gold-citrate syntheses, the citrate and its oxidized product have been shown to affect the growth process.[1,45] Next, despite the decreased silver solution concentration and decreased temperature, the data in figure 4 shows an increase in the number of particles in solution. Furthermore, it is unclear how reproducible is the data in all of these experiments, and whether or not the reaction has been allowed to run to completion. Presently, there is more evidence to dispute the applicability of the 1950 model to this system than there is to support it.	16

Table S2 Summary of literature on the formation of semiconductor nanoparticles relating to the 1950 model.

Entry	Title	System	Evidence & Insights	Comments and/or Relevance to the 1950 model	Ref.
1	The mechanism of particle formation during homogeneous precipitation of zinc sulfide	Zinc sulfide particles were prepared from $ZnSO_4$ in sulfuric acid and water/glycerin. Thioacetamide was added and the reactor was headed to 80 °C. Next, a polyvinylalcohol solution was added and the ZnS particles were separated by filtration. Particles were characterized by SEM.	An induction period was observed before ca. 0.8 micron sized particles appeared after 22 minutes. It is believed this induction period is, partly, due to the decomposition of thioacetamide. The particles are believed to form, under a Brownian coagulation model, from primary particles that are 50 nm or less. Further, the authors claim "the diameter of the ZnS sphere, as obtained from SEM micrographs, is given as a function of the viscosity of the liquid phase relative to the viscosity of pure water at the reaction temperature of 80 °C."[17]	The authors cite the 1950 model to describe the formation of monodisperse particles. But, they state "nucleation now is not restricted to a short period in the beginning of the process, but does occur during a much larger time span."[17] Important here is the recognition of a continuous nucleation process.	17
2	Model of Controlled Synthesis of Uniform Colloid Particles: Cadmium Sulfide	The paper focuses on the development and application of a model for nucleation and growth of cadmium sulfide nanoparticles. The experimental data analyzed was from a previous paper by the same corresponding author.[18] Cadmium sulfide nanoparticles were prepared from aqueous solutions of $Cd(NO_3)_2$, thioacetamide, and nitric acid, and then particles were characterized using SEM, XRD, EDS, and TGA.[18]	The authors found "the analysis of the experimental data for CdS colloid particle synthesis suggests that a model with cluster-cluster aggregation of secondary particles containing up to approximately 25 primary particles can provide the desired mechanism of obtaining a smaller number of larger final particles." "This model mechanism yields the width of the distribution much closer to that experimentally observed, than earlier approaches."[19]	While the model in question focuses on the aggregation of primary particles, the formation of those particles is assumed to occur by the 1950 model. This initial formation process is incorporated into their model, as the rate of primary particle formation is a necessary input. Effectively, the authors built this new aggregative model upon a foundation of CNT and the 1950 model without any direct evidence to support doing so.	19
3	In Situ Observation of the Nucleation and Growth of CdSe Nanocrystals	Cadmium selenide nanoparticles were formed from a solution of CdO, stearic acid, trioctylphosphine oxide, and hexadecylamine heated to 280 °C, where selenium powder, dissolved in trioctylphosphine, was injected into the reaction solution. The reaction temperature was reduced to 250 °C and allowed to run for 30 minutes. During the reaction, aliquots were characterized using photoluminescence and absorption spectroscopies. These data were used to calculate the	The results from the photoluminescence experiments show the temporal evolutions of the CdSe particle concentration, cadmium (precursor) concentration, and particle size. These results lead the authors to suggest a four-stage crystallization process: (1) "total number of particles increased as a result of prolonged formation of relatively small particles in the solution."[20]; (2) particle concentration decreases and size-distribution focuses; (3) a 'stable' stage, where there is a "broadening of the particle size distribution…most likely due to the concentration fluctuation."[20]; and (4) a defocusing of the size distribution as a result of Ostwald ripening. Based on their four-stage crystallization model, the authors deduced that growing particles are able to interact with each other, and, hence, do not grow independently.	The authors note "classical crystallization theories assumed that the concentration of crystals should not be a function of the monomer concentration in the solution. Evidently, this is contradictory to the results shown in Figure 4."[20] Here, the authors have reported direct evidence against the classic theories of CNT and the 1950 model. Additionally, the authors make the relevant observation that "the understanding of crystallization, especially the nucleation process, has been very much limited mainly due to a lack of quantitative experimental data."[20]	20

		particle size, particle concentration, and size distribution. Size measurements were corroborated with TEM.			
4	Nucleation Kinetics vs Chemical Kinetics in the Initial Formation of Semiconductor Nanocrystals	Indium phosphide nanoparticles were prepared by two methods. The first from $In(He)_3$, hexanoic acid, and tri-trimethylsilyl phosphine ($P(TMS)_3$), octylamine in 1-octadecene at 178 °C under argon. The second from $In(Ac)_3$, myristic acid, $P(TMS)_3$, and 1-octylamine in 1-octadecene at 178 °C under argon. Cadmium sulfide nanoparticles were prepared from cadmium(II) stearate and steric acid in 1-octadecene at 300 °C under argon.	From the experimental data, the authors reach the following, important, series of conclusions: (1) "'magic sized clusters' have often been mistaken as the critical sized nuclei. However, the model in Figure 1 tells us that these local thermodynamic minima could just be shallow traps in a crystallization system."[21]; (2) "Consequently, the growth of 'magic sized clusters' has been observed to be slow. However, if these nanoclusters are qualified as critical sized nuclei, the CNT would require the formation of the 'magic sized clusters' to be slow and the following growth to be much faster, which is *opposite* to the experimental results."[21]; and (3) "theoretical treatment of the growth of nanoclusters/nanocrystals probably should not ignore the size dependent chemical properties of the particles although the formation process—nucleation in traditional meaning—could concentrate on the initial chemical reaction(s)."[21]	The results indicate Classical Nucleation Theory is not applicable to semiconductor crystallization due to extremely low solubility of the product. In other words, the bonding and lattice energy in $(CdS)_n$ and $(InP)_m$ are, respectively, strong and high. Furthermore, the authors insightfully remark that "the theoretical challenge for understanding nucleation is well-known to the field. However, lack of reliable and systematic experimental data in the early stage of a crystallization system implies that there are no sufficient insights for solving such a challenge."[21]	21
5	Precursor Conversion Kinetics and the Nucleation of Cadmium Selenide Nanocrystals	Cadmium selenide nanoparticles were formed from the reaction of cadmium octadecylphosphonate (Cd-ODPA) with three different alkyphosphine selenide precursors: (i) tri-*n*-octylphosphine selenide, (ii) di-*n*-butylphenylphosphine selenide, or (iii) *n*-butyldiphenylphosphine selenide in trioctylphosphine. Reactions were monitored by UV-vis and ^{31}P NMR spectroscopies.	The authors found "changes to Q_o [initial precursor conversion rate] influence the final number of nanocrystals and thus control particle size."[22] The authors interpret their results "in light of a mechanism where the precursors react in an irreversible step that supplies the reaction medium with a solute form of the semiconductor."[22] They claim CdSe is continuously produced, "causing supersaturation, nucleation, and NC growth."[22]	While the author's results are characterized as being like the 1950 model, their observation of continuous production of CdSe precursors is in opposition to the 1950 model. The authors report kinetics sensitivities to reaction impurities, important observations that merit further study in order to have a better mechanistic understanding of the system.	22
6	Formation Mechanisms of Uniform Nanocrystals via Hot-Injection and Heat-Up Methods	This paper reviews studies on how uniform nanocrystals are obtained by two common synthetic methods: hot-injection and heat-up. The review covers the "Basic Concepts of Size-Distribution Control", "Theoretical Description of Nucleation and Growth Processes", "Studies on	The authors explanation of the basic concepts behind particle size-distribution control and their theoretical description is based, entirely, on CNT and the 1950 model with its postulate of 'burst nucleation' followed by 'diffusion-controlled growth'. The author final claim is "the hot-injection process can be regarded as a special case of the 1950 model, omitting the first stage."[23]	While this review does provide a thorough summary of many cases where the 1950 model and CNT have been applied to nanocrystal cases, it *does not provide any disproof-based evidence* for the stated claims. There is no explanation for how the 1950 model is able to be 'adapted' from a model for the formation of hydrosols to metal nanocrystals.	23

		Nanocrystal Formation Processes", and reviewer conclusions.[23]			
7	Precursor-dependent shape variation of wurtzite CdSe crystals in a microwave-assisted polyol process	Cadmium selenide nanoparticles were prepared from combining CdO, $CdCl_2$, Se powder, ethylene glycol, and glycerol. A total of 1 molar equivalent of cadmium (with varied amounts of CdO and $CdCl_2$) was added, so the ratio of Cd to Se would be 1-to-1. The reaction solution was irradiated with microwave radiation at 50 °C. The resulting CdSe particles were characterized by TEM, FE-SEM, EDX, HR-XRD, HR-XPS, and photoluminescence spectroscopy.	The ratio of CdO to $CdCl_2$ precursor resulted in differing CdSe morphologies. With only CdO as the cadmium precursor, the result was spherical CdSe nanoparticles. However, with increasing amounts of $CdCl_2$, the formation of tetrapods appears at the ratio of 0.33 to 0.67 (CdO to $CdCl_2$) in the solvent ethylene glycol. The authors' explanation for the differing morphology is "the formation of cadmium-polyol complexes could modify the reactivity of the $CdCl_2$ precursor significantly to retard the formation of monomers. As a result, the monomers are unevenly produced and depleted during the reaction, and then the nucleation of CdSe proceeds over an extended period of time, leading to variation in growth rates."[24]	The 1950 model is accepted by the authors and for their data in terms with only a rather cursory, qualitative discussion of the results. No kinetics data were collected to assist in an actual mechanistic investigation. No discussion of an alternative hypothesis, such as increased chloride ligand, is proposed nor subsequently tested.	24
8	The Importance of Nanocrystal Precursor Conversion Kinetics: Mechanism of the Reaction between Cadmium Carboxylate and Cadmium Bis(diphenyldithiophosphinate),	Cadmium sulfide nanoparticles were prepared from $Cd(S_2PPh_2)_2$ and cadmium tetradecanoate in 1-octadecene under argon. The particles were prepared by the heat-up method to 240 °C. Aliquots were taken throughout the reaction and analyzed using UV-vis and fluorescence spectroscopies. Characterization was done ex situ using ^{1}H, ^{13}C, and ^{31}P NMR, FT-IR, TEM, and XRD.	It was observed the heating-up of $Cd(S_2PPh_2)_2$ alone was not sufficient to produce CdS particles; the inclusion of cadmium tetradecanoate is required. The full stoichiometry was written out and the byproducts from the nanoparticles formation reaction were quantified by NMR spectroscopy. The conversion of precursors to CdS particles was monitored with respect to time and shows an approximate 7 minutes induction period. Nucleation is shown to have "a first-order dependence on total precursor concentration."[25] The authors note there could be competing parallel reduction pathways based on the complexity of the reaction solution.	The authors suggest a mechanism like the one used for Ref. 21 (Entry 4 of this Table (S4)) is likely applicable, based on the data presented.) That mechanism is in opposition to CNT and the 1950 model. The approach in this paper to fully characterize and study the system is commendable. A deeper analysis of the mechanistic implications is worthy of further effort with this system, in our opinion.	25
9	Infrared emitting property and spherical symmetry of colloidal PbS quantum dots	Lead sulfide quantum dots were prepared by the hot injection of sulfur (dissolved in oleylamine (OLA)) into $PbCl_2$ (also in OLA), all under N_2. The reaction took place at 70-80 °C for 1 to 25 minutes. Characterization was done by photoluminescence spectroscopy and TEM.	The authors conclude "lower reaction temperature, higher supersaturation, and longer growing time are suited for the synthesis of spherical PbS QDs."[26] This was determined on the basis of the 1950 model being qualitatively applied to the photoluminescence data, which the authors used to determine the particle size-distribution.	The authors apply the 1950 model to their system, but do not present any quantitative, kinetics data to support that application. The 'supersaturation' for their system was not measured.	26
10	Growth mechanism of Ag_2S nanocrystals in a nonpolar organic solvent	Silver sulfide (Ag_2S) nanocrystals were prepared from sulfur powder and either DDA-Ag^{+} ions (DDA=dodecylamine) or pre-	TEM images were collected at several points in the growth stage (1 h, 2 h, 5 h, 15 h, 25 h, 40 h, 80 h, and 1 month), all at 10 °C. At elevated temperature (60 °C), the entire process took less than 4 hours, indicating a clear	The authors have observed a drastically different formation process than described by the 1950 model. The authors remark that "according to the 1950 model, the	27

		formed silver nanoparticles in toluene. The Ag_2S nanocrystals were characterized by TEM, HR-TEM, XRD, and UV-vis spectroscopy.	temperature dependence of the growth process. Overall, the authors found their synthetic approach "revealed a 'coalescence-fracture-ripening' mechanism for the growth of Ag_2S nanocrystals, which is different from the widely accepted LaMer nucleation growth mechanism."[27] This model was also shown to effectively describe the formation of Ag_2S from pre-formed Ag nanoparticles and sulfur.	molecular Ag_2S should firstly appear in the solution, the concentration of which rises up quickly to the super-saturation level. Nevertheless, our observations indicated that the synthesis of Ag_2S NCs in toluene underwent a growth process consisting of the nanowire network stage, hollowing occurrence and expansion, fragment of the nanowires, formation of quasi-spherical and uniform spherical particles."[27]	
11	Conversion Reactions of Cadmium Chalcogenide Nanocrystal Precursors	This review focuses on the mechanism and kinetics of cadmium selenide and cadmium sulfide particle growth. "Section I is dedicated to the role of precursor conversion as a source of monomers and the importance of the supply rate on nanocrystal nucleation and growth. Section II describes the structure and reactivity of cadmium carboxylates, phosphonates, and chalcogenolates. Section III describes the reaction chemistry of commonly employed chalcogenide precursors and the mechanisms by which they react with metal precursors."[28]	While the field of semiconductor synthesis has been extensively studied for the past three decades, the authors note there is still much to be learned. In particular, the fabrication of nanostructures and the complete mechanisms of reactions are still not well unknown. "More detailed investigations of precursor reactivity and coproducts are needed."[28]	Section I does deal with the precursor reaction kinetics and mechanisms of the nanoparticle formation. The authors predominantly use the 1950 model and its modified version, proposed by Sugimoto, to explain the observations in the synthesis of metal chalcogenide nanocrystals.	28
12	White Luminescence from CdS Nanocrystals Under the Blue Light Excitation	Trap-rich CdS nanocrystals were obtained from the thermal decomposition of cadmium(II) stearate and sulfur in octadecene at 260 °C before being quickly cooled to 170 °C to induce precipitation of the nanocrystals. Characterization was done by XRD, HR-TEM, UV-vis, and fluorescence spectrophotometry.	Cadmium sulfide nanocrystals with an average diameter between 5.5 and 6.2 nm were reported to have been synthesized. "When using blue light to irradiate CdS NCs, white light is produced by mixing broad emission across 500-700 nm from CdS [nanocrystals] excited by blue light."[29]	The authors use the 1950 model "to explain the phenomenon that the intensity of the trap emission gradually decreases as reaction time increases in contrast with that of the band-edge emission."[29] However, the concentration or even existence of a monomer species is unknown by the authors current method of preparation. The reaction is not followed by any method and only characterized after the reaction is over, so any discussion of a mechanism of formation is only conjecture.	29
13	Continuous Microwave-Assisted Gas–Liquid Segmented Flow Reactor for Controlled Nucleation and	Copper indium selenide ($CuInSe_2$) nanocrystals were prepared with a continuous microwave-assisted flow reaction	The authors claim there is a burst of nucleation in the microwave heating zone that is followed by growth in a constant temperature bath. They report "the first example of ternary $CuInSe_2$ [nanocrystal] synthesis using a	The authors assume and apply the 1950 model to their system. They claim the microwave heating zone induces burst nucleation and the constant temperature	30

	Growth of Nanocrystals	(CMAFR). Solutions of CuCl, $InCl_3$, and Se in oleylamine were continuously pumped and microwave heated. Nanocrystals were characterized by EDS, TEM, and UV-vis.	CMAFR system."[30] In addition, they claim this is an example of a reproducible and monodisperse system.	bath allows for diffusion-controlled growth. However, they have no direct evidence for burst nucleation besides a drawing of their reaction set-up. Furthermore, the authors claim "slower and more controlled [nanocrystal] growth continues"[30] following nucleation. This is contradictory to the 1950 model that claims growth is diffusion-controlled (e.g., $k \sim 10^9$ M^{-1} s^{-1} for smaller species).	
14	Gain High-Quality Colloidal Quantum Dots Directly from Natural Minerals	Lead sulfide quantum dots (PbS QDs) were prepared from suspensions of galena in oleic acid and irradiated with a millisecond Nd:YAG laser (1064 nm, 20 ms, 2 Hz, 60 J/cm^2). Samples were irradiated for 1 hour between 0 and 5 °C. PbS QDs were characterized using TEM, XRD, and DLS.	The PbS QDs were measured using both TEM and DLS. The authors hypothesize the QDs are formed by the nanosecond laser pulse fragmenting the galena into monomers, as the laser irradiation in expected to cause momentary local temperatures of 14854 K. Hence, the authors hypothesize the mineral PbS fragments and forms monomers and follow the 1950 model.	The 1950 model is used in words-only form to rationalize the syntheses. "Supersaturation" is claimed but no measurements of supersaturation are provided. Furthermore, no kinetics data were collected.	31
15	The nature and implications of uniformity in the hierarchical organization of nanomaterials	The authors have presented a perspective article describing colloidal frameworks under "the topic of hierarchical organization: atoms arranged into crystalline nanoparticles, ligands arranged on nanoparticle surfaces, and nanoparticles arranged into crystalline superlattices."[32]	The authors note "surface ligands form the interface between a nanoparticle and its surroundings to dictate how nanoparticles interact with each other and their environment. Thus, stabilizing ligands determine the size and size dispersion of the final nanoparticles obtained in the synthesis as well as the properties of materials."[32]	The authors make the point that nanoparticle size is determined by nature of the surface ligands. The 1950 model has no provision for ligand effects, and only more recent work has demonstrated the role of ligands being added to the 2-step mechanism, that is, the work cited in Table S1, entries 59 and 62.[103,106] Overall, the 1950 model is employed merely as an explanation / rationalization for hot-injection techniques.	32
16	Chemistry of InP Nanocrystal Syntheses	In this review, "the fundamental differences in the syntheses of InP nanocrystals are highlighted with respect to established II–VI and IV–VI semiconductor nanocrystals comparing their nucleation and growth stages. Next, [the authors] inspect in detail the influence of the nature of the phosphorus and indium precursors used and of reaction additives, such as zinc carboxylates or alkylamines, on	The authors summarize the seven drawbacks and suggested directions for the field of InP quantum dot synthesis: (1) "low availability of suitable phosphorus precursors"; (2) "in-depth *in situ* and *ex situ* studies are of prime importance for the design of efficient synthesis methods, as they provide the necessary insight into precursor conversion kinetics, eventual side-reactions, internal structure and surface state of the obtained [nanocrystals]"; (3) "supplying additional precursors externally during the growth stage…is a promising yet underexplored alternative"; (4) "it has been demonstrated that the presence of traces of water or hydroxide impurities limit the size tunability", yet "the pure	The 1950 model is used to describe the growth process in all the examples the authors provide. Unfortunately, looking through the list of references, there are no reports that consider any other types of growth. Furthermore, the authors have not included any of the kinetics data that might bear on the claim of the 1950 model—kinetics being essential to decide on the applicability (or not) of the1950 model to InP.	33

		the properties of the [nanocrystals].”[33]	crystalline phase of bulk InP is assumed”; (5) “the recent observation and isolation of [magic size clusters] is very promising and may hold the key for further improving the quality of III-V nanocrystals”; (6) “improved understanding of surface/interface passivation would benefit designing core/shell structures with tuned optical properties”; and (7) “very few works exist on the doping of InP-based [nanocrystals], which demonstrate nonetheless the potential of this approach for introducing a further way for tuning their optical and electronic properties.”[33]		
17	Continuous Growth of Metal Oxide Nanocrystals: Enhanced Control of Nanocrystal Size and Radial Dopant Distribution	Indium oxide nanocrystals were formed from indium(III) acetate in oleic acid under N_2. This solution was heated to 150 °C for several hours and then added to oleyl alcohol heated to 290 °C. Preparation of indium tin oxide (ITO) core with indium oxide shell particles was done by preparing a 10% tin-doped indium oleate solution using tin(IV) acetate and indium(III) acetate in oleic acid. The ITO solution was added first to the oleyl alcohol and then followed by the indium oleate solution. Characterization was done by SAXS, TEM, STEM, XPS, and UV-vis.	Continuous growth is observed as long as there is metal precursor present. Particle sizes from 6 to 16 nm were observed by SAXS and TEM. SAXS analysis suggests the number of particles remains effectively constant throughout the addition of metal precursor, which would mean additional metal precursor is only consumed as surface growth on the present particles. Addition of more oleyl alcohol produces larger particles. The authors “suspect that the surface hydroxyl groups are responsible for sustaining nanocrystal growth (or, alternatively, terminate growth if the hydroxyls become passivated or dehydrate to an oxo species).”[34]	The 1950 model (or as the authors call it, the ‘classic LaMer theory’) is cited and used as the theoretical background behind the heat-up and hot-injection methods. However, the results in the paper are not explained in terms of the model and no test/experiment was done of the 1950 model. Hence, there is no evidence to support (or refute) the applicability of the 1950 model to indium-oxide nanoparticles.	34
18	Synthesis of Semiconductor Nanocrystals, Focusing on Nontoxic and Earth-Abundant Materials	This is a review of “the synthesis of semiconductor nanocrystals/colloidal quantum dots in organic solvents with special emphasis on earth-abundant and toxic, heavy-metal-free compounds.”[35]	The main sections of the review are: (1) the introduction; (2) “terms related to the toxicity of nanocrystals and a comprehensive overview of toxicity studies concerning all types of quantum dots”; (3) “the basic concepts of nanocrystal synthesis… used to describe the nucleation and growth of monodisperse particles” and “a closer look at the chemistry of the inorganic core and its interactions with surface ligands”; (4) the synthesis of different families of semiconductor nanocrystals, namely elemental group IV compounds (carbon nanodots, Si, Ge), III-V compounds (e.g., InP, InAs), and binary and miltinary metal chalcogenides”; and (5) author perspectives on the field.[35]	The authors present a section in the review entitled the ‘LaMer Model and Its Extensions.’ Here, the authors say “the LaMer model links nucleation and growth of colloidal particles in homogeneous solution and represents, despite some shortcomings, the most widely applied model for describing the formation of [nanocrystals].”[35] However, the focus on the review is on the role of ligands in nontoxic and earth-abundant semiconductor materials, even though the 1950 model has no provision for ligand effects. Overall, the authors of this review accept the 1950	35

				model, but with insufficient critical analysis in our opinion.	
19	Aqueous Based Semiconductor Nanocrystals	"This review summarizes traditional and recent nonconventional, bioinspired methods for the aqueous synthesis of colloidal semiconductor quantum dots."[36] The review covers the "basic chemistry of aqueous synthesis", "aqueous synthesis of semiconductor nanocrystals" (growth mechanism and core/shell structures), "optical properties of quantum dots", "theoretical aspects of optical/electronic properties of quantum dots and heterostructures", and author perspectives.[36]	In a discussion of formation mechanisms, the authors note the added complexity of aqueous synthetic routes over non-aqueous routes "owing to the involvement of H^+, OH^-, and H_2O moieties that introduce a large number of thermodynamic and kinetic parameters."[36] The authors use the 1950 model and Ostwald ripening as the primary mechanisms of growth for aqueous nanocrystals. Of note, the authors remark "the binding strength of a surface capping ligand substantially affects its reactivity with metal precursors and in consequence influences both nucleation and growth kinetics of [nanocrystals] formed in solution."[36]	The 1950 model has not been reviewed; the model was only described at the beginning as the theoretical basis of aqueous nanocrystal growth.	36
20	Shining Light on Indium Phosphide Quantum Dots: Understanding the Interplay among Precursor Conversion, Nucleation, and Growth	The single author perspective describes the most commonly used nanocluster formation models, and then focuses on the author's previous work on the nucleation and growth of InP. Finally, the author presents and advances their two-step nucleation model for quantum dot synthesis.	The author found that "tuning precursor conversion kinetics appears insufficient to allow preparation of monodisperse samples at high yield over a range of sizes."[37] They "hypothesized that kinetically persistent magic-size cluster intermediates build up during InP [quantum dot] synthesis creating a low energy bottleneck in the reaction coordinate diagram."[37] This resulted in the development of their non-classical nucleation model, where monomers form cluster intermediate (pre-nucleation clusters) before being transformed ("in a series of steps that can be slow[37]) into nanoclusters.	This perspective presents the 1950 model and the underlining classical nucleation theory in its background information. However, the author draws the distinction between the 1950 model and CNT (calling CNT the 'classical' model) and the new non-classical model used by the author in recent publications. Specifically, the author notes that non-classical nucleation continues throughout the reaction time. Furthermore, ligand involvement in the formation of nanoparticles is in contrast to the 1950 model.	37
21	Tunable Room-Temperature Synthesis of Coinage Metal Chalcogenide Nanocrystals from *N*-Heterocyclic Carbene Synthons	Metal (Ag and Cu) sulfide quantum dots (QDs) were prepared from benzimidazolium metal salts and bis(trimethylsilyl)sulfide in 1-octadecene in an air- and moisture-free environment. Metal (Ag and Cu) selenides were prepared from benzimidazolium metal salts and bis(*tert*-butyldimethylsilane)selenide in	The authors claim they are able to tune the metal chalcogenide QDs by modifying the electronic properties of the ligands. They remark "this synthetic approach thus allows for QD size control from the molecular precursor, rather than reaction time or temperature."[38] The authors report an extremely narrow size distribution. However, they also report they precipitated the particles, extracted them by centrifugation, and discarded any agglomerates.	The authors explain the separation of nucleation and growth in high-temperature (hot-injection syntheses) using the 1950 model. The authors do not mention the 1950 model beyond this point. However, the authors recognize that at a much lower temperature (ambient/room temperature) the rate of nucleation will be slower.	38

		THF in an air- and moisture-free environment. Reactions were carried out for 60 minutes. The reaction was monitored using UV-vis-NIR spectroscopy. Further characterization was done with NMR, FT-IR, TGA, XPS, XRD, TEM, and ICP-OES.			
22	Large scale syntheses of colloidal nanomaterials	The review summarizes how the synthetic approaches developed for nanomaterials can potentially be used in large-scale, industrial applications. The review covers:[39] heat-up method (room temperature, elevated temperature, solvothermal and microwave irradiation), hot-injection, continuous flow, and multiphase flow.	The authors offer a series of recommendations for scaling up colloidal nanomaterial syntheses. First, for one-batch reactions, the heat-up method appears to be the easiest to scale up. Next, many isolation and precipitation processes are not optimized or automated, yet. Finally, "for further advancing the large scale production of nanomaterials, one would need an efficient coupling of the synthesis and post-synthetic treatment units with a high throughput analytical systems for in-line characterization and control of the processes and products."[39]	The 1950 model is used as the underlining principle leading to monodisperse colloidal particle formation. The authors specifically remark "the formation of monomers needs to be controlled so that during the growth stage the concentration should not cross the nucleation threshold, since that would create new nuclei which would have less time to grow compared to the ones formed before, a scenario that would ultimately lead to polydisperse particles. This can be achieved by several handles, like temperature, material supply, pH, etc."[39] However, no consideration of ligand effects on particle growth is taken into account, yet numerous papers where ligand effects are shown to control growth are referenced.	39
23	Surface activation of colloidal indium phosphide nanocrystals	Quantum dots (QDs) were prepared by heating metal (In or Cd) precursors to 185 °C or 250 °C, respectively, and then injecting phosphorus or selenium octadecene solutions. Heating was stopped once particles had reached a desired size. Metal precursors used were indium acetate or indium acetylacetonate in either decanoic acid, myristic acid, or stearic acid, and cadmium oxide in myristic acid. QDs were characterized by UV-vis, photoluminescence, TEM, XRD, XPS, and elemental analysis.	The authors found that "dense and tight ligand passivation on InP and III-V QDs was identified as the key barrier to the efficient growth of nanocrystals. This structural feature induced the tight entanglement of the nucleation and growth of the nanocrystals under typical synthesis conditions."[40] It was observed that stronger-bonding ligands slows the surface growth of the QDs more.	This important 2017 paper has only 6 citation as of February 2019. The demonstration of the role of surface ligand in the nucleation and growth of nanoparticle formation is strong evidence against the 1950 model. Showing that nucleation is not "instantaneous" and can dominate growth is an important part of this paper. Inapplicability of the 1950 model to the formation of the semiconductor nanoparticles examined is clearly demonstrated.	40
24	On-Surface Reactions in the Growth of High-Quality CdSe Nanocrystals in Nonpolar	Cadmium selenide (CdSe) quantum dots (QDs) were prepared from cadmium oxide and selenium	The kinetics and the mechanism for Cd-terminated QDs versus Se-terminated QDs were shown to be different. "While two elementary steps in the Se-surface half-	The demonstration that the particle growth is achieved through reaction of precursors with the species on the surface of	41

	Solutions	powder in lauric acid and 1-octadecene under argon gas at 260 °C. Particle formation and characterization was done using UV-vis, FT-IR, TEM, XRD, and photoluminescence. Selenium-terminated and cadmium-terminated QDs were prepared.	reaction can be quantitatively treated as parallel kinetics, two elementary steps for the Cd-surface half-reaction must be treated as consecutive steps."[41] "The growth of high-quality CdSe QDs can be realized using a cyclic scheme."[41] "Such a scheme enables quantitative and reproducible studies on chemical kinetics between the reactive Se (Cd) precursors in the bulk solution and the Cd-terminated (Se-terminated) QDs."[41]	nanoparticles is in contrast to "diffusion-controlled growth" where soluble monomer is assumed to be attached to nuclei. The 1950 model in inapplicable to these systems because it has no provision for the existence of ligands on the surface of growing particles.	
25	Antisolvent-assisted controllable growth of fullerene single crystal microwires for organic field effect transistors and photodetectors.	Fullerene (C_{60}) was purchased and used as received. Crystals of fullerene were grown using "a two-vial-based antisolvent vapor diffusion method."[42] Antisolvents used were isopropyl alcohol, ethanol, and methanol. Crystals were characterized using the following techniques: optical microscopy, AFM, SEM, TEM, XRD, and XPS.	The authors used "a facile solution-processed antisolvent vapor diffusion method…to grow one-dimensional millimeter-length C_{60} crystal microwires directly in solution."[42] The photodetectors that were constructed from these wires performed superior to those constructed from drop-casting. It is believed this antisolvent vapor diffusion method could be "further exploited for a broad range of other organic semiconductors to achieve desirable single crystal size and morphology."[42]	The 1950 model is adopted to rationalize the crystal growth, but in a "words only" fashion without supporting data or quantitative fits to any kinetics. Hence, the 1950 model has yet to be definitively supported or refuted for this system.	42
26	Real-Time in Situ Probing of High-Temperature Quantum Dots Solution Synthesis	Cadmium Selenide (CdSe) quantum dots were prepared from cadmium myristate (CdMyr) and selenium powder in 1-octadecene. The solution was mixed and sonicated under argon gas and heated from 150 °C to 240 °C at a rate of 1 °C/second. The reaction was monitored by in situ synchrotron SAXS and WAXS.	Particles under 1 nm were observed and claimed to be CdMyr micelles. Particles larger than 1 nm were claimed to be CdSe nanoparticles. A bimodal size distribution was observed until the end of the reaction time. Nucleation is claimed to end once the reaction has reached 240 °C. The authors claim the incorporation of the reduced selenium is the rate-limiting step in the formation reaction of CdSe.	The authors claim "a LaMer-type mechanism is observed where the concentration in monomer increases until the onset of nucleation. As long as the concentration in monomers is large enough, nucleation persists while newly formed nuclei grow. When the generation of monomers is not fast enough to fuel both processes, nucleation stops and only growth persists."[43] *However*, the authors have disproved that growth is diffusion-controlled. They explicitly state growth is several orders of magnitude lower than diffusion-controlled. Furthermore, they show, with their high-quality, in situ, synchrotron data, that nucleation is continuous. This nucleation continues beyond their claim of the temperature-dependent end at 240 °C.	43

Table S3 Summary of transition-metal nanoparticle literature relating to the 1950 model.

Entry	Title	System	Evidence & Insights	Comments and/or Relevance to the 1950 Model	Ref.
1	The Bakerian Lecture: Experimental Relations of Gold (and Other Metals) to Light.	Primarily, Faraday uses various forms of gold (gold-leaf, wire, film, from solution) and other metals. He describes the interactions the metals have with (primarily) light, heat, and pressure.	The findings reported in this lecture given by Faraday are one of the first, complete reports on the formation of colloidal gold in solution. The lecture focuses primarily on the physical observations of different forms of gold starting materials (and other metals) as they interact with changes in light, heat, and pressure.	This report is commonly referred to in the literature as the first study of gold sols. It has been >150 years since this original study was conducted, a classic paper that holds important historical accounts of the beginnings of gold colloid research. While Faraday did not know it at the time, he observed the formation of gold sols in solution, as he notes that "gold in a *certain state* can transmit a ruby light."[44]	44
2	A Study of the Nucleation and Growth Processes in the Synthesis of Colloidal Gold	By using various methods, the nucleation and growth of colloidal gold were studied under different conditions with different reducing agents. By using various methods including electron microscopy, nephelometry, monitoring the change in concentration of chloroauric ion, following the formation acetone dicarboxylic acid as the oxidation product from sodium citrate, it was shown that the formation of colloidal gold consists of a *slow nucleation and an exponential growth*.	Major findings: (i) The nucleation agent and reducing agent are identified to be same; (ii) Nucleation takes place parallel to reduction, whereby the reagent forms a complex with the chloroauric anion; (iii) *Both* nucleation and growth are observable; (iv) The particle size distribution depends on gold concentration, temperature, and the concentration and nature of reducing agent; (v) An induction period is observed during which reduction and nucleation occur; and (vi) Observation of exponential growth without induction period when preformed nuclei are added to reaction medium in the presence of mild reducing agent such as hydroxylamine hydrochloride.	Turkevich notes that slow nucleation cannot be explained by the fluctuation theory or the 1950 model, which is based on the assumption of instantaneous nucleation from a supersaturated solution (and we can now strongly suggest that such a supersaturation is never achievable with highly reactive metallic gold atoms). *This classic study disproves the 1950 model for at least for the formation of gold nanoparticles.* Nevertheless, the 1950 model continues to this day to be cited as how transition-metal nanoparticles form—a testament to how little, and how poorly, those citing the 1950 model for the formation of transition-metal nanoparticles have read and studied Turkevich's classic, insightful literature.	1
3	The Formation of Colloid Gold	Electron microscopy was used to study the reduction of chloroaurate(III) ion to colloidal gold.	The authors present nucleation and growth kinetics followed by a particle size-distribution for colloidal gold. Most importantly, a mechanism for the nucleation of gold sols is presented, which is termed, the "organizer mechanism."[45] The authors describe this as "the nucleating agents gradually build up a *chemical* complex between themselves and gold ions, organizing the latter into a macromolecular. When the size of the macromolecular inorganic-organic polymer is sufficiently great, it will undergo a molecular rearrangement to produce the metal nucleus and oxidation products of the organizer."[45]	This is another classic study by Turkevich and coworkers. It demonstrates a temporal alternative to the 1950 model's growth model. Furthermore, it explicitly presents particle number increasing with time, a direct disproof of the 1950 theory of burst nucleation. The concentration versus times curves are described as having an induction period where nucleation is occurring and an "auto-accelerating" growth period, which is inconsistent with the 1950 model, but completely consistent with modern	45

				studies of nucleation and growth.[48]	
4	Colloidal gold. Part I	The historical perspective by Turkevich focuses primarily on the formation of gold sols from the reduction of chloroauric acid by sodium citrate at 100 °C.	The author presents a summary of his work on colloidal gold formation and discusses, from a historical approach, the advances that have been made in the measurements of gold colloids. Specifically, he addresses the experimental preparation, the nucleation, growth, and coagulation steps, and the advancement of electron microscopy to determine particle sizes and morphology.	No new insights have been presented in this perspective than have already been cited in the preceding two entries (#2 and #3) to this table, Table S1.	46
5	Gold Sol Formation Mechanisms: Role of Colloidal Stability	The formation of gold nanoparticles from chloroauric acid, reduced by sodium citrate, was studied. The reaction kinetics were followed by monitoring the change in concentration of gold(III) ion by UV-vis absorption spectroscopy and iodometric titration. Particle size was monitored by electron microscopy, DLS, and absorption spectroscopy.	The formation of large gold particles is observed at the beginning of reaction. Over the course of the reaction, the large clusters break apart to form smaller, stable sols. It is hypothesized by the authors that "over the course of the reaction the particle surface potential increases and electrostatic forces due to increased citrate adsorbtion push the primary particles apart."[47] The mechanism proposed by the authors cites the 1950 model, but with a reversible aggregation of primary particles.	While the authors cite the 1950 model as the mechanism of gold colloid formation, the extent of reaction versus time data clearly exhibit sigmoidal character. The observed sigmoidal curve strongly suggests continuous, not burst, nucleation. One important insight the authors made is the importance of surface ligand to stabilize growing particles.	47
6	Transition Metal Nanocluster Formation Kinetic and Mechanistic Studies. A New Mechanism When Hydrogen Is the Reductant: Slow, Continuous Nucleation and Fast Autocatalytic Surface Growth	Iridium nanoparticles ($Ir_{\sim 190–450}$) are formed from $[(1,5\text{-COD})Ir^{I}\bullet P_2W_{15}Nb_3O_{62}]^{8-}$ under 40 psig H_2. The kinetics of the reaction were quantified by two methods: the catalytic hydrogenation activity of the $Ir(0)_n$ nanos and by gas-liquid chromatography of reaction byproducts. Controls were conducted to disprove all possible alternative hypotheses.	A 2-step mechanism consisting of slow, continuous nucleation and autocatalytic surface growth was proposed and used to explain and quantitatively account for the kinetics of formation of Ir(0) nanoparticles. A differential rate equation was derived for the above 2-step mechanism with resultant rate constants k_1 (nucleation) and k_2 (growth).	This is the first paper clearly indicating that the 1950 model is obsolete for at least the formation of transition metal nanoparticles. Nucleation was demonstrated quantitatively to be *slow and continuous*, and not a "burst" phenomenon as the 1950's 1950 model postulated. In addition, growth was shown to be far slower than diffusion controlled and, instead, chemically controlled, autocatalytic surface growth. The title of the paper states the new findings: A New Mechanism … Slow, Continuous Nucleation and Fast Autocatalytic Surface Growth".[48]	48
7	Nanocluster Size-Control and "Magic Number" Investigations. Experimental Tests of the "Living-Metal Polymer" Concept and of Mechanism-Based Size-Control Predictions Leading to the Syntheses of Iridium(0) Nanoclusters Centering about Four	Kinetic and mechanistic studies of the formation of $Ir(0)_{\sim 300}$ nanoparticles from the precursor $[(1,5\text{-COD})Ir^{I}\bullet P_2W_{15}Nb_3O_{62}]^{8-}$ reduced under 40 psig H_2.	Magic number clusters of average size close to the theoretical values of 147, 309, 561, and 923, particles were deliberately and rationally synthesized, namely $Ir(0)_{\sim 150}$, $Ir(0)_{\sim 300}$, $Ir(0)_{\sim 560}$, and $Ir(0)_{\sim 900}$ average-size nanoparticles. This study is an early, and probably the first, mechanism-based report of size-control for transition-metal nanoparticle formation. Furthermore, the authors state, "magic numbers are the expected, natural consequence of surface autocatalytic growth."[49]	The results are a direct disproof of the 1950 model and CNT for this specific system. The study employs a kinetically controlled syntheses, which is in opposition to CNT and the 1950 model, which claim thermodynamic control. In addition, this study further disproves the diffusion-controlled growth posited by the 1950 model and demonstrates growth for transition-metal nanoparticles occurs by	49

	Sequential Magic Numbers.			autocatalytic surface growth that is 10^{6-7} orders of magnitude slower than diffusion control, in this particular study.	
8	Nanocluster Formation Synthetic, Kinetic, and Mechanistic Studies. The Detection of, and Then Methods to Avoid, Hydrogen Mass-Transfer Limitations in the Synthesis of Polyoxoanion- and Tetrabutylammonium-Stabilized, Near-Monodisperse 40 ± 6 Å Rh(0) Nanoclusters	Rh(0) nanoparticles were formed from the precursor, $[(C_4H_9)_4N]_5Na_3[(1,5\text{-}COD)Rh^{I}\bullet P_2W_{15}Nb_3O_{62}]$, reduced by H_2 in acetone.	Rh(0) nanoparticles, stabilized by $P_2W_{15}Nb_3O_{62}^{9-}$ polyoxoanion, were synthesized and observed to be near-monodisperse, size = 4.0 ± 0.6 nm. Initial attempts resulted in polydisperse sizes from 1.6 to 11.6 nm Rh(0) nanoparticles. The hydrogen gas-to-solution mass-transfer limitation (MTL) was identified as a component of transition-metal nanoparticle syntheses, which must be controlled to produce near-monodisperse nanoparticles. Stirring rate, catalyst dependent and independent kinetic regimes, and TEM evidence were all used to determine MTL and non-MTL kinetic regimes. The authors state that "these lines of evidence support a mechanism with two parallel, competing, nanocluster growth steps: autocatalytic surface growth, leading to near-monodisperse nanoclusters, and diffusive agglomeration, leading to polydisperse nanoclusters."[50]	This paper presents strong evidence that both metal nanoparticle formation is a kinetic process, consisting of slow continuous nucleation followed by autocatalytic surface growth, *and* that the FW 2-step mechanism is a direct disproof of the 1950 model. The results from this study of Rh(0) nanoparticle formation provides a mechanistic explanation of how polydisperse and then near-monodisperse nanoparticles can be formed from a mechanistic understand and the effects of of H_2 gas-to-solution diffusion limitations..	50
9	Mechanism of Formation of Monodispersed Colloids by Aggregation of Nanosize Precursors	A model was constructed to analyze primary particle formation from kinetic and thermodynamic points of view. The model is intended for particles, where the nuclei are formed from supersaturated solution, grow to nanosized 'primary particles', and then coagulate into large final, micro-scale, particles. Finally, the model is checked, experimentally, against spherical gold particle dispersions produced from chloroauric acid reduced by ascorbic acid.	A kinetic model for particle formation with narrow size distributions is presented, where numerical simulations of the kinetic equations are used. The authors report "semi-quantitative values" for the "average size, width of the distribution, time scale of the process, and the fitted effective surface tension"[51] of the gold-sol system. The gold-sols were studied by field emission microscopy and dynamic light scattering. The primary gold particles had an average radius of 21 nm. The secondary gold particles had an average radius of ~1-2 microns.	The authors claim that, "with the increasing availability of monodispersed colloids of spherical and other shapes, it has become evident that the burst-nucleation/diffusional growth mechanism alone cannot explain many experimental observations."[51] Here, the authors have rejected the 1950 model because of the increased evidence that it does not fit the experimental data. Further, they presented an alternative, *kinetics-based model* to describe the same growth process.	51
10	Silver Nanoparticle Formation: Predictions and Verification of the Aggregative Growth Model	The formation of silver sols from silver perchlorate reduced by sodium borohydride is studied experimentally in an aqueous medium. An aggregative growth model was constructed using population balance equations. Experimental results were collected using AFM, TEM, UV-vis, and surface potential measurements.	The reduction of silver perchlorate to silver nanoparticles by sodium borohydride is observed to be fast, reported in the paper as taking only 5 seconds, and leads to the formation of ~2.5 nm silver particles with a polydispersity of ~20%. Over the next 30 minutes, the particles aggregated to form ~12 nm particles. The proposed aggregative growth model was able to model this behavior by assuming the particles interact by only electrostatic or van der Waals forces.	This study disproves both the proposed nucleation and growth concepts of the 1950 model. The authors demonstrate (i) nucleation is non-instantaneous, and (ii) growth is not diffusion-controlled, but rather that growth is aggregative past initial silver nanoparticle formation. Importantly, the authors present both experimental and theoretical /modeling results.	52

11	Is It Homogeneous or Heterogeneous Catalysis? Identification of Bulk Ruthenium Metal as the True Catalyst in Benzene Hydrogenations Starting with the Monometallic Precursor, Ru(II)(η^6-C_6Me_6)$(OAc)_2$—Plus Kinetic Characterization of the Heterogeneous Nucleation, then Autocatalytic Surface-Growth Mechanism	The formation kinetics of bulk Ru(0) metal from a monometallic precursor, Ru(II)(η^6-C_6Me_6)$(OAc)_2$, were observed. The reaction kinetics were monitored by the hydrogenation of benzene and by quantifications of reaction byproducts. Further characterization of the Ru(0) film was done using TEM and XPS.	The sigmoidal kinetics curves for the formation of bulk Ru(0) film were quantitatively fit using the FW 2-step mechanism. The authors state the most important findings from this study, are that the FW 2-step mechanism "quantitatively accounts for the formation of bulk metal via *heterogeneous* nucleation then autocatalytic surface growth. This is significant for three reasons: (i) quantitative kinetic studies of metal film formation from soluble precursor are rare; (ii) a clear demonstration of such A $\rightarrow$ B, then A + B $\rightarrow$ 2B kinetics, in which both the induction period and the autocatalysis are continuously monitored and then quantitatively accounted for, has not been previously demonstrated for metal thin-film formation; yet (iii) all the mechanistic insights from the soluble nanocluster system[48,49,50] should be applicable to metal thin-film formations which exhibit sigmoidal kinetics."[53]	This study presented strong evidence for the broader applicability of the 2-step mechanism—this time to bulk Ru(0) metal formation as a benzene hydrogenation catalyst. The result are, again, a disproof of the 1950 model for the Ru(II) to 1/n $Ru(0)_n$ system examined.	53
12	In Situ Spectroscopic Analysis of Nanocluster Formation	Chloropalladous acid, chloroauric acid, and silver nitrate were all reduced by sodium borohydride or tetraoctylammonium acetate in DMF. Nanoparticle formation kinetics were monitored by UV-vis. Characterization of the resulting nanoparticles was done by TEM and EDX.	The authors collected time-resolved UV-vis spectra of the formation of Pd, Au, and Ag nanoparticles. The spectra were analyzed using a combination of net analyte signal (NAS) analysis and principal component analysis (PCA), referenced as NAS/PCA. The bulk of the kinetics data were collected on the Pd system, where an induction period followed by a fast growth period was observed. Furthermore, the authors describe the in situ NAS/PCA approach as a "quick and quantitative assessment of the system without the need to quench and isolate the clusters."[54]	The observation of an induction period and continuous nucleation disproves the 1950 model's posit of burst, or instantaneous, nucleation. This study uses UV-visible spectroscopy to perform needed kinetics studies, but does not discuss the mechanistic implications of their results.	54
13	Transition-Metal Nanocluster Kinetic and Mechanistic Studies Emphasizing Nanocluster Agglomeration: Demonstration of a Kinetic Method That Allows Monitoring of All Three Phases of Nanocluster Formation and Aging	A 3-step kinetic method following nucleation, growth, and then agglomeration is presented. Formation of catalytically active Ir(0) nanoparticles stabilized by $P_2W_{15}Nb_3O_{62}^{9-}$ polyoxoanions in acetone were studied. The Ir(0) nanoparticles were formed in situ from the precursors [(1,5-COD)$Ir^{I}(CH_3CN)_2$][BF_4] and $[Bu_4N]_9[P_2W_{15}Nb_3O_{62}]$.	The authors report the "nucleation, growth, and then agglomeration [steps] are treated kinetically for the first time for a modern, prototype transition-metal nanocluster."[55] The authors ran numerous controls to rule out various alternative hypotheses (solvent effects, salt effects, etc.) and found the kinetics data were only able to be fit with the inclusion of the third step (B + B $\rightarrow$ C, bimolecular agglomeration) in the mechanism.	The 2-step mechanism was expanded to account for agglomeration. In this study, B is the active catalyst and C is the deactivated, agglomerated catalyst, via B + B $\rightarrow$ C. This new, proposed mechanism describing nucleation, growth, and agglomeration of transition-metal nanoparticles directly disproves the applicability of the 1950 model as do previous entries in this table.[48,49,50,53]	55
14	A Mechanism for Transition-Metal Nanoparticle Self-Assembly	Platinum(0) nanoparticles were formed from the reduction of (1,5-COD)$Pt^{II}Cl_2$ by H_2 in acetone at room temperature. The Pt(0)	The results in this paper build upon the 3-step mechanism presented in entry 13 (ref. 55). Here, they have added a fourth, autocatalytic agglomeration, step to a proposed, new 4-step mechanism. The proposed 4-step	The 4-step mechanism provides the first particle formation mechanisms that include agglomeration and double autocatalysis.	56

		nanoparticles were stabilized by tributylamine and chloride. Kinetics data were collected using a catalytic reporter reaction. Further investigation was performed using numerical simulations (MacKinetics). Characterization was performed by TEM and ^{31}P NMR.	mechanism contains of: (i) slow, continuous nucleation, A $\rightarrow$ B; (ii) autocatalytic surface growth, A + B $\rightarrow$ 2B; (iii) bimolecular agglomeration, B + B $\rightarrow$ C; and then (iv) autocatalytic agglomeration, X + C $\rightarrow$ 1.5C, where A is the organometallic precursor, B is a M(0) nanoparticle, C is bulk-metal, and X is either A or B. The authors tested 15 alternative mechanism and found that only 2 were able to fit the data: X + C $\rightarrow$ 1.5C, where X = A or B. Finally, the possibility and implications of size-dependent metal-ligand bond dissociation energies are raised and addressed.		
15	Nanocluster Nucleation, Growth, and Then Agglomeration Kinetic and Mechanistic Studies: A More General, Four-Step Mechanism Involving Double Autocatalysis	The same system from the above entry 14 (ref. 56) was studied that resulted in the formation of Pt(0) nanoparticles stabilized by tributylamine and chloride. Kinetics were collected using a catalytic reporter reaction. Byproduct quantification was done by ^{1}H NMR and GLC. Further investigation was done by TEM and XPS.	The findings in the above entry 14 (ref. 56) are further supported with an additional kinetic and mechanistic investigation. The authors state that the mechanism with the addition of the fourth step, B + C $\rightarrow$ 1.5C, "accounts *quantitatively* for the unusual, approaching step-function-like nature of the curves."[57] They report the 4-step mechanism accounts for not only the kinetics from the catalytic reporter reaction, but also to the formation of the cyclooctane byproducts. In addition, the kinetics were simulated by MacKinetics and shown to be consistent with the experimental data.	The authors state, in this 2005 paper, that the 1950 model "was for *sulfur sol*, and not transition-metal, formation."[57] Furthermore, the 1950 model "is completely different from the expanded, more general mechanism published herein for transition-metal nanocluster formation and then agglomeration under reductive conditions."[57] In short, the authors disprove the 1950 model and show how a 4-step mechanism can quantitatively fit and explain, physically, the observed data.	57
16	New Insights on the Nanoparticle Growth Mechanism in the Citrate Reduction of Gold(III) Salt: Formation of the Au Nanowire Intermediate and Its Nonlinear Optical Properties	The reduction of aqueous tetrachloroaurate(III) anion by sodium citrate to produce gold nanospheres, which self-assemble into networks of nanowires, was studied. Nanowires were directly observed by TEM. UV-vis measurements were performed. Nonlinear optical (NLO) activities were studied with femtosecond Z-scans and pump-probe at 780 nm with a 150 fs laser (at a rate of 1 kHz).	The authors report the reduction of Au(III) to Au(0) and the formation of 3-5 nm nanoparticles. These nanoparticles self-assembly into interconnected long nanowires (diameter = ~8 nm). Eventually, spherical nanoparticles (diameter = 13-15 nm) are produced from the ends of the nanowires until all the nanowires are consumed and only nanospheres remain. UV-visible spectroscopy displays the continuous red-shift from dark purple to ruby-red throughout this process.	The authors remark that "in the present study, we focused on the particle growth process in the citrate-reduction method and found that the growth process differs remarkably from the commonly accepted LaMer nucleation-growth model."[58] However, no explanation is provided for the role of the citrate in the final particle size or the growth process.	58
17	Size Control of Gold Nanocrystals in Citrate Reduction: The Third Role of Citrate	Gold nanocrystals were prepared by the Frens's synthesis (chloroauric acid reduced by sodium citrate in water). Kinetics data were collected using UV-vis. Particle size and size distributions were obtained by TEM	The authors report the reactivity of Au(III) is greatly diminished at pH values of 6.2 and 7.2. They also state, "dependent on the reaction pH, gold nanocrystals could be formed through either the nucleation-growth pathway or nucleation-aggregation-smoothing pathway, pH roughly being 6.2-6.5 as the switch point."[59] Finally,	The authors claim there is an induction period in the formation of their gold nanocrystals, something inconsistent with the 1950 model's burst/instantaneous nucleation. The authors also report time-resolved UV-vis data (i.e., concentration	59

		and DLS.	they claim citrate, in addition to being a reducing agent and ligand in the Frens's process, acts as a pH mediator. This was determined by varying the gold:citrate ratio and measuring the solution pH.	versus time kinetics data) that does not support the 1950 model.	
18	Transition-Metal Nanocluster Stabilization versus Agglomeration Fundamental Studies: Measurement of the Two Types of Rate Constants for Agglomeration Plus Their Activation Parameters under Catalytic Conditions	$Ir(0)_{\sim 900}$ nanoclusters stabilized by $P_2W_{15}Nb_3O_{62}^{9-}$ (POM^{9-}) were formed from the precursor [(1,5-COD)Ir•POM]$^{8-}$, reduced under H_2 and studied by a catalytic reporter reaction and TEM. Specifically, agglomeration and temperature dependence were studied.	The authors report a method to "quantitate nanocluster stability and thereby rank stabilizers."[60] Agglomeration kinetics were measured, specifically rate constants for bimolecular agglomeration, B + B $\rightarrow$ C, and autocatalytic agglomeration, B + C $\rightarrow$ 1.5C, were studied, where B is reported as an average $Ir(0)_{\sim 900}$ and C is an average $Ir(0)_{\geq 2000}$.	The evidence presented in this paper support the mechanisms these authors have uncovered for nucleation and growth (2-step, 3-step, and 4-step), kinetic / mechanistic models.[48,49,50,53,55,56,57]	60
19	The Four-Step, Double-Autocatalytic Mechanism for Transition-Metal Nanocluster Nucleation, Growth, and Then Agglomeration: Metal, Ligand, Concentration, Temperature, and Solvent Dependency Studies	The 4-step mechanism (previously reviewed in entries 14 & 15)[56,57] was applied to 5 different transition-metal systems. Complexes studied were $[Ir^{I}(1,5\text{-COD})Cl]_2$, $[Rh^{I}(1,5\text{-COD})Cl]_2$, $Pt^{II}(1,5\text{-COD})Cl_2$, $Pd^{II}(1,5\text{-COD})Cl_2$, and $Ru^{II}(1,5\text{-COD})Cl_2$. Kinetics were studied by a catalytic reporter reaction.	The authors found "the four-step, double-autocatalytic mechanism discovered previously[56,57] for the reduction of the platinum salt $Pt^{II}(1,5\text{-COD})Cl_2$ is more general to the reduction of the analogous salts of Ru^{II}, Ir^{I}, Rh^{I}, and Pd^{II} in the presence of appropriate ligands and under the conditions examined."[61] Furthermore, it was suggested that for any transition-metal complex displaying step-function-like kinetics, the 4-step mechanism should be tried to fit the data quantitatively.	The 4-step mechanism for the nucleation, growth and two types of agglomeration of transition metal nanoparticles is further supported.[48,49,50,52,53,55,56,57,60]	61
20	Fitting Neurological Protein Aggregation Kinetic Data via a 2-Step, Minimal/"Ockham's Razor" Model: The Finke-Watzky Mechanism of Nucleation Followed by Autocatalytic Surface Growth	A summary of fitting 14 representative literature data sets of neurological protein aggregation to the FW 2-step mechanism.	This paper reveals the broader applicability of the 2-step mechanism to systems beyond metal nanoparticle formation, notably to protein aggregation in neurological diseases such as Alzheimer's, Parkinson's, and Huntington's diseases.	This paper provides evidence for the broader generality of the 2-step mechanism, now to gain a understanding of protein aggregation.	62
21	Fitting Yeast and Mammalian Prion Aggregation Kinetic Data with the Finke-Watzky Two-Step Model of Nucleation and Autocatalytic Growth	An expansion of the above study (Entry 20, Ref 62) is presented, where the authors focused on applying the FW 2-step mechanism to "27 representative prion aggregation kinetic data sets obtained from the literature."[63]	The authors report their biggest finding to be that "twenty-seven prion aggregation curves from the literature, measured by seven different physical methods, were successfully fit using the F-W model, allowing for the deconvolution of average nucleation (k_1) and growth (k_2) kinetic parameters for the first time in all cases."[63]	As stated above in Entry 20 (ref 62), this study shows the growing evidence for the broader generality of the 2-step mechanism.	63
22	Nanocluster nucleation and growth kinetic and mechanistic studies: A review emphasizing transition-metal nanoclusters	The authors present a literature review of the kinetic and mechanistic studies for transition-metal nanocluster formation. Specifically analyzed were the following: classical nucleation	As of 2008, the authors report that there is "no clear, experimentally quantitative description of what happens during the nucleation of transition-metal nanoclusters in solution."[64] Furthermore, the authors point out several issues that still remain in the study of nucleation of nanoclusters: the timing of formation of the nuclei in	The authors of this review specifically discuss the 1950 model in relation to transition-metal nanocluster formation. They state that "while it may be a viable mechanism for the specific system of *sulfur sol formation*, it is not expected to be the	64

		theory, the 1950 model, techniques for studying nanocluster formation in solution, factors affecting nanocluster preparation, and systems including Au, Ag, Bi, Co, Cr, Cu, Fe, In, Ir, Pd, Pt, Rh, Ru, Sn, CdSe, CdO, and $AgMnO_4$.	relation to reduction/oxidation of metal precursor, the role of ligands in nucleation, and the importance of the metal—metal bond strength.	mechanism by which transition-metal nanoclusters nucleate and grow from dilute solutions. Despite this, LaMer's pioneering mechanistic work…has been applied to nanocluster preparations. This has led the opinion that LaMer's work has been 'overcited'; Finke and Watzky[48] have pointed out that this statement is unfair to LaMer and coworkers, given that LaMer's model was the only one available for almost 50 years.The problem is more that people are citing LaMer's model where it should not be cited, and beyond the limits imposed by the assumptions behind the LaMer model.	
23	Is There a Minimal Chemical Mechanism Underlying Classical Avrami-Erofe'ev Treatments of Phase-Transformation Kinetic Data?	This paper focuses on fitting literature data sets using both the FW 2-step mechanism and the AE model for solid-state kinetics. Twelve solid state systems were analyzed with 7 of them discussed in the main text. Those seven were as followed: Bi_3NbO_7, $Zr_{55}Cu_{30}Al_{10}Ni_5$, $CuAlCl_4$, poly(ethylenephthalate), $Al_{75}Cu_{15}V_{10}$, $Fe_{80}B_{20}$, and $Pd_{75}Cu_6Si_{10}P_5$.	The curve-fits to the two models demonstrate that the classical AE model and the FW 2-step mechanism provide generally equivalent fits to the data sets examined. The primary difference between the two models is the meaning behind the resultant two parameters: for the FW 2-step mechanism, k_1 and k_2 are well-defined rate constants for nucleation and autocatalytic surface growth, respectively. For the semi-empirical AE equation, the rate *parameter*, k, and the Avrami exponent, n, do not have unambiguous physical meaning. The authors state that "mathematical analysis…reveal that one alternative way to view the AE parameters k and n are that they are convolutions containing the FW rate constants k_1 and k_2."[65]	The paper provided addition evidence for the broader applicability of the 2-step mechanism—in this case to the solid-state, phase transformation literature. Importantly, the authors offer additional information to mark the distinction between the 2-step mechanism the 1950 model for the mathematical application in Footnote 25a, where they say "let us define what we mean by 'continuous nucleation'. We mean the process by which many single nucleation events occur over a period of time to achieve *average* nucleation. This is the process measured by the composite nucleation rate constant k_1. The use of the term 'continuous' nucleations historically served to distinguish the FW models from the 1950 model, in which a hypothesized 'burst nucleation' takes place due to an essentially infinite nucleation rate."[65]	65
24	In Situ Time-Resolved XAFS Studies of Metal Polymer Formation by Photoreduction in Polymer Solutions	Rhodium and palladium nanoparticles are formed from metal-chloride precursors in aqueous ethanol with PVP polymer. Particles are formed by photoreduction and studied by UV-vis, TEM, and *in situ* QXAFS.	Harada and Inada investigated the mechanisms of formation for rhodium and palladium stabilized by PVP polymer in aqueous ethanol. Analysis of the kinetics data was performed using the same differential equation as the FW 2-step mechanism. Specifically, a long induction period was observed in the kinetics of $Rh(0)_n$ nanoparticle formation.	The data and results presented support the 2-step mechanism using a direct, synchrotron technique (XAFS). The observed kinetics data from multiple techniques do not support the 1950 model. The data demonstrate continuous nucleation, and the data do not show diffusion-controlled growth. Therefore, the	66

				1950 model is disproved for this classic study and its systems.	
25	Monitoring Supported-Nanocluster Heterogeneous Catalyst Formation: Product and Kinetic Evidence for a 2-Step, Nucleation and Autocatalytic Growth Mechanism of $Pt(0)_n$ Formation from H_2PtCl_6 on Al_2O_3 or TiO_2	The formation of Pt(0) nanoparticles, via the reduction of H_2PtCl_6 on Al_2O_3 (or TiO_2) by H_2 in a solution of ethanol and cyclohexene, was examined. The reaction stoichiometry was confirmed by detecting the HCl by-product (using a pH meter) and by TEM and EDX measurements. Kinetics were studied by a catalytic reporter reaction.	Precatalyst preparation was done by deposited H_2PtCl_6 on either Al_2O_3 or TiO_2. Hydrochloric acid byproduct formation was quantitatively observed by $pH_{apparent}$ measurements. Sigmoidal kinetics data were successfully fit using the FW 2-step mechanism.	The 2-step mechanism is used to fit the kinetics data and to provide a physical explanation for the nucleation and growth process in preparing a supported, heterogeneous nanoparticle catalyst, $Pt(0)_n$, formation.	67
26	Development Plus Kinetic and Mechanistic Studies of a Prototype Supported-Nanoparticle Heterogeneous Catalyst Formation System in Contact with Solution: Ir(1,5-COD)Cl/γ-Al_2O_3 and Its Reduction by H_2 to $Ir(0)_n$/γ-Al_2O_3	The conversion of Ir(1,5-COD)Cl/γ-Al_2O_3 to $Ir(0)_{\sim 900}$/γ-Al_2O_3, under H_2, was studied directly by XANES and EXAFS and indirectly by a catalytic reporter reaction. Reactants were characterized by ICP-OES, CO adsorption, FT-IR, and XAFS. Products were characterized by reaction stoichiometry, TEM, GLC, and XAFS.	The nucleation and growth kinetics were fit using the 2-step mechanism. The catalytically active product, $Ir(0)_{\sim 900}$/γ-Al_2O_3, was observed to have a lifetime of ≥220,000 total turnovers (for cyclohexene hydrogenation). Importantly, the authors state the ability to fit the kinetics to the FW 2-step mechanism is "significant" as "it means that the nine synthetic and mechanistic insights[65] from the two-step mechanism should, at least in principle, be applicable to the synthesis of supported-nanoparticle heterogeneous catalyst in contact with solution."[68]	The nanoparticle formation kinetics data, in this study, are monitored directly by synchrotron x-ray techniques. The synchrotron data show the inapplicability of the 1950 model, the data being fit by continuous nucleation and autocatalytic growth (the FW 2-step mechanism) and *not* by burst nucleation and diffusion-controlled growth (LaMer) model.	68
27	Mechanism of Gold Nanoparticle Formation in the Classical Citrate Synthesis Method Derived from Coupled *In Situ* XANES and SAXS Evaluation	Tetrachloroauric acid was reduced by trisodium citrate in aqueous solution at 75 ºC and 85 ºC. The reaction was monitored by tandem SAXS/XANES using an acoustic levitator as the sample holder. Further characterization was done by UV-vis, SEM, and TEM.	The authors report *high-quality* tandem, *in situ*, SAXS/XANES data, where they have time-resolved size, number of particles, polydispersity, and oxidation state. The authors then propose a 4-step 'mechanism'—really just a scheme—for the formation of their Au nanoparticles by "fast initial formation of small nuclei, coalescence of the nuclei into bigger particles, slow growth of particles sustained by ongoing reduction of gold precursor, and subsequent fast reduction ending with the complete consumption of the precursor species."[69]	The authors state that "although one can describe the initial step as burst nucleation, the growth mechanism proposed in the present article is not in complete agreement with the classical nucleation theory by LaMer."[69] However, we argue burst nucleation is not occurring, as is observed in Figure 3d, where the number of particles initially increases with time. Unfortunately, the authors did not use any kinetics scheme to fit, qualitatively nor quantitatively, their high-quality kinetics data.	69
28	Mechanistic insights into seeded growth processes of gold nanoparticles	As with the above, Entry 27, gold nanoparticles were prepared from tetrachloroauric acid being reduced by trisodium citrate in aqueous solution. Samples were analyzed *ex*	The authors report "analysis by SAXS, SEM, and UV-Vis confirm that the radius of GNP can be precisely adjusted by 7 and 20 nm in GNP synthesis from $HAuCl_4$ and citrate, by adding incremental amounts of reactants in the absence of additional stabilizing or reducing	Overall, the data presented depicts sigmoidal kinetics suggestive of slow nucleation followed by fast, autocatalytic growth. However, because no differential equation or fully balanced stoichiometry is	70

		situ by SAXS/XANES (in tandem), UV-vis, and pH measurements.	agents."[70] The authors claim these results further support the 4-step 'mechanism' proposed in Entry 27 (ref. 69).	used to fit their data, they do not have conclusive nor even strong evidence for their mechanism. For comments on the connection to the 1950 model, see the above, Entry 27.	
29	Nucleation and Growth of Gold Nanoparticles Studied *via in situ* Small Angle X-ray Scattering at Millisecond Time Resolution	The synthesis of gold nanoparticles using a procedure originally published by Wagner *et al*. is examined: tetrachloroauric acid is reduced with sodium borohydride in water using a microstructured, static caterpillar mixer employing a total liquid flow rate of 50 mL per minute to allow for continuous mixing. The gold nanoparticles were monitored by SAXS measured with a CCD detection system and processed with SAXSQuant software. The same experimental set up was used for XANES analysis at the synchrotron facility BESSY II.	The use of SAXS and XANES (along with UV-vis) provide support for a 2-step mechanism of nanoparticle nucleation and growth, thereby supporting prior work on the Turkevich system. The number of particles increases at the beginning of the reaction (observable due to the excellent time-resolution within the first second of the reaction—see Figure 5b therein). Importantly, the authors utilize a new "microstructured mixer for fast continuous-flow mixing for nanoparticle synthesis with small-angle X-ray scattering" to allow for "'in house' SAXS at a time resolution of about 100 ms without requiring a synchrotron radiation facility."[71] Excellent *in situ* XANES data monitoring the gold reduction process was also obtained.	Unfortunately, no specific balanced-equation-based mechanism nor associated differential equation is provided in this paper to try to fit their excellent, expertly obtained kinetics data. Their resultant mechanism is, then and again, unfortunately an unconvincingly "words only" explanation of what the authors believe to be occurring in their reaction. Further studies using mechanism-derived differential equations to fit both their kinetics and size data are necessary in order to support their proposed 2 step mechanism and to try to disprove other conceivable mechanisms. Their data, particularly that shown in Figure 5b therein, do disprove the applicability of 'burst' nucleation per the 1950 model.	71
30	Pathway from a Molecular Precursor to Silver Nanoparticles: The Prominent Role of Aggregative Growth	A mechanistic study of Ag-nanoparticle growth, by reaction of $[Ag(PPh_3)_2(O_2CC_{13}H_{27})]$ and azoisobutyronitrile (AIBN) in the presence of a polymeric stabilizer, is reported. The reaction stoichiometry is established by NMR and MS. The reduction of precursor is followed by ^{31}P NMR. Nanoparticle formation is monitored by UV-vis spectroscopy.	The ^{31}P NMR monitoring of phosphine detachment from the precursor gives a pseudo first order kinetics. The Ag(0) nanoparticle formation is followed by UV-vis spectroscopy and TEM. However, none of two methods can measure small particles formed at the beginning earlier than 3 minutes. NMR does show the detachment of phosphine from the complex, but UV-vis spectroscopic results demonstrate that Ag(0) nanoparticles appear at a much later time than the detachment of phosphine, a point supported by TEM and the particle-size distribution data.	A valuable part of this work is that different techniques have been used to follow the reaction. However, the interpretation fails to consider all of the results together. The authors claim the observation of a sigmoidal growth curve for the size versus time data, at least in the so-called active growth regime. Afterword, the particle size continues to increase. The authors do conclude that the 1950 model does not apply to their system, albeit primarily because the 1950 model does not include aggregative growth in its model.	72
31	Insights into Initial Kinetic Nucleation of Gold Nanocrystals	Using a continuous-flow *in situ*, time-resolved XAFS spectroscopy, the initial kinetics of Au cluster formation under 1 nm for a classical Au(0) nanoparticle synthesis via the reduction of $AuCl_4^-$ with citric acid in the presence of PVP stabilizer in aqueous solution was studied..	The *in situ* XAFS reveal the formation of a Cl_3Au-$AuCl_3$ dimer and then subsequent longer-order complexes in the initial, prenucleation stage. A three-step mechanism involving the initial prenucleation, slow growth, and eventual coalescence for the Au(0) nanoparticle formation is proposed.	The 1950 model is found to *not* be applicable to the formation of gold nanoparticles. However, the key nucleation period could not be investigated because of the inability of their EXAFS to detect particles smaller than 1 nm, which means the authors were unable to observe any nucleation kinetics data because the needed	73

				data are below their limit of detection.	
32	Nucleation Control in the Aggregative Growth of Bismuth Nanocrystals	Kinetics of Bi-nanoparticle growth from $Bi[N(SiMe_3)_2]_3$, with added amounts of $Na[N(SiMe_3)_2]$, are investigated. Time-resolved TEM data were presented for the formation of Bi nanoparticles.	The Bi nanoparticles were prepared at 180 ºC and monitored by TEM, where initially a bimodal particle size distribution is observed. The distribution narrows with time, but eventually broadens, which the authors attribute to Ostwald ripening. Prior to the section attributed to Ostwald ripening, the authors observe sigmoidal particle-formation kinetics.	The authors state that "nanoparticles grown from molecular precursors are typically assumed to result from classical (LaMer) nucleation and growth, and nanoparticles grown from smaller nanoparticles are typically assumed to result from Ostwald ripening. However, neither the classical mechanism nor Ostwald ripening can produced the bimodal size distributions in Figure 2a-d."[74] Furthermore, the authors claim the diffusion-controlled growth process does not apply to the formation of Bi nanoparticles, but instead they propose aggregative growth to be a major contributor.	74
33	A review of the kinetics and mechanisms of formation of supported-nanoparticle heterogeneous catalysts	A comprehensive review of the literature of the kinetics and mechanisms of formation of supported-nanoparticle heterogeneous catalyst systems is presented. The review is split into two primary focuses: (1) supported-nanoparticles at the gas-solid interface; and (2) supported-nanoparticles in liquid-solid systems. All the systems studied in this review contain supported-nanoparticles that start as molecular precursors.	This first review of the mechanisms of supported heterogeneous catalyst formation highlights and illustrates: (i) the types of techniques (especially direct techniques) that are most successful at collecting high-quality kinetics data for mechanistic study; and then (ii) the most significant literature for supported-nanoparticle systems, including what kind of kinetics data has been produced and what kind of mechanism(s), if any, are used to explain the observed results.	This review makes apparent the surprisingly crude, state-of-the-art in mechanistic understanding of supported heterogeneous catalyst formation. While the 1950 model is not addressed directly because there is no evidence it is applicable to the nucleation and growth of supported heterogeneous catalyst formation.	75
34	Nucleation and Aggregative Growth Process of Platinum Nanoparticles Studied by in Situ Quick XAFS Spectroscopy	The reduction of precursors $PtCl_6^{2-}$ and $PtCl_4^{2-}$ in aqueous ethanol solution stabilized by PVP was quantitatively investigated by QXAFS. The resulting kinetics data were analyzed by the following models: Avrami-Erofe'ev (A-E), FW 2-step mechanism, and Ostwald ripening. Data were further corroborated using TEM and UV-vis.	The data presented by Harada represents direct observation of slow, continuous nucleation and rules out "burst or instantaneous" nucleation. The kinetics are fit to the A-E model and to the FW 2-step mechanism. At extended time after 6000 seconds, the particle growth follows a different path, ascribed to Ostwald ripening.	Of note, the direct technique of QXAFS allows the observation of the initial kinetics phase of the reaction, with the smallest nuclei observed being $Pt(0)_4$, and important part of this valuable study. The direct observation of such very small clusters is evidence against the 1950 model (or any other model or mechanism) that implies the reversible formation of a particle with a $M(0)_n$ of $n >> 4$). Furthermore, the observed kinetics are sigmoidal curves that are not possible under the 1950 model.	76
35	Effect of Surfactant Concentration and	Nickel nanoparticles were formed from the hydrogen reduction of	Based on the synchrotron SAXS data, the Ni nanoparticles are observed to follow a slow nucleation	The Ni nanoparticle formation kinetics data were fit to the FW 2-step mechanism. The	77

	Aggregation on the Growth Kinetics of Nickel Nanoparticles	nickel(II) acetylacetonate hydrate in oleylamine and trioctylphosphine. *In situ* synchrotron SAXS measurements were taken at the Stanford Synchrotron Radiation Light-source. Particles were later characterized *ex situ* by HR-TEM.	followed by an autocatalytic growth process. The kinetics data were fit using the FW 2-step mechanism. The authors propose four phases of Ni nanoparticle growth: (i) reduction of Ni(II) to Ni(0); (ii) autocatalytic growth of Ni nanoparticles; (iii) uneven aggregation on the surface of larger particles; and (iv) settling of large aggregates ("evidenced by a decrease in the total volume of particles"[77]).	kinetics are shown to follow continuous nucleation, which disproves the applicability of the 1950 model to this system.	
36	Colloid chemistry of nanocatalysts: A molecular view	The review is centered on the fabrication and design of nanocatalysts. Sections focus on the synthesis of nanoparticles and mesoporous materials, the preparation of nanocatalysts, and the catalytic behavior.	The review cites hot-injection as the synthetic pathway to produce monodisperse nanoparticles. The 1950 model is stated dogmatically as the "simplest and often most used model for particle nucleation and growth."[78] In addition, the authors discuss other size controlling measures, such as, concentration and identity of stabilizer.	The review has several weaknesses. First, it only cites, uncritically, the 1950 model as a means to obtain monodisperse particles. Second, the review does provide any data supporting the 1950 model; rather the review just claims in words only the 1950 model. Third, all other models and mechanisms for the synthesis of nanocatalysts are omitted. Overall, this review needs greater depth in its understanding of nanoparticle formation models and mechanisms to be deemed very useful mechanistically.	78
37	Implementing atomic force microscopy (AFM) for studying kinetics of gold nanoparticle's growth	Gold nanoparticles were prepared from tetrachloroauric acid and trisodium citrate in water at 70 ºC and 90 ºC. Kinetics data were collected using TEM, DLS, UV-vis, and AFM.	Kinetics data were analyzed using the FW 2-step mechanism. The reported AFM and UV-vis spectroscopic techniques were found to be comparable to each other. They were compared to two well-established size methods, TEM and DLS, to further support the findings. The authors report that their "results support strongly the preliminary conclusion that Turkevich's 'organizer' words-only mechanism is really the F-W 2-step mechanism, and therefore should be replaced by the F-W mechanism."[79]	The authors of this study comment that the first attempt to understand nucleation and growth in solution was done by LaMer. However, they show that the 1950 model "lacked the detailed mechanistic explanation e.g. precise chemical equations with corresponding rate constants for the nucleation and growth steps."[79] They report the FW 2-step mechanism contains the needed precise chemical equations, and they successfully used it to quantitatively fit and physically explain their data.	79
38	Kinetic Factors in the Synthesis of Silver Nanoparticles by Reduction of Ag^+ with Hydrazine in Reverse Micelles of Triton N-42	Within droplets of water, inside reverse micelles of oxyethylated surfactant Triton N-42, silver nitrate is reduced by hydrazine. Micelles were dispersed in decane. Kinetics were measured by UV-vis. Resultant silver nanoparticles were characterized by DLS, TEM, EDX, XRD, UV-vis and FT-IR.	The kinetics data were successfully fit to the FW 2-step mechanism. A complete chemical mechanism was reported for the slow, continuous nucleation and autocatalytic growth of silver nanoparticles. The authors showed that the kinetics were sensitive to temperature, salt effects, and hydrazine (reductant) concentration.	Once again, the quantitative accounting of the data using the FW 2-step mechanism consisting of the nucleation and growth is a quantitative disproof of any applicability of the 1950 model to this transition-metal nanoparticle formation system.	80
39	On the Mechanism of Metal Nanoparticle Synthesis in the	By using Population Balance Modeling (PBM), a mechanism for	Only final product distribution was analyzed by the	The authors claim their proposed mechanism is similar to the 1950 model,	82

	Brust-Schiffrin Method	the formation of thiol-stabilized gold nanoparticles was tested consisting of continuous nucleation, growth, and then capping ligand passivation of the particles.	PBM methods employed. The important part of this work is arguably two-fold: the application of PBM and the finding that a capping step is important to account for the particle-size distribution.	whereas in fact it is completely different. They state "the *continuous* nucleation-growth-capping mechanism unraveled in the present work…suggests that if the conditions in the reaction system are maintained constant, the particle born at different times through continued nucleation will grow to the same size before getting fully capped."[82] This is a drastically different proposed mechanism, which is *actually* similar to the one proposed in the FW 2-step mechanism, and recently supported by Mechanism-Enabled Population Balance Modeling (see ref 81).	
40	Time-Resolved Small-Angle X-ray Scattering Study on the Growth Behavior of Silver Nanoparticles	Silver nanoparticles were prepared from aqueous silver nitrate reduced by sodium borohydride in the presence of 1.5 molar equivalents of the stabilizer, polyvinylpyrrolidone (PVP). The solutions were prepared at 2.0, 4.0, 6.0, and 8.0 mM.	By SEM, the Ag nanoparticles are observed to be spherical. For their kinetics analysis, the authors comment that they "think that such an initial stage is not a pure nucleation process. In fact, it is difficult to divide completely the nucleation and growth stages for almost all preparation processes of nanoparticles."[83] The time-resolved SAXS results produced size versus time data that the authors fit to their diffusion-coalescence model to extract predicted critical radii.	The authors state that "the LaMer model is often used to describe the kinetic process of nanoparticles. Although the diffusion coefficients cannot be determined quantitatively, the 1950 model describes qualitatively the necessary conditions to develop the monodisperse nanoparticles."[83] Experimentally, the authors did not use the 1950 model for their data. Instead, they introduced a new Diffusion-Coalescence (DC) model. Unfortunately, the diffusion coefficient in their differential equation cannot be determined independently. In addition, the assumption is made that the first observable particles are the 'critical nuclei', which we would argue is a result of the limit of detection for the instrument rather than the CNT-predicted putative, critical nucleus. The authors are correct, however, that nucleation and growth are difficult to completely deconvolute.	83
41	A Four-Step Mechanism for the Formation of Supported-Nanoparticle Heterogeneous Catalysts in Contact with Solution: The Conversion of Ir(1,5-COD)Cl/γ-Al_2O_3 to $Ir(0)_{\sim 170}$/γ-Al_2O_3	The precursor Ir(1,5-COD)Cl/□-Al_2O_3 is reduced under H_2 gas to form $Ir(0)_{\sim 170}$/□-Al_2O_3 in organic solvent. Characterization of the resultant nanoparticles was done by TEM. Kinetics were monitored using a catalytic reporter reaction and verified by GLC cyclooctane evolution. Further controls were	The authors examine the FW 4-step mechanism for supported nanoparticle formation. They found the autocatalytic **B** + C → 1.5 C step cannot account for all the data. Instead, an **A** + C → 1.5 C step was found to be applicable for supported transition-metal nanoparticle heterogeneous catalyst formation in contact with solution. This new, Alternative (Alt.) 4-step mechanism "was obtained following the disproof of 18 alternative mechanisms."[84]	A new 4-step mechanism was discovered after rigorous disproof of 18 alternative mechanisms. As stated previously in this Table (S1, ref 61), the quantitative, chemically-precise fitting of kinetics data to the FW 4-step mechanism is direct disproof of the 1950 model with its assumption of burst nucleation.	84

		performed using UV-vis, MacKinetics curve fitting, and COPASI curve fitting.			
42	Nucleation is Second Order: An Apparent Kinetically Effective Nucleus of Two for $Ir(0)_n$ Nanoparticle Formation from $[(1,5\text{-COD})Ir^{I}\bullet P_2W_{15}Nb_3O_{62}]^{8-}$ Plus Hydrogen	The precursor, $[(1,5\text{-COD})Ir^{I}\bullet POM]^{8-}$, is reduced under H_2 to produce $Ir(0)_{\sim 300}$ nanoparticles stabilized by POM^{9-}, where POM^{9-} is $P_2W_{15}Nb_3O_{62}^{9-}$. Kinetics data were collected using a catalytic reporter reaction at several different starting concentrations of $[(1,5\text{-COD})Ir^{I}\bullet POM]^{8-}$, a 30-fold concentration range.	The authors found, experimentally, nucleation to be second-order with respect to the iridium precursor. Overall, the paper provides strong evidence that nucleation is, indeed, under kinetic, not thermodynamic, control for strongly bonded systems. Numerous alternative hypotheses were tested and disproven en route to the final, reported results and conclusions.	The authors report that "the demonstration in 1997 that nucleation is slow and continuous,[48] and not a 'burst' phenomenon as the 1950s LaMer mechanism postulated, is upheld by the present studies and is, in hindsight, a seminal finding in nucleation and growth studies across nature."[85] Furthermore, the authors found that the foundation for the 1950 model, CNT, "is simply not applicable to the present nanocluster formation system."[85] Finally, the concepts of the kinetically effective nucleus (KEN) was introduced to replace the, now outdated, thermodynamic critical nucleus of CNT as well as the concept of a First Observable Cluster (FOC) by the resolution of whatever physical method one is using.	85
43	Mechanisms of Nucleation and Growth of Nanoparticles in Solution	This review claims to cover the available models and mechanisms for the formation of nanoparticles, albeit *without sufficient critical analysis,* in our opinion.	The review covers CNT, the 1950 model, Ostwald ripening, the FW 2-step mechanism, coalescence, orientated attachment, and intraparticle growth.	Unfortunately, this non-critical review looks to have been written by researchers with a primarily synthetic or condensed matter nanophysics background—that is, by non-experts lacking the needed kinetic and especially mechanistic background to write a critical, reliable review in the title area. *Our recommendation is that this review be used and cited only with considerable caution*. Specific criticisms of this review are provided in the SI associated with Whitehead, C. et al. *Chem. Mater.* **2019**, *31*, 2848-2862).	86
44	On the Two-Step Mechanism for Synthesis of Transition-Metal Nanoparticles	The authors use the FW 2-step mechanism as the basis for their Population Balance Model (PBM). In addition, they use data published in Watzky, Finney, and Finke from 2008 to test their PBM.[87]	The authors attempt their PBM using first- and second-order nucleation. However, they show that neither are able to properly model the nucleation behavior observed in the data. Hence, they intentionally shorten the time of nucleation by delaying the onset of nucleation until 75% of the induction period is done. Nucleation is then only allowed to take place over a 30-minute window before it is manually 'shut off.'	The authors state "the LaMer model…explains neither the long induction time nor the rapid sigmoidal decrease in precursor concentration thereafter."[88] This paper demonstrates, again, that the 1950 model does not apply to system that exhibit sigmoidal kinetics. Unfortunately, the authors of this work performed PBM on this well-studied $Ir(0)_n$ nanoparticle system without know the true	88

				nucleation mechanism, what turns out to be a fatal flaw in this otherwise valuable contribution. This work has been corrected in recent Mechanism-Enabled Population Balance Modeling.[81]	
45	Turkevich in New Robes: Key Questions Answered for the Most Common Gold Nanoparticle Synthesis	Gold nanoparticle synthesis by the Turkevich method of citrate reduction of $HAuCl_4$, is examined by addressing five key questions that focus on the growth mechanism, final particle size, synthetic parameters, and the effect of citrate reduction on silver nitrate versus auric acid. Conclusions were developed from analyzing data collected using SAXS, XANES, DLS, UV-vis, SEM, and TEM.	The general growth mechanism that is proposed by the authors, based on the Turkevich synthesis, is the reduction of Au(III), formation of 'seed particles' of Au(0), slow growth on seed particles, and, finally, fast growth on seed particles. The authors state that the proposed seed-mediated growth mechanism is reason for the highly uniform preparation of Au(0) nanoparticles. Temperature, pH, and order of addition have observed to greatly affect the resultant particle size and polydispersity. Finally, it is experimentally determined the citrate reduction of silver nitrate is not analogous to the Turkevich synthesis.	A comprehensive picture of the Turkevich synthesis is provided demonstrating the inapplicability of the 1950 model to gold nanoparticle formation. Recent Mechanism-Enabled Population Balance Modeling[81] offers a more likely explanation for the formation of near-monodisperse particles.	89
46	Fundamental growth principles of colloidal metal nanoparticles - a new perspective	This single-authored perspective focuses on growth mechanisms for Au nanoparticle formation. The perspective emphasizes the application of CNT and the 1950 model, as well as, the previous publications of the author.	A detailed discussion of growth principles for gold nanoparticles is provided for time-resolved SAXS, XANES, and UV-vis experiments. The author claims that "to explain the underlying processes of colloidal formation of [gold nanoparticle] syntheses, the classical nucleation theory with its transformation to NPs by LaMer and co-workers in the 1950s is still seen as the basic model."[90] Finally, while the perspective focuses on growth mechanisms, it is important to note that nucleation is described as a wholly thermodynamic process.	The author appears to blindly support the 1950 model, without questioning any weaknesses and shortcoming of the model. In that sense, they are unaware of or ignore all the papers listed to this point that provide evidence against the 1950 model. Further, it is our belief they are unaware of the original LaMer research, as LaMer and co-workers in the 1950s were *not* working on strongly bonded nanoparticles, but instead of weakly associated sulfur sols. Surprisingly, the author cites their own previous report[89] as support of the 1950 model, yet in that paper, they explicitly state the opposite that the 1950 model *does not apply to their system!* *Overall, we recommend this perspective be read and used only with considerable caution.*	90
47	Rapid continuous microwave-assisted synthesis of silver nanoparticles to achieve very high productivity and full yield: from mechanistic study to optimal fabrication strategy	Silver nanoparticles were prepared from silver nitrate or silver acetate in ethylene glycol using a continuous-flow microwave-assisted polyol-reduction method. Nanoparticles were characterized using DLS, UV-vis, HR-TEM, EDX, and XRD.	Nanoparticle size and size distributions were attributed, in word form only, to the 1950 model. It was observed that reaction temperature and choice of silver precursor (silver nitrate versus silver acetate) had the greatest impact on the final size and size distribution.	The 1950 model is used as an explanation for the size and size distribution results, yet there is no experimental data to support this words-only assertion. The application of the 1950 model is in words only; the authors have not attempted to use any other models or mechanisms, and the authors have not applied any kind of disproof of	91

				alternative hypotheses to their research.	
48	The Kinetic Rate Law for the Autocatalytic Growth of Citrate-Stabilized Silver Nanoparticles	Silver nanoparticles are prepared from the reduction of aqueous silver nitrate by sodium citrate and hydrazine. Citrate is assumed to be the stabilizer, but it is unclear if it also participates as a co-reductant. The formation and growth processes were monitored by UV-Vis. Particles were characterized using XRD and TEM.	The silver nanoparticle formation kinetics data were fit using the FW 2-, 3-, and 4-step mechanisms. The sigmoidal kinetics data are well-fit by all three mechanisms. A complete kinetics derivation is provided in the main text of this paper. Additionally, this paper demonstrates the importance of autocatalytic growth in $Ag(0)_n$ nanoparticle formation.	The use of the three different FW mechanisms demonstrates the inapplicability of the 1950 model to the silver nanoparticle formation, as continuous (not burst) nucleation is observed.	92
49	Formation of gold nanoparticles during the reduction of $HAuBr_4$ in reverse micelles of oxyethylated surfactant: Influence of gold precursor on the growth kinetics and properties of the particles	Tetrabromoauric acid in water was reduced by hydrazine in reverse micelles, of the surfactant Tergitol NP 4, to form gold nanoparticles. Following nucleation and growth of the gold nanoparticles, the particles were phase transferred into a solution of 6-mercaptopurine monohydrate. Kinetics were followed by UV-vis. Characterization was done by TEM, EDX, and FT-IR.	The gold nanoparticle formation, for this system, is observed to follow the FW 2-step mechanism of slow, continuous nucleation followed by fast, autocatalytic surface growth. Changes in the concentration of hydrazine, reaction temperature, and size of initial micelles are all observed to affect the nucleation and growth rate constants. Additionally, the phase transfer, from micelles to DMSO does not change the size or shape of the gold nanoparticles.	Once again, the quantitative accounting of the data using the 2-step mechanism consisting of the continuous nucleation and autocatalytic growth is observed. Hence, the application of the 1950 model to this transition-metal nanoparticle formation system is disproved.	93

50	Synthesis of 1 nm Pd Nanoparticles in a Microfluidic Reactor: Insights from in Situ X-ray Absorption Fine Structure Spectroscopy and Small-Angle X-ray Scattering	A microfluidic reactor is used to investigate the synthesis of palladium nanoparticles from palladium acetate. Two different solvent stabilizer mixtures were used. In a 1:1 toluene:methanol solvent mixture, palladium was reduced at 60 °C with a 1.0 molar equivalent of oleylamine (OLA). In a 1:1 toluene:hexanol solvent mixture, palladium was reduced at 100 °C with a 1.0 molar equivalent of trioctylphosphine (TOP). The reaction was monitored using *in situ* SAXS and XAFS. The nanoparticles were characterized using dark-field STEM.	The synthesis was found to proceed through slow, continuous nucleation as evidenced by a continuous increase in the number of particles, in accordance with the FW 2-step mechanism. Also, growth was observed to be autocatalytic and fast at the early times; then, despite the availability of a large percentage of unreacted precursor, growth slows dramatically and the Pd nanoparticle diameter reaches a plateau while more nanoparticles continue to form—again emphasizing the continuous nature of the nucleation step(s). Notably, the authors "showed [by EXAFS] that an increase in the coordination of Pd with the capping ligands coincided with the change in the growth rate."[94] Furthermore "the combined SAXS and XAFS results strongly suggest the ligands play an important role in affecting the nucleation and growth rates leading to the self-limiting nanoparticle size observed in [this] work."[94]	This is an important contribution on the role in the kinetics of capping ligands. The authors make the insightful t comment that "it is crucial to obtain direct, in situ structural and chemical information on the nucleation, growth, and more importantly, the Pd interaction with the capping ligands to provide insight into the synthesis mechanism and role of the ligands."[94] In this case of Pd nanoparticles, the mechanism is supported by the data and the expanded, ligand-modified FW 2-step mechanism accounts quantitatively for ligand effects on the particle formation process. All the observations reported in this paper are inconsistent with, and hence evidence against, the 1950 model for this Pd/ligand nanoparticle formation system. The authors furthermore note that there are numerous "examples in the literature where the LaMer mechanism was not applicable."[94]	94
51	Formation Mechanism of Gold Nanoparticles Synthesized by Photoreduction in Aqueous Ethanol Solution of Polymers Using In Situ Quick Scanning X-ray Absorption Fine Structure and Small-Angle X-ray Scattering,	Gold nanoparticles were prepared by the photoreduction of $[AuCl_4]^-$ in ethanol with the stabilizer, poly(N-vinyl-2-pyrrolidone) (PVP). Formation kinetics were monitored using *in situ* QXAFS and SAXS.	Sigmoidal kinetics curves are observed for the formation of Au nanoparticles. The kinetics curves were fit with both the A-E model and FW 2-step mechanism. (These two models have already been shown in the literature to be equivalent in many cases for data fitting purposes.[65]) The authors deduce a three-stage gold nanoparticle formation process: (i) initial reduction from Au(III) to Au(I) by alcohol radicals; (ii) slow continuous nucleation and autocatalytic growth; and (iii) aggregative growth and interparticle coalescence. Particle sizes are observed to be ~30 nm. Ostwald ripening was not observed in this study.	Notably, the authors did not try and ascribe the 1950 model to their system, even after discussing how it has been used to describe other gold nanoparticle formation studies. Overall though, the 1950 model was found to be inapplicable to this system as no burst nucleation is observed.	95
52	Synthesis of indium nanoparticles at ambient temperature; simultaneous phase transfer and ripening	Indium trichloride was reduced by lithium borohydride at ambient temperature in a non-polar solvent, where a phase transfer and ripening method was performed. The indium nanoparticles were characterized by TEM, SAXS, DLS, EDS, FT-IR,	Indium nanoparticles were found to be 6.4 ± 0.4 nm and were stable for up to 2 months. Two systems were characterized: (I) *n*-dodecane/oleylamine; and (II) *n*-dodecane/oleylamine-diphenylamine. The authors claim "the key factor for obtaining small diameter, size-monodisperse nanoparticle is due to the formation of the [tri-*n*-butylphosphine]-stabilised In(0) species which	The authors ascribe the 1950 model to their system in words only. They describe the 'burst of nucleation' as the reason for the small-sized indium nanoparticles. However, they provide *no kinetics or other evidence for this claim.* The only measurements they conducted were end-	96

		and NMR.	trigger the burst nucleation and formation of fine nanoparticles."[96]	time characterization of their resulting nanoparticles.	
53	Kinetic studies of nucleation and growth of palladium nanoparticles	Pd(0) nanoparticles are formed by the reduction of Pd(II) chloride in aqueous solutions of ascorbic acid. Varying amounts of chloride was added to influence the rate of the nanoparticle formation. Kinetics were followed by UV-vis spectroscopy.	Kinetics of palladium nanoparticle formation were studied under different experimental conditions such as initial concentration of metal ions, ascorbic acid, chloride ions, as well as at different temperature and ionic strength and fit using the FW 2-step mechanism. The nucleation rate constant as a function of Cl^- ion concentration does not appear to result in a general trend.	The FW 2-Step mechanism was used to fit the Pd(0) nanoparticle formation, sigmoidal absorbance kinetics data. Hence, burst nucleation as in the 1950 model is not observed in this Pd(0) nanoparticle formation system.	97
54	Palladium(0) Nanoparticle Formation, Stabilization, and Mechanistic Studies: $Pd(acac)_2$ as a Preferred Precursor, $[Bu_4N]_2HPO_4$ Stabilizer, plus the Stoichiometry, Kinetics, and Minimal, Four-Step Mechanism of the Palladium Nanoparticle Formation and Subsequent Agglomeration Reactions	Palladium acetylacetonate was reduced by hydrogen in propylene carbonate and stabilized by hydrogen phosphate. Kinetics were monitored using a catalytic reporter reaction and confirmed by GLC. Kinetics were fit using the FW 2- and 4-step mechanisms. Characterization of $Pd(0)_n$ nanoparticles was done by TEM and XRD.	The synthesis of 7.2 ± 1.8 nm Pd(0) nanoparticles were observed. The kinetics data reveal a slow, continuous nucleation process and a subsequent growth process that includes both autocatalytic surface growth and agglomeration. The data collected include verification of the reaction stoichiometry by quantification of the other reaction byproducts, quantified by GLC. The effect of different amounts of stabilizing ligand (HPO_4^{2-}) on the kinetics and apparent mechanism are studied.	The sigmoidal growth curves are well-fit by the FW 2- and 4-step mechanisms. The 1950 model is shown to be inapplicable to this system as it shows continuous nucleation.	98
55	Gaining Control over Radiolytic Synthesis of Uniform Sub-3-nanometer Palladium Nanoparticles: Use of Aromatic Liquids in the Electron Microscope	Palladium nanoparticles are produced from the reduction of palladium acetate by H_2. The reductant, H_2, is produced from the radiolysis of the solvent, toluene. $Pd(0)_n$ nanoparticles are stabilized by a 1:1.5 ratio of Pd:TOP (trioctylphosphine). In situ liquid STEM and in situ SAXS experiments were conducted. Similar ex situ experiments were conducted using hexanol as the reductant.	Resultant $Pd(0)_n$ nanoparticles were observed to be ~2.2 nm in diameter. Continuous, slow nucleation is observed in all experiments. Nucleation is followed by fast, autocatalytic growth of the particles. Particles then slow as they approach their final size, of ~2.2 nm, as the TOP caps the surface sites. Furthermore, this study demonstrates the importance and impact of correlating in situ and ex situ techniques to obtain a full understanding of the formation mechanism.	The authors specifically comment how their observed data differs from the 1950 model. "The linear trend of nucleation of Pd particles over time reported here does not follow the LaMer model for the formation of uniform particles."[99]	99
56	Burst nucleation by hot injection for size-controlled synthesis of ε-cobalt nanoparticles	A series of ε-Co nanoparticles were synthesized from $Co_2(CO)_8$ in dichlorobenzene (DCB) and oleic acid (OA). Particles were characterized by DLS, ICP-OES, XRD, and TEM.	By TEM measurements, Co nanoparticles are observed to be between 4-10 nm, based on experimental parameters. The particles are stabilized by OA and are found to be stable for at least 1 month. The Co:OA ratio and the temperature (of the OA-DCB solution) at the time of injection were the experimental parameters that had the greatest impact on the final size of the Co nanoparticles. No particle-formation kinetics data are reported.	The 1950 model was applied to this study by the authors as their claimed way "to produce monodispersed particles."[100] However, no direct kinetics measurements were taken of the nucleation process, so there is no nucleation kinetics data in support of their claimed mechanism.	100

57	Revitalizing the Frens Method To Synthesize Uniform, Quasi-Spherical Gold Nanoparticles with Deliberately Regulated Sizes from 2 to 330 nm	Gold nanoparticles were prepared from aqueous solutions of tetrachloroauric acid, sodium citrate, and silver nitrate. The particles were studied by DLS, zeta-potential measurements, and TEM.	The authors report near-monodisperse, quasi-spherical gold nanoparticles, where they have controlled the final size between 2 and 330 nm by varying reaction conditions. The authors state that for their model, "the formation of Au^{+}/[sodium acetone dicarboxylate] complex particles at the early stage of citrate reduction of $HAuCl_4$ is essential for the control of the size and shape of the resulting Au [nanoparticles]."[101]	Interestingly, the authors base their study off the original 1951 report by Turkevich[45], which rejects the 1950 model. Yet the authors apply the 1950 model as the mechanism by which the gold nanoparticles form—but provide no experimental evidence in support of this conclusion.	101
58	Quantitative Analysis of Different Formation Modes of Platinum Nanocrystals Controlled by Ligand Chemistry	The formation of Pt nanocrystals is achieved by CO reduction of platinum acetylacetonate, $Pt(acac)_2$, in the presence of oleylamine and oleic acid. Experiments were done using UV-vis, TEM, and MALDI-TOF MS.	The formation of platinum nanoparticles was followed by time-dependent TEM. Based on kinetics analysis, the authors present a new three-step 'mixed mechanism' that included the FW 2-step mechanism plus an additional slow growth step (slow, continuous nucleation, autocatalytic growth, and slow growth). Importantly, the authors identify the importance of the metal–ligand prenucleation complexation and its impact on the kinetics of metal nanoparticles formation.	The sigmoidal shape of nanoparticle formation curve, and its ability to be fit by the FW 2-step mechanism provide a compelling disproof of the 1950 model for this system. Furthermore, the authors note that "corresponding kinetic models were refined to account for the observed nucleation and growth of nanocrystals during chemical reaction and collision of primary nanoparticles, addressing some limitations of the classical 1950 model that was originally developed for the precipitation phenomenon in supersaturated solution. The molecular level understanding on this process however is still limited."[102] Important here is the remark that 'molecular level understanding' is still not readily available in the scientific community.	102
59	Nanoparticle Nucleation is Termolecular in Metal and Involves Hydrogen: Evidence for a Kinetically Effective Nucleus of Three $\{Ir_3H_{2x}•P_2W_{15}Nb_3O_{62}\}^{6-}$ in $Ir(0)_n$ Nanoparticle Formation From $[(1,5\text{-}COD)Ir^{I}•P_2W_{15}Nb_3O_{62}]^{8-}$ Plus Hydrogen	The prototypical iridium nanoparticle system, $(Bu_4N)_5Na_3[(1,5\text{-}COD)Ir^{I}•P_2W_{15}Nb_3O_{62}]$, $\{(COD)Ir^{I}•POM\}^{8-}$, was reduced under H_2. Kinetics studies was collected using a catalytic reporter reaction. Further experiments were done using TEM and ^{31}P NMR.	"The three most reasonable, more intimate mechanisms of nucleation [were] tested: bimolecular nucleation, termolecular nucleation, and a mechanism termed 'alternative termolecular nucleation' in which 2 $(COD)Ir^{+}$ and 1 $(COD)Ir•POM^{8-}$ yield the transition-state of the rate-determining step of nucleation."[103] Based on the experimental kinetics data and computer simulations, the 'alternative termolecular nucleation' with a kinetically effective nucleus (KEN) of 3, Ir_3, is the only reasonable mechanism. Furthermore, a replacement for the thermodynamic critical nucleus of CNT is proposed in the detailed KEN of $\{Ir_3H_{2x}POM\}^{6-}$.	This state-of-the-art study of nucleation established a rare KEN and its molecular composition to the level of $\{Ir_3H_{2x}POM\}^{6-}$. This study disproves both CNT and the 1950 model for the strong-bonding, $Ir(0)_n$ nanoparticle system. This study disproves the applicability of the thermodynamic critical nucleus of CNT for the $Ir(0)_n$ system and notes that the critical nucleus of CNT is a purely theoretical concept of the highest energy species and cannot be observed experimentally.	103
60	Toward a Quantitative Understanding of the Reduction Pathways of a Salt Precursor in the Synthesis of Metal	Tetrabromopalladate(II) and tetrachloropalladate(II) were reduced in aqueous solutions of ascorbic acid and poly(vinylpyrrolidone) (PVP) in the	Two pathways were studied for the reduction of Pd(II): (i) solution reduction or homogeneous nucleation; and (ii) surface reduction or heterogeneous, seed-mediated, nucleation. Under standard preparation procedures, the $PdCl_4^{2-}$ followed a combination of both pathways, hence,	While the 1950 model is cited in this paper as an example of attempts to understand nucleation and growth in the literature, the kinetics are all fit using the FW 2-step mechanism. The effective fitting of the	104

	Nanocrystals	presence of Pd(0) nanocubes. Resulting particles were characterized by TEM. Kinetics were measured by UV-vis.	forming new, small particles, as well as growing on the edges and corners of the existing nanocubes in solution. However, the $PdBr_4^{2-}$ resulted in no new particles and only heterogeneous nucleation. The kinetics from both experiments were fit quantitatively to the FW 2-step mechanism. It was concluded that one could switch between reduction pathways by "manipulating the experimental parameters such as the type of precursor and the reaction temperature, to modulate the reduction kinetics."[104]	experimental kinetics data is disproof of the 1950 model. Further, the observation of slow, continuous solution phase reduction rules out the 1950 model's assumption of burst nucleation.	
61	Synthesis of Au Nanoparticles with Benzoic Acid as Reductant and Surface Stabilizer Promoted Solely by UV Light	Aqueous solution of tetrachloroauric acid and benzoic acid (1:5 ratio) were irradiated with 254 nm light for 200 minutes. Particles were dispersed in toluene solutions of 1-dodecanethiol. Characterization was done with DLS, XPS, NMR, UV-vis, and TEM.	Au nanoparticles are formed from 30 to 350 nm. Modifications in the intensity of light allow for control over the final particle size. Additionally, the concentration of benzoic acid contributes to the size control. Gold reduction occurs as a result of the photoexcitation of the complexation of auric acid and benzoic acid. The gold nanoparticles were dispersed in organic solvent and placed on a TiO_2 support.	The authors claim growth of gold nanoparticles can only follow "two mechanisms for the growth of AuNPs such as the classical LaMer mechanism (formation of Au nuclei followed by their aggregation) and the autocatalytic surface growth mechanism (formation of Au nuclei, catalytic Au^{3+} reduction on the surface, followed by Au deposition)."[105] However, the formation curve of gold nanoparticles is found to be sigmoidal (slow nucleation and autocatalytic growth), indicating the inapplicability of the 1950 model or the model presented by Polte[69].	105
62	Colloidal nanoparticle size control: experimental and kinetic modeling investigation of the ligand–metal binding role in controlling the nucleation and growth kinetics	The reduction of palladium(II) acetate in either pyridine or toluene was studied. Different amounts of the stabilizer trioctylphosphine (TOP) and the co-solvent 1-hexanol were added. Synthesis was carried out at 100 °C. Particles were characterized by dark-field STEM. Kinetics data were collected using *in situ* synchrotron SAXS and fit using the Schultz distribution model for spherical particles.	The results demonstrate the effect of ligands and solvents on the rate of nucleation, rate of growth, and the final particle size. The kinetics data were fit using an expanded FW 2-step mechanism. The first two steps were the same (slow, continuous nucleation and autocatalytic surface growth), but then followed by 2 additional ligand binding steps of an A + L ⇌ A•L equilibrium and a B + L ⇌ B•L equilibrium. The data were fit quantitatively, and the final particle size is demonstrated to depend on the initial growth/nucleation rate ratio.	This study is paradigm-shifting as it is incorporating and expanding upon the current understand of nucleation and growth. The addition of the two equilibrium ligand binding steps (to the precursor and to the nanoparticle) is a huge step for nanoparticle synthesis. Furthermore, it is direct disproof of the 1950 model for the system at hand. The authors even state, that "despite the wide application of the LaMer mechanism in describing nucleation and growth of nanoparticles, there are studies where it fails to capture the kinetics of nanoparticles formation, especially for metal nanoparticles where temporal overlap between nucleation and growth is often observed."[106]	106
63	Tuning Precursor Reactivity	Palladium acetylacetone was reduced	The particle size diameter was collected as a function of	The valuable *in situ* SAXS kinetics data	107

	toward Nanometer-Size Control in Palladium Nanoparticles Studied by in Situ Small Angle X-ray Scattering	to Pd(0) nanoparticles in 1-octadecene. Prior complexation with trioctylphosphine (TOP) is observed and the Pd-TOP complex is thermally decomposed under reaction temperature of 280 °C, where either oleylamine or oleic acid are added as ligands. Kinetics were measured in situ using synchrotron SAXS and characterization was done ex situ with TEM.	time using SAXS. Oleylamine is observed to not affect the prior equilibrium of the Pd-TOP. The final particle size is dependent on the ligand used and the concentration of that ligand (TOP with oleylamine or oleic acid). A detailed picture of the size, size distribution, and concentration of Pd NPs was obtained during the syntheses. Different ligands strongly affect the precursor reactivity. A theoretical model was developed to explain the dependence on both precursor reactivity and ligand.	collected were not fit to any chemical mechanism. Instead, the data wre modelled against a CNT-based classical growth kinetic model. The authors state that "in the presence of large excess of TOP, a classical growth kinetic model does not provide a good fit to the experimental results."[107] Unfortunately, this model does not provide any physical information concerning this Pd-TOP system. The kinetics data and size formation data do not support the 1950 model, yet this study uses the 1950 model as its theoretical basis for particle formation.	
64	Solvent-free synthesis of monodisperse Cu nanoparticles by thermal decomposition of an oleylamine-coordinated Cu oxalate complex	Copper nanoparticles were synthesized by the thermal decomposition, at 200 °C, 220 °C, 240 °C, and 260 °C, of the precursor Cu(II) oxalate complexed with oleylamine (OA-Cu(ox)). Characterization of the starting material and/or the final product was done using XRD, FT-IR, TGA/GC-MS, and UV-vis. TEM was used to collect end particle sizes for particle size-distributions.	TEM micrographs reveal that as the reaction temperature increases (from 200 °C to 260 °C in 20 °C increments) the average particle size changes and the size-distribution narrows. At 200 °C and 260 °C, the average particle size is ~13 nm, while at 220 °C and 240 °C, the average particle size is ~16 nm.	The authors state dogmatically that "based on LaMer's law, a short nucleation period is required to synthesize monodisperse NPs."[108] However, the paper presents no direct evidence of the nucleation and growth processes in the formation of copper nanoparticles, but rather, the authors only present characterization of the copper precursors and final product, copper nanoparticles. No kinetics data are presented in this study.	108
65	Highly Tunable Hollow Gold Nanospheres: Gaining Size Control and Uniform Galvanic Exchange of Sacrificial Cobalt Boride Scaffolds	"Hollow gold nanospheres (HGNs) were synthesized through galvanic exchange (GE) using cobalt-based nanoparticles as sacrificial scaffolds."[109] Co_2B nanoparticles were synthesized from Co^{2+} and $NaBH_4$ in the presence of citrate in water and used as sacrificial scaffolds in the formation of HGNs. Co_2B nanoparticles and HGNs were studied using XPS, UV-vis, DLS, ^{11}B NMR, SEM, HR-TEM, XANES, and cyclic voltammetry.	The formation of Co_2B nanoparticles was studied by UV-vis with respect to time, specifically at 220, 230, and 500 nm, which is representative of Co^{2+} + $B(OH)_4^-$, Co_2B, and Co^{2+}, respectively. Sigmoidal formation and loss curves are observed. $B(OH)_4^-$ is observed to be a crucial component of the growth process of Co_2B. Formation of HGNs was conducted in both aerobic and anaerobic conditions, as "oxygen must be regarded as a reactant in GE as it affects both the structural and optical properties."[109] Size tunability in Co_2B, and the subsequent HGN, is proposed to be controlled by the ratio of $B(OH)_4^-$ and BH_4^-.	The authors state that "in classical nucleation theory as set forth by LaMer in the 1950s, particle diameter is said to be governed by the extent of initial nucleation."[109] We would argue that this is a misrepresentation of LaMer's statement that nucleation is "effectively…instantaneous". Also arguing against this claim is that the particle diameter is dependent on factors such as ligand coverage.[106]	109
66	Chemistry and Structure of Silver Molecular Nanoparticles.	This account of chemical research is on silver molecular nanoparticles (mNPs). In particular, it focuses on the synthesis, structure, and reactivity	The authors summarized their extensive work in the field of Ag mNPs. In particular, they focused on the 'ultrastability' of the Ag_{44} archetype. Despite silver's similar properties to gold, it was demonstrated that even	The authors note their ability to synthesize exceptionally stable Ag_{44} mNPs. They remark that the 1950 model is the "canonical method of preparing a	111

		these authors have researched over the past two decades. Several techniques have been used: ESI-MS, MS-MS, UV-vis, PAGE (polyacrylamide gel electrophoresis), computational efforts, and extensive literature analysis.	under identical conditions (solvent, surface ligand, size, etc.) different properties are exhibited.	nanoparticle product with a narrow size distribution." However, "in the case of the Ag_{44} synthesis, nucleation was not limited or controlled. Instead, nucleation occurred randomly over a significant period during the synthesis." [110,111] In short, these authors note the inapplicability of the 1950 model to their silver nanoparticle system.	
67	Influence of Reduction Kinetics on the Preparation of Well-Defined Cubic Palladium Nanocrystals	Palladium nanocubes were synthesized from K_2PdCl_4 in water with PVP, ascorbic acid, KBr, and specific amounts of acetate (KOAc, NH_4OAc, or HOAc). The reaction took place at 85 °C for 3 hours prior to the nanocubes being characterized by HR-TEM. Ex situ UV-vis measurements were taken throughout the reaction to monitor Pd(II) reduction kinetics.	The type of acetate species and its concentration are observed to impact the final Pd nanocube size and size dispersity. Morphology is observed to be fairly consistent regardless of nanocube size. The growth kinetics of the Pd nanocubes is quantitatively monitored by taking UV-vis measurements of the reaction supernatant throughout the reaction. Growth kinetics are ascribed as the apparent reduction kinetics of the Pd(II). The authors draw a mathematical connection between the first-order rate constant of reduction and the cubic width of the nanocubes.	The authors ascribe CNT and the 1950 model to their growth kinetics, as they claim there is *fast* nucleation and slow growth. They ascribe this as words-only evidence to demonstrate the unsuitability of the FW 2-step mechanism to their system. However, from inspecting their kinetics curves (UV-vis versus time), it appears that with the addition of certain acetate species, agglomeration is taking place in the growth phase. This is not addressed in their kinetics fits. Furthermore, their reaction is taking place at an elevated temperature, which has been shown throughout the literature to increase the rate of nucleation. Hence, it should be investigated whether greater time resolution at early time would result in observation and measurement of the nucleation kinetics. In short, this system merits careful reinvestigation.	112
68	Toward Rationally Designing Surface Structures of Micro- and Nanocrystallites: Role of Supersaturation	The authors report, "in this Account, on the role of supersaturation in controlling the surface structures of micro- and nano-crystallites during crystal growth."[113] "Key experimental factors related to supersaturation are discussed and some detailed cases, including ionic crystals, molecular crystals, noble metals, metal oxides, and MOFs, are then presented."[113]	The authors conclude the role of supersaturation is key to understanding and gaining control over surface structure of nanocrystalline materials. The method in which to maintain high levels of supersaturation is reported to be very system dependent. They report that "although progress has been made in explaining and controlling the growth behaviors of crystals by considering kinetics, it is still particularly complicated to clarify the specific roles of numerous kinetic parameters (including reaction temperature, diffusion, and mass transport) in different reaction conditions."[113]	The discussion, within this account, of the effects of supersaturation on growth kinetics, is thought-provoking and deserves further study and attention. The 1950 model, specifically the LaMer diagram, is used to rationalize the nanoparticle formation process.	113
69	In Situ Time-Resolved XAFS Studies on Laser-Induced Particle Formation	The synthesis of palladium nanoparticles from $PdCl_4^{2-}$ in aqueous ethanol solution by high-fluence laser	Both TEM and DXAFS data demonstrate the increase in laser fluence is directly proportional to particle size and nucleation rate constant. The time-resolved DXAFS data	The authors note that the FW 2-step mechanism is different from the 1950 model and that their data are well-fit l	114

	of Palladium Metal in an Aqueous/EtOH Solution.	irradiation (226 nm) is reported. No photoactivator was used. Kinetics were collected using DXAFS and three methods of XAFS data analysis. Kinetics data were fit using the FW 2-step mechanism. TEM was used to determine final particle size.	were fit successfully using the FW 2-Step mechanism. Palladium nanoparticles size-distributions were observed to be broad across sizes 25-150 nm. Some nanoparticles were observed to be below 10 nm.	using the FW 2-step mechanism. The authors claim, based on literature SAXS evidence, that Ostwald ripening is taking place in their system, but clear, direct evidence for this would seem to be lacking. The authors to have *high-quality kinetics and size data* that indicate some kind of agglomerative growth step in their Pd(0) nanoparticle formation mechanism. A more complete, disproof-based approach to all alternative hypotheses would be needed to determine exactly what mechanism is taking place, but the again high-quality kinetics data in this work merit additional attention.

Table S4 Summary of the literature on oxide-based nanoparticles relating to the 1950 model.

Entry	Title	System	Evidence & Insights	Comments and/or Relevance to the 1950 Model	Ref.
1	Controlled Growth of Monodisperse Silica Spheres in the Micron Size Range	Tetraalkyl esters of silicic acid were studied in saturated alcoholic ammonia solutions (methanol, ethanol, *n*-propanol, or *n*-butanol). TEM images were collected after 120 minutes and particle sizes were analyzed.	The reaction's condensation rate was determined to be strongly correlated to the concentration of water. A lack of ammonia resulted in amorphous particle formation. At standard and high concentrations of ammonia, only spherical particles were observed with 5-8% polydispersity. The rate of particle formation was slowed when longer alkyl alcohols were used. Increased concentrations of alkyl ester and ammonium hydroxide resulted in large particles.	This is a classic, synthetic paper from Stöber and co-workers. Although this paper does not cite the 1950 model (or any particle formation model or mechanism) this seminal work describes a reference point of a very narrow size distribution, still to this day (in 2019) one of the narrower particle size-distributions in the literature.	115
2	Ferric Hydrous Oxide Sols: III. Preparation of Uniform Particles by Hydrolysis of Fe(III)-Chloride, -Nitrate, and -Perchlorate Solutions	Sols were prepared by heating ferric hydrous oxide dispersions in acidic solutions of chloride, nitrate, or perchlorate. SEM, X-ray analysis, and electrophoresis were conducted on the resultant particles.	The effects of several experimental parameters were analyzed. An increase in reaction temperature resulted in increased rate of precipitation. Further, lower temperatures produced rod-like particles, whereas as elevated temperatures produced more irregularly shaped particles. The $FeCl_3$ solutions produced a mixture of β-FeOOH and α-Fe_2O_3, whereas $Fe(NO_3)_3$ and $Fe(ClO_4)_3$ produced primarily α-Fe_2O_3. Variations in anion concentration and solution pH resulted in morphologic changes.	The authors were attempting to determine the growth mechanism of iron-oxide particle formation. However, the authors find that this is "by no means an easy task. In order to succeed it is necessary to have well-defined systems generated in an environment of which the composition is completely understood."[116] Here, the authors have recognized two important points: first, the need to know the complete reaction stoichiometry and, second, the limitations of the system and available techniques.	116
3	Monodisperse colloids of transition metal and lanthanide compounds	The article by J. K. Beattie is a review of well-known colloidal systems: gold, sulfur, silicon dioxide, latex, metal hydroxides, metal oxides, and sulfides.	The 1950 model is described and used to explain how each of these systems displays monodispersity. The chemical control over particles of varying size is claimed to be limited. Furthermore, the author states that "understanding the kinetics and mechanisms of the complex dynamics of particle formation and growth is necessary before particles of particular sizes can readily be prepared."[117]	This review concisely summarizes the previous reports on the aforementioned colloidal systems. It does not, however, describe the reaction kinetics or differential equation / rate law that led to the use of the 1950 model. Further investigation and attempts at disproof of the 1950 and other models are needed to determine the exact formation mechanism for the systems described.	117
4	Colloidal Interactions during the Precipitation of Uniform Submicrometre Particles	SiO_2 and TiO_2 particles were synthesized from tetraethylortho-silica and -titanate in ethanol. Measurements and characterization were performed with ^{29}Si NMR, DLS, TEM, and electrophoresis.	The authors report the final size versus several experimental parameters for SiO_2 and TiO_2 particles. The authors determine that an aggregative growth model is most appropriate to describe the particle formation model. They pointedly reject and disprove the 1950 model as an explanation for the particle uniformity.	The authors state explicitly that "for the systems studied…the nucleation period is a substantial fraction of the total reaction time."[118] "Final particle size can be altered without changing rates of reaction between soluble species. For uniformity to result under conditions where small particles are	118

				continuously produced requires that these particles be lost by some mechanism. Aggregation is shown to provide such a loss route."[118] These authors have systematically disproven the 1950 model for this system and, instead, provide data supportive of a different, in this case aggregative, growth model.	
5	Precipitation of Uniform Particles: The Role of Aggregation	A summary of recent results by the authors is reported. The focus of these results is on the formation of uniform SiO_2 and TiO_2 particles. The formation is described by an aggregative growth model.	It was found that the loss of silicate or titanate concentration was independent of the final size or density of the resulting SiO_2 and TiO_2 particles. The used aggregative growth model reports the loss of titanate to be pseudo-first order. In addition, "the success of the aggregation model in predicting the trends observed in the silica system suggest that…attention should be paid to the colloidal interactions of growing particles."[119]	In addition to what these authors stated in ref. 118 (Entry 4 of this Table S2), they also remark that "a decrease in number density is difficult to rationalize within the 1950 model but is very suggestive of a growth mechanism where aggregation occurs."[119] This is further evidence the 1950 model is not suitable for at least this SiO_2 or TiO_2 system.	119
6	Mechanism of Silica and Titania Colloidal Particle Formation from Metal Alkoxides	Colloidal silica and titania were formed from tetraethoxysilane with ammonia and water in *n*-propanol and titanium isopropoxide with water in *n*-propanol, respectively. Growth was monitored by quenching the reaction at specific points throughout the formation process and directly observing the particles by cryo-TEM.	Increased concentration of water resulted in faster reactions, as determined by the onset of turbidity. It was noted for micrographs taken during the reaction that the observed particles were of different sizes suggesting the particles were at different stages of the growth process. The titania particles are observed to be more morphologically uniform than the silica particles.	The paper proposed that silica and titania particles form by an aggregative growth process. They authors do not cite or mention the 1950 model, but their conclusions support the work of Bogush and Zukoski, summarized above in Entries 4 and 5.[118,119]	120
7	Studies of the Kinetics of the Precipitation of Uniform Silica Particles through the Hydrolysis and Condensation of Silicon Alkoxides	Tetraethylortho-silicate (TEOS) in aqueous ethanol and ammonium hydroxide to produce silica particles. Particle formation was monitored and characterized using TEM, AA, ^{29}Si NMR, volume, and conductivity.	The precipitation reaction kinetics were monitored for the formation of silica particles. The rate of the reaction was monitored against 5 experimental parameters: particle size, silica concentration, TEOS concentration, solution conductivity, and solution volume. Changes in the particle size-distribution suggest that "growth does not occur by a diffusion limited mechanism and is more closely matched by surface reaction limited or aggregative growth mechanisms where the time rate of change in particle radius is independent of particle size." [12	The results "reported in this paper are not consistent with the 1950 model. Instead, these data are consistent with an aggregative growth mechanism…and the observation of aggregation in the growth of a variety of other uniform submicrometer particles."[121,122,123]	121
8	Uniform Silica Particles Precipitation: An Aggregative Growth Model	Silicate particles are prepared from tetraethylortho-silica in aqueous ethanol solutions with ammonia. The authors "take the extreme perspective that particles grow solely by aggregation and see how far this point of view can go in predicting observed trends."[124]	Population balance equations are used to model the aggregation behavior. The proposed aggregation model "provides good estimates of final particle size distribution parameters from silicon alkoxide reaction rates."[124]	The authors note that "this growth mechanism is clearly a limiting case. However, by assuming that particle growth occurs by this mechanism and solving the relevant equations making reasonable estimates of particle interaction potentials, surprisingly good comparisons between predicted and measured final particle size	124

				distributions are found."[124] Additional investigations, not limited to the extreme case the authors investigates, seem highly warranted as a follow-up to this important work and aggregative-growth model.	
9	Formation of colloidal silica particles from alkoxides	Silica colloids were prepared from tetraethoxysilane in aqueous solutions of *n*-propanol with ammonia. Cryo-TEM was used to measure particles in a liquid solution. NMR (^{29}Si) studies were conducted using aqueous ethanol.	The goal of this paper was to reconcile the differing reports on the nucleation and growth mechanisms of silica colloid formation. Unfortunately, due to the nature of cryo-TEM and this system, the authors were unable to definitively reconcile the differences between previous research reports. Instead, based on their cryo-TEM data, they postulate a growth mechanism where "hydrolyzed monomer reacts to form microgel polymers which collapse upon reaching a certain size and cross-link density which makes them insoluble. Collapsed particles densify by condensation and are colloidally stable with respect to each other."[2]	Overall, an aggregative-growth mechanism was supported by the data in this report. As the authors state, such a mechanism is not consistent with the 1950 model's diffusion-controlled growth.	2
10	Monodisperse Colloidal Silica Spheres from Tetraalkoxysilanes: Particle Formation and Growth Mechanism	Silica particles were formed from tetraethoxysilane in aqueous ethanol with ammonia. Experiments were conducted using ^{13}C NMR, ^{29}Si NMR, and cryo-TEM.	The silica formation process proceeds by "an aggregation process of siloxane substructures that is influenced strongly by the surface potential of the silica particles and the ionic strength of the reaction medium."[125] The particle size-distribution was observed to be bimodal. "The overall rate of the particle growth is limited by the first-order hydrolysis rate of the alkoxide."[125]	An aggregative growth mechanism, consistent with the work by Bogush and Zukoski,[118,119,121,124] is supported by the results reported in this paper.	125
11	Preparation and Properties of Uniform Size Colloids	The author note that "the purpose of this review is to describe more recent advances in the field of well-defined colloids, generated by the precipitation from homogeneous solutions"[126] as of 1993. Sections include: metal oxides, metal non-oxides, coated and hollow particles, and mechanisms of uniform particle formation.	The final section of this review highlights the mechanisms of uniform particle formation. The author focuses on the different mechanisms and models that have been proposed in the literature up to 1993, when the review was published. Specifically, he focused on the 1950 model (LaMer & Dinegar 1950) and the aggregative growth model (Bogush & Zukoski 1990).[121,124] The author concludes that the literature evidence is "inadequate" to support the concept of a short-lived burst of nucleation. The author summarizes the advances that have been made on the synthesis and characterization of near-monodisperse particles, but acknowledges that an understanding of the nucleation and growth mechanism have yet to be determined.	This review was one of the early reports that refutes the 1950 model on the basis of experimental observation. The author explicitly states "it has been amply demonstrated that LaMer's approach is applicable in a limited number of cases and often only to the initial stages of the precipitation process."[126] This is consistent with our claim in this Part II review that the 1950 model should be applied *only when quantitative kinetics data demonstrating burst nucleation can be and is obtained*.	126
12	Growth Mechanisms of Iron Oxide Particles of Differing Morphologies from the Forced Hydrolysis of Ferric	Iron oxide particles (β-FeOOH and α-Fe_2O_3) were prepared from solutions of $FeCl_3$ and aqueous HCl. Final samples were monitored by TEM and	The different morphologies are observed based on the concentration of the two starting materials. Three different morphologies are present: spheres, cubes, or double ellipsoids. All three morphologies exhibit β-	Unfortunately, and in the words of the authors, "this study provides no support for a support for a mechanism of simultaneous nucleation and aggregation for particles	127

	Chloride Solutions	cryo-TEM.	FeOOH rods first and then transition into α-Fe_2O_3 as the final particle morphology. Furthermore, "the results of this study indicate that the size and aggregation of the metastable phase influences the morphology of the final particle."[127]	formed by the forced hydrolysis of ferric chloride solutions."[127]	
13	Formation of uniform precipitates from alkoxides	The book chapter focuses on the experimental work done by the authors on the hydrolysis and condensation of alkoxides (Ti and Si) en route to colloid formation. Parallels are then drawn to formation of latex particles and metal-oxide precipitates. Primary methods used were TEM, ^{29}Si NMR, and conductivity.	Through a decade of study, the authors identify the overarching themes in their research. "Precipitation of uniform particles requires two conditions to be met. First, at a point early in the reaction, a constant number of colloidally stable particles must be established. Second, these particles must remain stable to mutual coagulation throughout the subsequent reaction. If the primary particles formed are unstable with respect to larger particles, a short nucleation period is not a prerequisite of a narrow final particle-size distribution. Indeed, continuous slow nucleation with the correct aggregation rate kernels can produce very uniform particles."[128]	In this summary report by Zukoski, Look, and Bogush, they reiterate that a burst of nucleation is not a requirement to establish uniform particles. In contradiction to the 1950 model, they propose their aggregative growth mechanism for the formation of SiO_2 and TiO_2 particles from alkoxide precursors. This is seminal work that merits much closer repetition, expansion, and overall attention.	128
14	And they all look just the same	A short review of the reports[115,119,120,125,126] which disagree the 1950 model.	The authors conclude that "different systems seem to show quite different behavior. There should be a single explanation for why monodisperse particles are formed, but there is evidence against each available model."[3]	This paper demonstrates the important point that each model (including the 1950 model) that has been presented has pieces of evidence against it. Hence, all scientists must be aware of the limitations of the models they are using and proposing, and they must be aware of the systems they are working on. In this summary report, the evidence is strong that the 1950 model is not correct for describing uniform silica and titania particle formation.	3
15	Synthesis of Monodispersed Silica Powders I. Particle Properties and Reaction Kinetics	Silica particles were formed from tetraethylorthosilicate (TEOS) in aqueous ethanol solution with ammonia. Trimethylsilation (using $(CH_3)_3SiCl$) was done as a characterization end-capping method. Other characterization was done using TEM, gas adsorption, density measurements, and light-scattering.	The author studied the silica formation process by varying the following experimental parameters: TEOS concentration, ammonia concentration, water concentration, and reaction temperature. The resulting particle size, shape, and size-distribution were all analyzed as function of the experimental parameters. Reaction kinetics were obtained and revealed that "the particle growth could best be described by a first-order process relative to the TEOS concentration."[129] Finally, the author noted that the growth process changed "at a later stage in the reaction and thereafter particles grew solely by condensation of monomeric and dimeric silicate units at the particle surface."[129] This is contrary to early in the reaction when particles grew by	The author observes an induction period and claims there needs to be a 'build-up' of pre-nucleation species. However, and consistent with other reports,[125] the author conducted a control with silica seeds, where he states "the silicic acid concentration should be already at or above its equilibrium value" and thus, "the condensation reaction or the particle growth reaction should take place. Nonetheless, an induction period was again observed."[129] This control experiment and observations disprove the utility of the 1950 model for this silica formation	129

			aggregation of primary nuclei.	system.	
16	Kinetic study of the formation reaction of colloidal silica spheres by transmitted-light-intensity and dynamic light-scattering measurements.	Colloidal silica was formed from tetraethyl orthosilicate in aqueous ethanol with ammonia. Formation kinetics were monitored by transmitted-light intensities (TLI), specifically at 600 nm. Silica particle diameters were determined by DLS.	Particle size versus time data, obtained by two independent methods, are in agreement. In particular, they agree in the initial stage of the reaction. The condensation (polymerization) starts after an induction time of 0.1 – 500 seconds, depending on the concentrations of ethyl silicate, water and ammonia.	The results presented are supportive of the aggregative growth model previously described in the above entries. The absorbance versus time data are of a sigmoidal shape that include an induction period and autocatalytic growth, results inconsistent with the 1950 model.	130
17	Morphology development and crystal growth in nanocrystalline aggregates under hydrothermal conditions: Insights from titania	Anatase (TiO_2) particles were prepared by the sol gel method. They were analyzed by TEM and XRD. Further characterization on the particles was done using acid digestion, dialysis, and pH measurements. Hydrothermal conditions were 100-250 °C and 15-40 bars.	It was observed that two different coarsening mechanisms—really *models*—take place in the growth of the anatase particles. First, XRD peak broadening shows fast growth occurs along the [001] axis due to high surface energy and reaction adsorption sites. In addition, topotactic attachment along the [112] resulted in elongation of the particle. Furthermore, oriented attachment is suggested to be an important factor in the coarsening of particles.	The authors state that "understanding the fundamental processes of crystal growth and morphology evolution is important in attaining control of material properties."[131] The authors note that they have suggestive evidence for their proposed growth processes, but correctly do not claim they *know* the mechanism of anatase particle formation.	131
18	Solubility-Controlled Synthesis of High-Quality Co_3O_4 Nanocrystals	Cobalt nitrate and sodium dodecyl benzenesulfonate in *n*-octanol were reacted at elevated temperature (90 °C for 6 hours and then 180 °C for the rest of the reaction time) to form Co_3O_4 nanocubes. The product was characterized by XPS, XRD, FT-IR, TGA, and HR-TEM. The reaction kinetics were monitored by UV-vis.	The metathesis reaction produced low polydispersity Co_3O_4 nanoparticles. Particles at 2.0 nm were spherical, whereas the particles at 2.5 and 4.7 nm were cubelike. TEM images are given for the particles and the standard deviations for the sizes is given to be approximately 10%. All products, regardless of size, are found to be pure spinel phase, as determined by XRD.	The authors claim that "the evolution of the absorption curves over time shows the separation of nucleation and growth in the solubility-controlled synthetic process."[132] Further, they claim "the absorption curve evolution from b1 to b2 reflects the nucleation process, and curve b2 could be roughly regarded as the burst-nucleation point."[132] However, curves b1 and b2 occur at 20 minutes and 40 minutes, respectively, another explanation for which is that autocatalytic growth has taken place during this time, as the particle sizes corresponding to these two curves are in the range of 2.0 – 4.7 nm. In summary, the evidence provided is not definitive for what they claim nor for the exact mechanism of their reaction.	132
19	Aggregative Growth of Silicalite-1	The all-silica zeolite, Silicalite-1, was synthesized in this study. It was prepared from tetraethylorthosilicate (TEOS) and tetraporpylammonium hydroxide (TPAOH) in aqueous ethanol. The nucleation and growth of the silica particles was monitored by SAXS, cryo-TEM, and HR-TEM.	Particle size following hydrolysis was observed to be ~4.0 nm. After heating the reaction solution, for 2 hours, from room temperature to 90 °C, secondary, larger particles were observed. These secondary particles are shown, by HR-TEM, to be crystals of silicalite-1. Evidence suggests this growth takes place by oriented attachment.	The evidence provided by the authors supports an oriented aggregative growth mechanism, although alternative possible mechanisms were not ruled out. Hence, the conclusions in this paper need to be taken with caution, and further control and other experiments are needed.	133
20	Hydrothermal Synthesis of	Barium hexaferrite ($BaFe_{12}O_{19}$) was	Experiments run at 280 °C for 5 hours produced	The authors claim the 1950 model is the	134

	Ba-Hexaferrite Nanoparticles	synthesized in a Parr autoclave by combining maghemite, barium hydroxide, sodium hydroxide, and water at 180 - 280 °C for 1-5 hours. The resulting $BaFe_{12}O_{19}$ particles were characterized using XRD, TEM, and Mössbauer spectroscopy.	primarily Ba-hexaferrite with some minor impurities ($BaCO_3$ and $BaFe_4O_7$). The prepared particles have a platelet morphology with a 50 nm diameter and a 5 nm thickness. TEM shows a stacking of the platelets, but that the platelets are non-uniform. The Mössbauer spectrum is well-resolved, but exhibits a smaller magnetic field splitting than expected.	explanation for this $BaFe_{12}O_{19}$ platelet formation. Furthermore, they claim that "by applying the LaMer-Dinger principle and considering the Ostwald ripening process, it is possible to control the morphology of $BaFe_{12}O_{19}$ crystallites during hydrothermal synthesis."[134] Unfortunately, the evidence the authors provide do not support this conclusion. The TEM images shown in Fig 3 (of their paper) are not uniform at all. Furthermore, the authors appear to have run only experiments that support their hypothesis—and example of confirmation bias vs the desired disproof of multiple alternative hypotheses. Additionally, the authors do not appear to have a true grasp of the 1950 model (or are at least a bit sloppy) in light of the incorrect reference to LaMer's paper (co-authors name spelled wrong and an incorrect journal cited in the reference).	
21	Kinetics of Monodisperse Iron Oxide Nanocrystal Formation by "Heating-Up" Process	The formation of iron oxide from iron oleate in 1-octadecene via a "heating-up" (to 320 °C)1 method was reported. The process was monitored in situ using TGA-MS, UV-vis, and SQUID. Ex situ measurements of crystallization yield (ICP) and size-exclusion chromatography (with HPLC) were performed. TEM and electrochemical impedance spectroscopy were used. The resulting iron oxide particles were understood to be a mixture of magnetite and maghemite.	The authors draw a theoretical parallel between the "heating-up" and the "hot-injection" methods. They claim there is a rapid nucleation process followed by a quick narrowing of the size-distribution. They compare their results to the 1950 model. Size of particles, number of particles, crystallization, and impedance were all measured as a function of time. The exact rate of nucleation and rate of growth are not reported.	While the authors claim there is a sudden appearance of particles, effectively making nucleation instantaneous, their TEM data suggests otherwise. In Figure 5, it is observed that at 0 and 1 minutes, there are an increasing number of particles. Furthermore, the particles are of various sizes, whereas at 3 and 6 minutes, their appears to be uniform particles. While we would agree with the authors that there are certainly parallels to be drawn between the "heating-up" method and the "hot-injection" method, the actual evidence in this paper does not support of the 1950 model nor the author's claims of that model. Disproof-based experiments ained at ruling out continuous nucleation and autocatalytic growth are needed, for example.	135
22	Colloidal Chemical Synthesis and Formation Kinetics of Uniformly Sized	In this account, the authors summarize the four different synthetic approaches to uniform particle formation. The	The authors used a variety of techniques to study nanoparticle formation. Primarily, they used *ex situ* TEM, in situ spectroscopies (FT-IR and UV-vis), and	No kinetics data were fit using the 1950 model – merely described in words only. Sigmoidal shape kinetics are reported for	136

	Nanocrystals of Metals, Oxides, and Chalcogenides	approaches they have used are: thermal decomposition, nonhydrolytic sol-gel, thermal reduction, and reactive chalcogen precursor. All four of these have been monitored, reproduced, and explained using the 1950 model.	magnetism (when appropriate). The authors claim their "kinetics studies reveal a three-step mechanism for the synthesis of nanocrystals through the heat-up method with size distribution control. First, as metal precursors thermally decompose, monomers accumulate. At the aging temperature, burst nucleation occurs rapidly; at the end of this second phase, nucleation stops, but continued diffusion-controlled growth leads to size focusing to produce uniform nanocrystals."[136]	the formation of crystals for the iron oxide and zirconia particles synthesized, kinetics suggestive not of the 1950 model, but instead suggestive of a continuous nucleation and autocatalytic growth mechanism. Further investigation and disproof of all alternative hypotheses need to happen before the 1950 model can be definitively assigned or rejected for these systems.	
23	Mechanism of Formation of Uniform-Sized Silica Nanospheres Catalyzed by Basic Amino Acids	Silica nanospheres are prepared from an emulsion of tetraethylorthosilicate (TEOS), water, and basic amino acids. Reaction takes place under basic conditions (pH 9-10). The formation is monitored using FE-SEM, SAXS, and ^{29}Si NMR.	The liquid-state NMR results suggest that hydrolysis of TEOS continues for eight hours, where the silicate species are immediately consumed as part of the growth process. However, the FE-SEM and SAXS results suggests that new particle formation does not take place. The resultant particle size is claimed to be controlled by changes to either the stirring rate or precursor concentration.	The authors note that the two prominent mechanisms in the field of silica formation are the 1950 model and Bogush & Zukoski's continuous nucleation and aggregative growth model. Neither model is explicitly applied to this system. This is because the authors conclude that "although the whole formation mechanism has still been unclear, the growth mechanism can be explained by the diffusion-controlled addition of monomer species on primary particles."[137] Unfortunately, there is no definitive evidence for these conclusions. The authors do note that further studies are needed.	137
24	Hybridized Nanowires and Cubes: A Novel Architecture of a Heterojunctioned $TiO_2/SrTiO_3$ Thin Film for Efficient Water Splitting	A thin-film heterojunctioned $TiO_2/SrTiO_3$ photocatalyst was prepared by hydrothermal precipitation. TiO_2 nanowires were prepared. Then, in an autoclave, with water, NH_4OH, and $Sr(NO_3)_2$, $SrTiO_3$ nanocubes were deposited on the TiO_2 wire. Characterization and experimentation were done using XRD, FE-SEM, FE-TEM, EDX, XPS, and UV-vis.	The authors claim "this paper is the first to report the successful photocatalytic cleavage of water using a hybrid $TiO_2/SrTiO_3$ thin-film."[138] Furthermore, the heterojunctioned thin-film has 2.1 and 4.9 times the efficiency than $SrTiO_3$ and TiO_2 alone, respectively. This is understood as a result of the "negative redox potential shift in the Fermi level."[138]	The authors invoke the 1950 model as the explanation for the formation of $SrTiO_3$ nanocubes. As observed in the FE-SEM, "no discernible discrepancy was noted in terms of the size of the $SrTiO_3$ nanocubes obtained throughout the hydrothermal reactions from 1 to 8 h; thus the reaction mechanism proceeded in good agreement with the 1950 model."[138] Unfortunately, the kinetics data that is required to to support this claim was not provided and remains to be obtained.	138
25	Synthesis of uniform, spherical sub-100 nm silica particles using a conceptual modification of the classic 1950 model	Silica particles (sub-100 nm) are formed from solutions of tetraethylorthosilicate, NH_4OH, and water in ethanol and/or methanol. Characterization was done using SEM and TEM. Further analysis of previous	The authors propose a modification to the 'classic' 1950 model. They propose a quantitative explanation in 3-dimensional space for the synthesis of sub-100 nm silica particles. The third parameter the authors include is the particle number, as a function of time. This model can be viewed in Figure 1b of the text. An important final	The authors make the important observation that while "rigorous quantitative models for burst nucleation have been recently reported,[139,140] these are predicated on key simplifying assumptions that, for the Stöber process, have been	141

		literature SAXS data was conducted.	note the authors make is that the "reaction conditions were adjusted using relatively large changes; thus, the particle properties obtained in our syntheses have not been globally optimized across all parameter space."[141]	demonstrated experimentally to be invalid."[141] The authors have presented their 'modification' to the 1950 model; however, because the authors demonstrate that "the particle number first increases and then decreases during nucleation"[141] our opinion is that the authors data are more in line with the reports of Bogush and Zukoski where aggregation occurs.	
26	Controllable preparation and formation mechanism of monodispersed silica particles with binary sizes	Silica particles are prepared from solutions of tetraethylorthosilicate (TEOS), NH_4OH, and ethanol. Particles were analyzed using FE-SEM, LSA, DLS, and XRD. Three parameters (TEOS feed rate, ammonia:ethanol ratio, and reaction temperature) were adjusted to determine their effect on the final particle size and size-distribution.	At the optimal conditions, a bimodal size-distribution is observed, where large (~375 nm silica particles) are surrounded by small (~50 nm silica particles). By SEM and LSA, the smaller particles are not observed until after 60 minutes. By increasing the ratio of ammonia:ethanol from 0.1 to 0.15, 0.2, or 0.25, a unimodal distribution is observed. The same result is observed when the reaction temperature is increased from 25 °C to either 50 or 60 °C. Intriguingly, doubling the feed rate of TEOS results in a broader distribution of smaller particles. To describe the bimodal size-distribution in the standard conditions, the authors present a modified 1950 model, in which a second nucleation event occurs.	The 1950 model was qualitatively reconsidered as a four-step model to include "prenucleation (I), nucleation (II), second nucleation (III), and growth stages (IV)."[142] This modification, they claim, explains the formation of the bimodal size distribution. But, the second nucleation event is just a convenient rationalization of the results, not disproof-based science. Why would a second nucleation event occur, much less a "2nd burst nucleation" event? The scholarship with the prior literature of the Stöber process is poor in this paper, the majority of the mechanistic work performed by others on the Stöber process not being cited.	142
27	Magnetic Iron Oxide Nanoparticles: Reproducible Tuning of the Size and Nanosized-Dependent Composition, Defects, and Spin Canting	Iron oxide nanoparticles were prepared from solutions of iron stearate, oleic acid, and solvent. Solvents tested were octyl ether, heaxdecene, octadecene, eicosene, docosene, and hexadecanol. Characterization and analysis was performed on the nanoparticles using TGA, TEM, XRD, FT-IR, SQUID, and ^{57}Fe Mössbauer spectroscopy.	Changes to the solvent and the reaction reflux temperature were investigated for their effect on the resultant particle size. It was observed that at least 6 hours was required for particle size to stabilize. The end size was shown to be dependent on the reaction reflux temperature, and subsequently the stability of the iron complex at that temperature. The composition of the iron-oxide nanoparticles shows a combination of maghemite and magnetite that is dependent on the size of the particles. Particles less than 8 nm were observed to be almost all maghemite, whereas larger particles had increasing amounts of magnetite as the core of the particle with an oxidized shell.	The authors state that one goal of the paper was "to explain how some synthesis parameters affect the nucleation and growth step by considering the LaMer model."[143] However, in their conclusions, the authors claim the 1950 model only helps to explain "the evolution of the size as a function of synthesis parameters."[143] Unfortunately, there was no form of data analysis performed in this paper to support such a claim. In addition, no kinetics were collected for the formation of the iron oxide nanoparticles.	143
28	LaMer diagram-type approach to study the nucleation and growth of Cu_2O nanoparticles using supersaturation theory	Copper(I) oxide nanoparticles are prepared by the reduction of copper(II) hydroxide (from copper(II) acetate and sodium hydroxide) by using ascorbic acid or maltodextrine in the presence of PVP stabilizer. UV-vis	UV-vis spectra show ascorbic acid reduces the Cu(II) to Cu(I) faster than maltodextrine. Addition of the reducing agent dropwise, instead of adding it all-at-once, results in larger resultant particles (89 nm compared to 74 nm, all determined by Scherer analysis of the XRD spectra).	Unfortunately, the UV-vis spectra have not been deconvoluted correctly, resulting in unreliable concentration versus time data. Specifically multiple species (at a minimum $Cu(OH)_2$, Cu_2O, and larger aggregates) all look to be contributing to	145

		spectroscopy was used to follow the reduction. Characterization was done by XRD and SEM.		the "Cu_2O" concentration versus time plot. Further, the LaMer diagram they prepared (concentration versus time), Figure 13, show extended periods of nucleation—a time dependence which is in direct contradiction of the 1950 model. **This is yet another of many studies to this point where one feels compelled to note that *reliable science requires disproof of multiple alternative hypotheses!*** [144]	
29	Celebrating *Soft Matter's* 10th Anniversary: Monitoring colloidal growth with holographic microscopy	Polydimethylsiloxane (PDMS) spheres were prepared from mixtures of dimethyldiethoxysilane (DMDES) and methyltriethyoxsilane (MTES) with ammonium hydroxide in water. Polymerization occurred at room temperature "on a rotating frame at 20 rpm for up to three hours."[146] Holographic video microscopy was used to measure the particle size and refractive index. Further characterization was done with SEM.	The colloidal particles were observed by holographic characterization. The authors believe they can expand this type of characterization to additional systems. They claim that the holographic microscopy "offers insights into the mechanisms of growth and aging that cannot be obtained by conventional characterization techniques."[146]	The data do not provide the complete particle size versus time plot–which might be sigmoidal—and, hence, this work is not definitive. Failure to consider not even one other hypothesis [144] than 1950 model is a flaw of this work, as is the glaring neglect of all the prior literature inconsistent with the 1950 model as of this 2015 paper. It speaks to the larger problem of poor scholarship with the prior literature, a problem seen throughout much of the literature citing the 1950 model.	146
30	Enhanced Nanoparticle Size Control by Extending LaMer's Mechanism	The precursor material, iron(III) oleate, was prepared from $Fe(acac)_3$ in oleic acid under nitrogen at 320 °C for ca. 30 minutes. The reaction was quenched, and the, believed-to-be, iron(III) oleate was used directly in the synthesis of magnetite nanoparticles. Here, docosane and oleic acid were mixed under nitrogen at 350 °C before iron(III) oleate in 1-octadecene was injected dropwise at a rate of 3 mL/h. Characterization of nanoparticles was performed using FT-IR, GATR, TEM, SAXS, SAR measurements, XRD, and SQUID.	Iron(III) oleate is assumed to be the precursor forming the monomer, although this is not certain. The reaction forming the magnetite is not known. The IR data are not reliable because of uncertain deconvolution of the CO stretching bands of a questionable intermediate, iron(III) oleate; thus, the interpretation of the early part of the kinetics is speculative. The only reliable data are the particle sizes, but size measurement are missing in the first 30 minutes. The size versus time data starts at 30 minutes, with the smallest particle measured being an already large 9.3 nm at that time—and, hence, way beyond any reasonable initial nucleation phase. It is not 100% clear why earlier samples were not measured, although the measurement of four aliquots at that first 30 min time yields different sizes, suggesting the unreliability of the measurements and perhaps the inability of the SAXS method employed to measure particles formed before 30 min. However, when the particle volume is plotted versus time, a straight line was obtained that did pass through zero, but only if the first four points were taken out. There is no reason/evidence	This paper is an intellectual mess. First, the authors are not using a proper disproof-based scientific method.[144] Second, the key, early (<30 min) part of the process remains unmonitored. Third, the attempt to blend the 1950 model with the FW mechanism (in a words-only form) is literally trying to blend "burst nucleation" with FW "slow, continuous nucleation" and "diffusion –controlled growth" with FW "non-diffusion, chemical reaction controlled, autocatalytic surface growth"—a literally non-sensical, illogical blend. Then there is the use of an empirical power function to fit the data, a function unconnected rigorously to either mechanism, while, fifth, calling the results an "Extending LaMer's Mechanism". *This paper should be discarded.* A do-over study of this system by a proper, disproof-based scientific method would be a	147

			to assume a sudden large deviation from the linearity in the early part (<30 min)—unless one fails to discard their original hypothesis of putative burst nucleation. The size versus time data were fit to a power function, not the 1950 model that the paper's title claims to be "Extending".	welcome addition to the literature.	
31	Formation mechanism of apex-truncated octahedral Cu_2O microcrystal	Cu_2O particles were synthesized from $Cu(OH)_2$ gel, where glucose was used as a reducing agent. The product was collected by centrifugation. $Cu(OH)_2$ gels were prepared from $CuSO_4$ and NaOH. Characterization was performed using XRD, FT-IR, SEM, and TEM. Modifications to the above synthetic procedure were performed to investigate the effect of additives, stabilizers, and different copper sources.	Octahedral Cu_2O microcrystals are formed on the micron-scale. The growth process is understood to a sol-gel growth mode. The sulfate ion (SO_4^{2-}) was determined to be necessary to obtain octahedral morphology. Overall, the authors note the "detailed mechanism is still not revealed."[149]	In the authors investigation of the mechanism, they note "the fact that the nucleation of Cu_2O began at an early stage of the reaction and carried on subsequently is in great contrast to Lamer nucleation-growth model."[149] The authors instead apply a growth model, previously proposed by Sugimoto[148] for a sol-gel system, as the explanation for the 'prolonged' nucleation period. Unfortunately, there are no kinetics data nor any associated differential equation-based rate law to support this hypothesis.	149
32	Experimental and numerical insights into the formation of zirconia nanoparticles: a population balance model for the nonaqueous synthesis	Zirconia nanoparticles were prepared from zirconium *n*-propoxide in 1-propanol and benzyl alcohol. Standard synthesizes took place at 250 °C and constant pressure. The product was collected by centrifugation. Characterization was done by XRD, SAXS, TEM, and light transmittance measurements. Population balance modeling (PBM) was performed with Matlab using the Garlekin *h*-*p*-method.	The kinetics data collected by different techniques show different trends. The zirconium ion concentration determined by the analysis of supernatant solution sample shows a linear decay of the precursor zirconium ion concentration, indicating a zero-order reaction. The light transmission measurements give a sort of sigmoidal shape (with agglomeration) for the zirconium ion concentration with an induction period. The SAXS scattering curves were given for samples withdrawn at four different reaction times.	The kinetics appear to have an induction period followed by agglomerative growth. The authors discuss the FW 2-step mechanism as an explanation for the long induction period, but unfortunately do not attempt to fit their kinetics data with either the FW 2-step or 4-step mechanisms. Instead, the authors attempt to fit their zero-order kinetics data to power functions, rather than mechanism-derived differential equations (or their integrated forms) derived for this interesting system.	150
33	Monodisperse mesoporous silica nanoparticles of distinct topology	The MSNs were prepared by combining the following molar equivalents: 2 TEOS, *x* EtOH, *y* CTAB, 1 NaOH, and 2950 H_2O, where x = 225-275 and y = 0.125-0.2. All MSNs were characterized using powder XRD, TEM, SEM, and N_2 physisorption. [MSNs = mesoporous silica nanoparticles; TEOS = tetraethyl orthosilicate; CTAB = cetyltrimethylammonium bromide]	"In the absence of ethanol only hexagonal mesoporous silica with ellipsoidal and spherical morphology are obtained. The presence of ethanol drives a mesophase transformation from hexagonal to mixed hexagonal /cubic, further to purely cubic, and finally to a mixed cubic/lamellar structure and morphology. This is accompanied by a morphology evolution involving a mixture of ellipses/spheres, regular rods, uniform spheres, and finally a mixture of spheres /flakes."[151] The authors hypothesize "that such structural mesophase transformations are due to ethanol-driven changes of the surfactant packing structure and charge matching at the surfactant/silicate interface."[151]	The authors note the 1950 model as *the model* for metal nanoparticle formation. Whereas, they claim the model for MSNs is more complicated due to additional factors, "such as surfactant concentration, interactions between surfactant and inorganic silicate frameworks, and condensation of ethoxysilanol species in aqueous solution involving pH control."[151] We contend that homogeneous metal nanoparticle formation deals with many of the same issues and is not as 'straightforward' as these authors claim it	151

				to be. Overall, the authors provide only a plot (Fig. 6) of pH versus time as their evidence for a separation of nucleation and growth. A plot that is not definitive evidence of such a claim. Furthermore, it remains unclear whether or not nucleation and growth are actually separated in time for the MSN system.	
34	Monodisperse Iron Oxide Nanoparticles by Thermal Decomposition: Elucidating Particle Formation by Second-Resolved in Situ Small-Angle X-ray Scattering	Iron oxide nanoparticles were prepared from the thermal decomposition of $Fe(CO)_5$ with oleic acid in dioctyl ether. In situ SAXS/WAXS were collected and ex situ TEM measurements were taken.	The authors claim that "the final particle size is directly related to a phase of inorganic cluster formation that takes place between precursor decomposition and particle nucleation."[152] The only kinetics data are the size vs time plots in Figure 8B, which, depending on the run, have widely different first observable clusters. We believe the authors have correctly labeled these curves as 'growth curves' as they do not account for the nucleation at all. The authors present an expanded LaMer-like explanation for the formation of the iron oxide nanoparticles.	The formation of near-monodisperse iron oxide nanospheres is rationalized with a LaMer-type explanation of the separation between claimed burst nucleation and the growth phase, whereas the size of the population is set by the precursor-to-surfactant ratio. Unfortunately, the needed balanced reactions are not given, and the mechanistic claims and assumptions are not backed up by experimental data. The authors present powerful, commendable *in situ SAXS/WAXS* data, but for a system that is *not well-characterized nor easily monitored*.	152
35	Unraveling the Growth Mechanism of Silica Particles in the Stöber Method: In Situ Seeded Growth Model	Silica particles were prepared following the (classic) Stöber process of tetraethylorthosilicate, ethanol, ammonia, and water. The effect of the ammonia concentration and the presence of LiOH were investigated. Characterization was done using TEM, FT-IR, UV-vis, ESI+ MS, and a Brookhaven ZetaPALS apparatus to collect the hydrodynamic diameter and ζ-potential.	The authors present their hypothesis that the silica particle formation process occurs in two steps. The first step "is the incubation stage, where nucleation and growth of silica particle is determined predominantly by TEOS hydrolysis."[153] "The second is the stage of size enlargement of silica particles, at the incubation stage, by adding newly formed silanol monomers atop via condensation."[153] The Stöber process is observed only when $[NH_3] > 0.95$ M. Sizes were obtained between 15-230 nm, which was dependent on the amount of LiOH present in the reaction solution.	In reviewing the literature (in the introduction), the authors claim that "generally, the monomer-addition model can describe the formation of monodisperse silica particles at high ammonia concentration, while the aggregation-only model can explain the formation of polydisperse silica particles at low ammonia concentration."[153] The authors assume the 1950 model as the basis for the monomer-addition model. Ultimately, the authors ascribe mechanisms to their results without using differential equations, kinetics, or any kind of disproof.	153
36	Optimizing the Binding Energy of the Surfactant to Iron Oxide Yields Truly Monodisperse Nanoparticles	Iron oxide nanoparticles were prepared from Fe(III) acetylacetonate in benzyl ether. The reducing agent 1,2-hexadecandiol was used. Oleylamine (OAM) and oleic acid (OAC) were	Metal to surfactant ratio was kept at 1:6. The molar amount of surfactant was kept constant, but the ratio of OAC to OAM was varied from 1:0 to 0:1. The optimal ratio of OAC:OAM was 3:1, which was determined by analyzing the surfactant binding energies. This ratio of surfactant produced the lowest polydispersity and did	The results are rationalized using the 1950 model, but in words only, claiming that "less nuclei with larger sizes are formed and therefore nanoparticles of larger size result."[154] No kinetics data have been provided to support this claim. More	154

		used as surfactants. Reactions were down under N_2 and heated from 110 °C to 180 °C for 2 hours and then to 300 °C for 1 hour. After cooling to room temperature, nanoparticles were precipitated with ethanol. Characterization was done using TEM, HR-TEM, XRD, SAED, TGA, and magnetic hysteresis.	not require further, post-synthesis work-up to narrow the dispersity.	importantly, no other explanation or formation mechanisms have been tested or even considered.	
37	On Grounds of the Memory Effect in Amorphous and Crystalline Apatite: Kinetics of Crystallization and Biological Response.	"Two different CP [(calcium phosphate)] nanopowders were synthesized and compared in this study."[155] The first CP, HAp, $Ca_5(PO_4)_3OH$, was synthesized from $Ca(NO_3)_2$ in water with NH_4OH and $NH_4H_2PO_4$ at 80 °C. After addition of reactants, the solution was left under atmospheric conditions from 24 hours. The other CP, ACP, amorphous calcium phosphate, were synthesized from the same reactants, but the precipitate was collected with 15 seconds of formation instead of being allowed to grow for 24 hours. The precipitate was stored at 4 °C "to prevent spontaneous transformation to HAp."[155] Products were characterized by SEM, TEM, XRD, and biological assays.	The normalized concentration versus time was collected based on the results from XRD analysis. This data yields sigmoidal growth curves, which the authors ascribe to the following "three stages: (i) the induction time period; (ii) the cooperative growth process, which is indicative of the interface-controlled, heterogeneous growth; and (iii) deceleration due to depletion of the concentration of growth units."[155] These data were subsequently fit using Classical Nucleation Theory.	The authors initially claim that "La Mer's classical, diffusional growth was dismissed as a real possibility long ago in favor of the aggregational growth"[155], yet later in their analysis, the authors claim that the "prenucleation species with circa 9 Å in size are expected to form via diffusional growth. This type of growth is fostered by the intensely hydrated and diffusive particle interface that is characteristic of the hydroxylated crystal structure of HAp."[155] Furthermore, the authors use only Classical Nucleation Theory-based equations and explanations for their data with no discussion *and more importantly no testing of any alternative hypotheses*. The induction period seen suggests continuous, not CNT-based burst, nucleation. Additional studies and alternative analyses of this data and system seem warranted.	155
38	Influence of experimental parameters on iron-oxide nanoparticle properties synthesized by thermal decomposition: size and nuclear magnetic resonance studies	Iron(III) acetylacetonate was reduced by 1,2-hexadecanediol in benzylether in the presence of the surfactant oleylamine and/or oleic acid. Iron oxide nanoparticles were prepared by hot injection at 200 °C, 250 °C, and 300 °C. Characterization was performed using ^{1}H NMR, TEM, PCS, ICP-AES, XRD, and TGA.	Under the experimental conditions, it was determined "that the reaction temperature and the surfactant concentration have larger effects than the reaction time" on "the production of monodisperse iron oxide nanoparticles."[156] Syntheses performed at 300 °C yields average sized particles of ~8 nm. The average polydispersity was 25-30%, yet the authors claim narrow size distributions.	The 1950 model is used to rationalize the hot-injection synthesis results, but without supporting evidence and using words only. Furthermore, adaptations have been made to the 1950 model without justification. Badly needed here are *real-time, fast kinetics measurements of the nucleation and growth stages of hot-injection syntheses,* similar to that obtained by the heating up method.[135]	156
39	Synthesis of Fine-Tuning Highly Magnetic $Fe@Fe_xO_y$ Nanoparticles through	Iron nanoparticles were prepared by hot injection under argon at 180 °C. Iron(0) pentacarbonyl in 1-octadecene	Iron nanoparticles were prepared at various sizes by varying the starting amount of $Fe(CO)_5$ with all other parameters remaining constant. Final particle sizes	The 1950 model is used to rationalize the formation of Fe nanoparticles using words only. There is no evidence that definitively	157

	Continuous Injection and a Study of Magnetic Hyperthermia	with hexadecylamine and oleylamine was used. Fe@Fe_xO_y particles were formed by aging samples in air. Characterization was performed using XRD, HAADF-STEM, EDS, SQUID, and DLS.	were 12.6, 15.9, 18.3, and 20.7 nm. Particles at ~12 nm were observed to oxidize entirely to iron oxide, while larger particles retained an Fe core with an Fe_xO_y shell. Particle size-distributions broadened after the average diameter exceeded 20 nm.	supports the 1950 model for this work. No other nanoparticle formation models or mechanisms were considered by the authors, that is the work is not disproof-based.

Table S5 Summary of other, alternative models or mechanisms for nanoparticle formation that cite or impact the 1950 model.

Entry	Title	System	Evidence & Insights	Comments and/or Relevance to the 1950 model	Ref.
1	The kinetics of precipitation from supersaturated solid solutions	The report prepares a mathematical explanation for "the process whereby diffusion effects can cause the precipitation of grains of a second phase in a supersaturated solid solution."[158] No specific, chemical system is assumed or studied.	The precipitation from supersaturated solution is considered to occur in two stages: "In the first, concentration fluctuations produce nuclei of the new phase, which grow directly from the supersaturated medium."[158] In the second stage, coalescence occurs producing larger particles from small ones. The kinetics of the coalescence is modeled by assuming that grains of new phase grow as the results of diffusion process.	The model proposed is for the kinetics of the diffusion-controlled coalescence producing larger grains from the smaller ones.	158
2	Imperfect Oriented Attachment: Dislocation Generation in Defect-Free Nanocrystals	Nanocrystalline TiO_2 (anatase) was prepared by the sol gel method. Dialysis was used to remove impurities. Particles were characterized by XRD and HR-TEM.	The authors present evidence showing how "spiral growth at two or more closely spaced screw dislocations provides a mechanism for generating complex polytypic and polymorphic structures."[159] The authors refer to this attachment at "a small misorientation in the interface" as the mechanism of "imperfect oriented attachment."[159]	The authors state that these "results are of fundamental importance to understanding crystal growth."[159] Furthermore, these dislocations or imperfections on the surface serve as nucleation sites. However, no kinetics data are provided to support a *reaction mechanism*. Hence, the authors have really only presented a *hypothesis* for growth.	159
3	Prediction of absolute crystal-nucleation rate in hard-sphere colloids	This mathematical study reports on simulations of the nucleation "process in a suspension of hard colloidal sphere, to obtain quantitative numerical predictions of the crystal nucleation rate."[160] Numerical and Monte Carlo simulations were performed.	The authors remark that the rate of nucleation is, historical, difficult to quantify. Even in this report, the authors "find large discrepancies between the computed nucleation rates and those deduced from experiments: the best experimental estimates of [probability of a spontaneous fluctuation will occur] seem to be too large by several orders of magnitude."[160]	An important part of this paper is the recognition that simulated and experimentally-determined nucleation rates are several order of magnitude apart—actually never much better than 10±1, and often 10±6-13 or more if one looks into the literature (see the section on Classical Nucleation Theory (CNT) in the main text). This indicates the inapplicability of CNT to systems like this one. Yet this work uses all the assumptions of CNT, including burst nucleation. Nucleation and growth processes are also mixed up throughout the explanations in the paper.	160
4	Formation of Monodispersed Nano- and Micro-Particles Controlled in Size, Shape, and Internal Structure	Primarily, this article serves as a summary report of the mathematical approaches to dealing with mechanisms of nucleation and growth. In particular, it focuses on the components that lead to size, shape, and internal structure control. Example systems used are AgBr,	This article was prepared in "an attempt to give systematic insights into the backgrounds for the formation of monodispersed particles, precisely controlled in size, shape, and internal structure, with some proposal of a condensed monodispersed system named 'gel-sol process'."[161] The nucleation process is assumed to follow the 1950 model of instantaneous nucleation and diffusion-controlled growth.	Again, the author assumes that monodisperse particles result from burst nucleation (an assumption of the 1950 growth model). No experimental evidence is presented to support this assertation.	161

		CdS, Fe_2O_3, and TiO_2.			
5	Kinetics of Oriented Aggregation	The paper presents a model for the mechanism of oriented aggregation and uses TiO_2, primarily, as a model system to demonstrate the application of the model. TEM and XRD data are observed.	The author state that "oriented aggregation is a special case of aggregation that provides an important route by which nanocrystals grow, defects are formed, and unique, often symmetry-defying, crystal morphologies are produced."[162] The model the author has applied "involves a rapid equilibrium for the association and dissociation of nanocrystals and an irreversible conversion of associated nanocrystals for producing oriented aggregates."[162]	The author cites the 1950 model as one of the two possible methods for obtaining monodisperse particles. The 1950 model is cited as an example of fast, instantaneous nucleation, but only *cited* with no direct evidence in support of its use.	162
6	A Mathematical Model for Crystal Growth by Aggregation of Precursor Metastable Nanoparticles	The authors have developed a mathematical model "to describe aggregative crystal growth, including oriented aggregation, from evolving pre-existing primary nanoparticles with composition and structure that are different from that of the final crystalline aggregate."[163] In the model, the authors consider the primary particles to be A, the mature (primary) particles as B, and the crystals to be C.	The authors ran simulations to test their various hypotheses, and then they compared their simulation results to experimental, literature data. The authors test two mechanisms (hypotheses): "(1) attachment of nuclei to nuclei, nuclei to crystals, and crystals to crystals, and (2) addition of partially transformed primary particles to nuclei and crystals."[163] The authors have "shown that the presence of an intermediate stage of primary particle, along with relatively slow higher-order coalescence (between crystals), are necessary ingredients for the formation of multiple peaks in a crystal size distribution."[163] The simulations were shown to be in agreement with the experimental data from SAXS and TEM.	This is an important study and paper that merits closer attention and additional study. The model was established to "describe the kinetic processes that have been proposed to occur during nucleation and crystal growth."[163] This study can account qualitatively for crystal size distributions, a current topic important to the field as more and more attempts to model and account for the particle-size-distributions are being published (i.e., via population balance modeling).	163
7	Formation Mechanisms of Uniform Colloid Particles	The authors present their aggregation mechanism, where primary particles aggregate together to form 'monodispersed' micro-sized particles instead of growth by diffusion. The authors use numerical integration models to test their proposed mechanism against literature data sets (XRD, SEM, and TEM) of Ag, CuO, and $MgNaF_3$.	The authors find that their model works well for the formation of silver particles. Next, they "explain the formation of cubic particles from small precursors" as a two-stage process: "(a) deposition of the building blocks on the surface of the primary particles located in a three-dimensional space, and (b) rearrangement of the particles arriving at the surface at the spot closest to the center of the surface."[165]	The authors acknowledge that the 1950 model was the most accepted model in the field. However, they cite experimental evidence (TEM) of ZnS spheres that disproveds the 1950 model.[164] This 2007 paper is of many papers in the literature to demonstrate quantitatively the inaccuracy of the 1950 model to numerous systems in the literature. Furthermore, the authors have shown "ample evidence [is] now available confirming that a large number, if not the majority, of monodispersed colloids [are] formed by aggregation of nanosized precursors."[165] Overall, the authors present a rebuke of the 1950 model.	165
8	Model of the evolution of nanoparticles to crystals via an aggregative growth mechanism	The authors have prepared a population balance model (a set of ODE, original differential equations) to describe the formation process of numerous crystals, claimed to be formed from the oriented	The authors have prepared a "mathematical model…that describes the evolution of precursor nanoparticles (PN) to crystals. The model treats PN as pseudospecies evolving through an arbitrary number of reversible first-order steps and having the ability to contribute to growth by	This paper is an early, successful use a series of ODEs to analyze the size distributions of particles.	166

		aggregation of precursors.	aggregation with existing crystals after they evolve beyond a certain stage."[166] The model is successful in being able to describe sigmoidal growth curves that have induction periods.		
9	Model of Nanocrystal Formation in Solution by Burst Nucleation and Diffusional Growth	The authors have presented "a model of burst nucleation which assume thermalization of clusters as long as they are below the critical size but diffusional growth of clusters large enough to have grown past the nucleation barrier."[139] The model was not applied to any specific experimental system in this paper.	The authors have applied the 1950 model and CNT (classical nucleation theory) to their analytical expressions. In the paper, the authors present the equations used in their model, equations for particle size-distributions, a scheme for numerical integrations, and a discussion of the limitations "of the model for interpretation of experimental results."[139]	The authors have created their model as a quantitative application of what they call "the qualitative explanation of LaMer…for burst nucleation and growth of nanoparticles in solution."[139] Furthermore, the authors note that numerous experimental results are not suitable for their model, like how they "assume instantaneous availability of all monomers, [while] the gold monomers are released slowly."[139] Unfortunately, the development of the model in this paper exhibits confirmation-bias rather than being disproof-based.	139
10	Mechanisms of Diffusional Nucleation of Nanocrystals and Their Self-Assembly into Uniform Colloids	The author summarizes his research in the field of modeling the growth of nanosized and colloid sized particles. The foundation of all the mathematical models described utilize the 1950 model and its assumptions. Particles are formed by instantaneous (burst) nucleation and growth is diffusion-controlled.	The author presents his "mathematical model of diffusive cluster growth by the capture of monomer 'singlets'."[140] Next, he presents "burst nucleation of nanoparticles in solution."[140] Then, finally, he presents a model for "the secondary process of aggregation of nanoparticles to form colloids and discuss[es] various aspects of the modeling of particle size distributions."[140] In this last model, the author shows that his model matches the average size of CdS colloids on the micron scale. However, the distribution, as a whole, is not well-fit.	Of note, the author states that he "avoided any quantitative or even qualitative modeling of the particle (nanosized and colloid) *shape* selection."[140] "The difficulty in modeling these processes is two-fold. First, they are presently not quantified and are difficult to probe experimentally. Second, their modeling would require extremely large-scale simulations. Thus, while one can venture guesses as to the key processes that balance to determine the particle shape distribution, derivation of quantitative predictions and their comparison with experimental data remain important open challenges in colloid and nanoparticle science."[140] Hence, *no mechanistic understanding* can be gained from this report. Mechanism *requires* the quantitative investigation that is not part of this empirical study.	140
11	Nucleation of Crystals from Solution: Classical and Two-Step Models	The article reviews the studies contributing to the development of what is denoted a two-step model for the nucleation of crystals from solution, where the first step is the formation of sufficient size clusters	The shortcomings of CNT discussed are: (i) "even for condensation of water, CNT predicts nucleation rates 1-2 orders of magnitude higher"[167,172] than experiments; "for condensation of *n*-alcohol vapors, the experimental and theoretical rates were found to differ significantly, with the ratio between two values ranging from about 10^{-10} for	This is a valuable, critical review. The "two-step" model, involving prenucleation cluster formation as the first step, is now gaining strength. It is completely different from the 1950 model and Classical Nucleation Theory, which underlies the	172

		of solute molecules and the second step is the reorganization of such *prenucleation clusters* into an ordered structure. The manuscript gives a comparison of the 1950 model (and Classical Nucleation Theory, CNT) and their two-step model for the nucleation in solution crystallization. The assumptions and shortcomings of CNT are discussed.	methanol to 10^7 for *n*-hexanol."[168,172] (ii) The assumption that the nucleation rate is constant "fails at the very beginning of the nucleation process since a certain time, called the transition time, is required to establish the steady-state distribution of sub-critical clusters."[169,172] (iii) The assumption that "a macroscopic thermodynamic description of a liquid drop can be used to model small clusters containing only a few of tens of molecules…fails for nuclei containing only 20-50 molecules, which are small enough that the center is not in the thermodynamic limit and the interface is sharply curved, changing its free energy."[170,172] (iv) "While CNT allows one to estimate the size of <the so-called> critical nucleus and nucleation rate, it does not provide any information about the structure of aggregates or pathways leading from solution to a solid crystal."[171,172]	1950 model. Unfortunately, there is not enough experimental data to support the proposed "two-step" model involving prenucleation cluster formation. Note here that this "2-step model" involving prenucleation clusters is distinct from the FW 2-step model of slow continuous nucleation and autocatalytic surface growth, steps A —> B, then A + B —> 2B, respectively.)	
12	Controlled synthesis of monodisperse nanocrystals by a two-phase approach without the separation of nucleation and growth processes	The account summarizes the different synthetic approaches that have been taken to obtain monodisperse nanocrystals in the authors' research and in the literature. They present summaries of research reports on burst-type nucleation, extended nucleation and growth periods, and a discussion of known data on CNT's 'critical nucleus'.	The authors state that "although the nucleation and growth processes have been observed in one-phase and two-phase systems through ex-situ and in-situ methods, the structures of critical nuclei and the early nucleation process are still unclear."[173] The authors have proposed two strategies to experimentally narrow the size distributions of nanocrystals. "First is to slow the reaction rate, including nucleation and growth rates."[173] "The second is to increase the surface tension at the solvent-nanocrystals interface, for instance by changing the capping agent or solvent polarity."[173]	The "current difficulties and future challenges in the synthesis and structural characterization" of so-called Critical Nuclei are presented because the authors note "there is little or no experimental data available on the atomic configurations of 'Critical Nuclei'."[173] This of course just shows the confusion surrounding Classical Nucleation Theory and its highest energy—*and thus transient, unobservable*—species, the putative 'Critical Nucleus'. This is one reason why replacement concepts of experimentally determinable "Kinetically Effective Nuclei (KEN)" and the "First Observable Cluster (FOC)" are introduced in the paper in entry 42 of Table 2.[85] The FOC is almost surely what is actually being detected in the few reports where people claim to have observed the 'Critical Nucleus' of CNT.	173
13	Nucleation and Growth of Nanoparticles in the Atmosphere	This review covers the following major topics: "overview of vapor nucleation", "nucleation of nanoparticles in the atmosphere", "growth of nanoparticles in the atmosphere", "numerical treatment of ambient nanoparticle nucleation and growth rates", and a summary	The authors report that "although CNT allows estimation of critical supersaturation reasonably well for systems that CNT was designed for, it fails frequently by many orders of magnitude in reproducing measured nucleation rates for a broader range of substances and experimental conditions. Specifically, the nucleation rates are underestimated at low temperatures and overestimated at high temperatures,[174] and critical supersaturations are	Measurement of nucleation rates and size of nanoparticles in aerosol formation in the atmosphere shows that Classical Nucleation Theory *fails* to explain the results.. As discussed in the main text of the Part I review,[176] the main problem here is not so much with CNT as it is with *researchers* that do not understand CNT and its	177

		with "future research needs."[177] The authors state "this review intends to critically assess recent findings related to nucleation and growth of atmospheric nanoparticles, with an emphasis on the understanding of these processes at a fundamental molecular level."[177]	significantly underestimated for even somewhat more strongly associated vapors, such as organic carboxylic acids.[175] One of the major reasons for the poor quantitative performance of CNT is the assumption that the Critical Nucleus of CNT can be approximated by a spherical droplet with a well-defined, sharp boundary and physical properties that are identical to those in the bulk phase"[177]—the so-called capillary approximation.	assumptions sufficiently so that they (try to) apply it beyond the intended limits of CNT—something that is not the "fault" of CNT!	
14	Use of Dispersive Kinetic Models for Nucleation and Denucleation to Predict Steady-State Nanoparticle Size Distributions and the Role of Ostwald Ripening	The author reports his case for the use of dispersive kinetic models, as CNT has limitations. The author uses dispersive kinetic models, based on power law functions using activation energy distributions to explain how denucleation, nucleation, and Ostwald ripening are involved in the nucleation and growth process.	The author concludes that "one can qualitatively assign the mechanisms of nucleation, denucleation, and/or [Ostwald ripening] to experimentally observed [particle size distributions] based on their different shapes and the time scales over which they operate."[178]	The author presents the limitations of CNT, specifically citing that "CNT predicts only one critical radius size for any given set of experimental conditions", whereas CNT "does not consider that nucleation might be a dispersive kinetic process, i.e., that the nucleation rate can be influenced by the system dynamics and thus give rise to a distribution of activation energies/*t*-dependent activation energy."[178] While the author has explained the inapplicability of CNT, he still utilizes numerous assumptions from CNT and the 1950 model in his various applications of dispersive kinetics to different literature systems.	178
15	A nanoscale-modified LaMer model for particle synthesis from inorganic tin-platinum complexes	Platinum nanoparticles are formed from $PtCl_4$ and $SnCl_2$ or $SnCl_4$ in concentrated aqueous HCl. The reaction was monitored by synchrotron EXAFS, UV-vis-NIR, UV-vis, and SAXS/WAXS. A proposed kinetic model was written.	The authors have applied a modified version of the 1950 model that holds the primary attributes of the original model. However, the authors have recognized that LaMer and coworkers had developed the model starting with "the smallest measurable particles"[179]—approximately 100 nm. Hence, "**LaMer's model examines the kinetics of particle growth after nucleation has completed**."[179] The authors of this study have attempted to reanalyze the derivation in terms of their system, incorporating nanoscale processes and ligand effects. Furthermore, the authors find that "particle size is determined by synthesis condition, particularly the ligand/Pt ratio."[179]	The authors' realization that LaMer's model is a growth model is one of the most important part of this paper. The authors present an interesting attempt at modifying the 1950 model to account for nanoscale size and for ligand effects. However, they fail to provide evidence to support their underlying hypotheses. They state the slowing effect on particle growth due to the presence of surface ligand, but then still use diffusion rate constants. Furthermore, they are still using thermodynamic equations to describe kinetic processes. Commendable in this work are the authors' acquisition of impressive synchrotron data and their above-noted insight that LaMer's model is a growth model. But, we retain our reservations over the data analysis and the lack of in-depth mechanistic study—mechanism-based differential equations and subsequent fitting of kinetics data are	179

				needed.	
16	Kinetics and Mechanisms of Aggregative Nanocrystal Growth	"In this review, [the authors] argue that advantages inherent in aggregative growth will potentially allow the systematic, rational control of nanocrystal size and size distribution to be achieved. In section 2, [they] summarize the conditions necessary to achieve such control, and [they] introduce the concept of a nucleation function. In section 3, [they] review the exciting recent developments in the direct observation of aggregative growth. Section 4 addresses the kinetics of aggregative growth. Section 5 reviews the experimental determination of aggregative nucleation functions, and their role in controlling nanocrystal size and size distributions. [They] hope to convince that mechanism-based synthetic control in nanocrystal synthesis is within reach."[180]	The goal of this review, as stated by the authors, is to advance the awareness and potential of aggregative growth and oriented attachment for mechanistic study. They claim that "nucleation functions in aggregative growth have now been shown to determine nanocrystal sizes and size distributions."[180] They claim to then have true control over nucleation, in aggregative growth, "will provide a firm mechanistic basis for size control in nanocrystal synthesis."[180]	Sigmoidal curves are observed for the nanoparticle formation kinetics, but the data were fit only to the Avrami semi-empirical equation, ruling out the possibility of any resulting mechanistic insight. Consideration of a Gaussian function for the aggregative-nucleation indicates adaptation of the short-fast nucleation concept of Classical Nucleation Theory. Aggregative growth of nanoparticles is, of course, not possible within the 1950 model. However, the significance and broader generality of aggregative growth is an important point emphasized by these author, one well-supported by multiple papers in the tables of this Supporting Information.	180
17	Analysis of reaction kinetics in the photomechanical molecular crystal 9-methylanthracene using an extended Finke-Watzky model	Polycrystalline thin films of 9-methylanthracene (9MA) were prepared under argon to remove any residual oxygen. Kinetics were collected using UV-vis, fluorescence, and ^{1}H NMR. Kinetics were fit using an extended version of the FW 2-step mechanism.	The FW 2-step mechanism has been extended to include the solid-state photochemistry of the excited state precursor and the ground state precursor for both the nucleation and growth steps. The full set of differential equations have been written and used to fit the collected reaction kinetics.	This is important work that (i) demonstrates how the use of minimalistic, disproof-based mechanisms composed of pseudo-elementary steps, such as the FW 2-step mechanism, can be extended naturally and as needed for more complex reactions and systems.	181

REFERENCES

[1] Turkevich, J.; Stevenson, P. C.; Hillier, J. A Study of the Nucleation and Growth Processes in the Synthesis of Colloidal Gold. *Discuss. Faraday Soc.* **1951**, *11*, 55–75.
[2] Bailey, J. K.; and Mecartney, M. L. Formation of colloidal silica particles from alkoxides. *Colloid Surface* **1992**, *63*, 151–161.
[3] Calvert, P. And they all look just the same. *Nature* **1994**, *367*, 119–120.
[4] Ginell, R.; Ginell, A. M.; Spoerri, P. E. Association phenomena. I. The growth of particles of silver chloride and the higher-order tyndall effect. *J. Colloid Sci.* **1947**, *2*, 521–525.
[5] Ottewill, R. H.; Woodbridge, R. F. The preparation of monodisperse silver bromide and silver iodide sols. *J. Colloid Sci.* **1961**, *16*, 581–594.
[6] Insley, M. J.; Parfitt, G. D. Precipitation of Silver Chloride from Homogeneous Solution. Part 1. – Particle Size and Shape Characteristics. *Trans. Faraday Soc.* **1968***, 64,* 1945–1954.
[7] Sugimoto, T. The Theory of the Nucleation of Monodisperse Particles in Open Systems and Its Application to AgBr Systems. *J. Colloid Interface Sci.* **1992**, *150*, 208–225.
[8] Sato, H.; Hirai, T.; Komasawa, I. Mechanism of Formation of Silver Halide Ultrafine Particles in Reverse Micellar Systems. *J. Chem. Eng. Jpn.* **1996**, *29*, 501–507.
[9] Sugimoto, T.; Shiba, F.; Sekiguchi, T.; Itoh, H. Spontaneous nucleation of monodisperse silver halide particles from homogeneous gelatin solution I: silver chloride. *Colloids and Surfaces A: Physicochem. Eng. Aspects* **2000**, *164*, 183–203.
[10] Sugimoto, T.; Shiba, F. Spontaneous nucleation of monodisperse silver halide particles from homogeneous gelatin solution II: silver bromide. *Colloids and Surfaces A: Physicochem. Eng. Aspects* **2000**, *164*, 205–215.
[11] Jeunieau, L.; Debuigne, F.; Nagy, J. B. Synthesis of Inorganic and Organic Nanoparticles in Microemulsions. In *Reactions and Synthesis in Surfactant Systems*; Texter, J., Ed.; Surfactant Science Series, Vol 100; Marcel Dekker, Inc.: New York, 2001; pp 609–631.
[12] Kimijima, K.; Sugimoto, T. Growth Mechanism of AgCl Nanoparticles in a Reverse Micelle System. *J. Phys. Chem. B* **2004**, *108*, 3735–3738.
[13] Shiba, F.; Okawa, Y. Relationship between Supersaturation Ratio and Supply Rate of Solute in the Growth Process of Monodisperse Colloidal Particles and Application to AgBr Systems. *J. Phys. Chem. B* **2005**, *109*, 21664–21668.
[14] Özkar, S.; Finke, R. G. Silver Nanoparticles Synthesized by Microwave Heating: A Kinetic and Mechanistic Re-Analysis and Re-Interpretation. *J. Phys. Chem. C* **2017**, *121*, 27643–27654.
[15] Li, Z.; Okasinski, J. S.; Gosztola, D. J.; Ren, Y.; Sun, Y. Silver chlorobromide nanocubes with significantly improved uniformity: synthesis and assembly into photonic crystals. *J. Mater. Chem. C* **2015**, *3*, 58–65.
[16] Naik, A. N.; Patra, S.; Sen, D.; Goswami, A. Evaluating the mechanism of silver nanoparticles in a polyer membrane under continuous precjursor supply: tuning of ultiple to single nucleation pathway. *Phys. Chem. Chem. Phys.* **2019**, *21*, 4193–4199.
[17] Eshuis, A.; Koning, C. A. J. The mechanism of particle formation during homogeneous precipitation of zinc sulfide. *Colloid Polym. Sci.* **1994**, *272*, 1240–1244.
[18] Libert, S.; Goia, D. V.; Matijević, E. Internally Composite Uniform Colloidal Cadmium Sulfide Spheres. *Langmuir* **2003**, *19*, 10673–10678.
[19] Libert, S.; Gorshkov, V.; Goia, D. V.; Matijević. E.; Privman, V. Model of Controlled Synthesis of Uniform Colloid Particles: Cadmium Sulfide. *Langmuir* **2003**, *19*, 10679–10683.
[20] Qu, L.; Yu, W. W.; Peng, X. In Situ Observation of the Nucleation and Growth of CdSe Nanocrystals. *Nano Lett.* **2004**, *4*, 465–469.
[21] Xie, R.; Li, Z.; Peng, X. Nucleation Kinetics vs Chemical Kinetics in the Initial Formation of Semiconductor Nanocrystals. *J. Am. Chem. Soc.* **2009**, *131*, 15457–15466.

[22] Owen, J. S.; Chan, E. M.; Liu, H.; Alivisatos, A. P. Precursor Conversion Kinetics and the Nucleation of Cadmium Selenide Nanocrystals. *J. Am. Chem. Soc.* **2010**, *132*, 18206–18213.
[23] Kwon, S. G.; Hyeon, T. Formation Mechanisms of Uniform Nanocrystals via Hot-Injection and Heat-Up Methods. *Small* **2011**, *7*, 2685–2702.
[24] Kim, H.–B.; Jang, D.–J. Precursor-dependent shape variation of wurtzite CdSe crystals in a microwave-assisted polyol process. *CrystEngComm* **2012**, *14*, 6946–6951.
[25] Hendricks, M. P.; Cossairt, B. M.; Owen, J. S. The Importance of Nanocrystal Precursor Conversion Kinetics: Mechanism of the Reaction between Cadmium Carboxylate and Cadmium Bis(diphenyldithiophosphinate). *ACS Nano* **2012**, *6*, 10054–10062.
[26] Nakashima, S.; Kikushima, K.; Mukai, K. Infrared emitting property and spherical symmetry of colloidal PbS quantum dots. *J. Cryst. Growth* **2013**, *378*, 537–541.
[27] Liu, H.; Hu, W.; Ye, F.; Ding, Y.; Yang, J. Growth mechanism of Ag_2S nanocrystals in a nonpolar organic solvent. *RSC Adv.* **2013**, *3*, 616–622.
[28] García-Rodríguez, R.; Hendricks, M. P.; Cossairt, B. M.; Liu, H.; Owen, J. S. Conversion Reactions of Cadmium Chalcogenide Nanocrystal Precursors. *Chem. Mater.* **2013**, *25*, 1233–1249.
[29] Li, B.; Zhang, X.; Li, L.; Li, M.; Xu, J.; Hong, Y. White luminescence from CdS nanocrystals under the blue light excitation. *J. Solid State Chem.* **2014**, *214*, 108–111.
[30] Kim, K.–J.; Oleksak, R. P.; Hostetler, E. B.; Peterson, D. A.; Chandran, P.; Schut, D. M.; Paul, B. K.; Herman, G. S.; Chang, C.–H. Continuous Microwave-Assisted Gas–Liquid Segmented Flow Reactor for Controlled Nucleation and Growth of Nanocrystals. *Cryst. Growth Des*. **2014**, *14*, 5349–5355.
[31] Wu, W.–T.; Liu, H.; Dong, C.; Zheng, W.–J.; Han, L.–L.; Li, L.; Qiao, S.–Z.; Yang, J.; Du, X.–W. Gain High-Quality Colloidal Quantum Dots Directly from Natural Minerals. *Langmuir* **2015**, *31*, 2251–2255.
[32] O'Brien, M. N.; Jones, M. R.; Mirkin, C. A. The nature and implications of uniformity in the hierarchical organization of nanomaterials. *P. Natl. Acad. Sci. USA* **2016**, *113*, 11717–11725.
[33] Tamang, S.; Lincheneau, C.; Hermans, Y.; Jeong, S.; Reiss, P. Chemistry of InP Nanocrystal Syntheses. *Chem. Mater*. **2016**, *28*, 2491–2506.
[34] Jansons, A. W.; Hutchison, J. E. Continuous Growth of Metal Oxide Nanocrystals: Enhanced Control of Nanocrystal Size and Radial Dopant Distribution. *ACS Nano* **2016**, *10*, 6942–6951.
[35] Reiss, P.; Carrière, M.; Lincheneau, C.; Vaure, L.; Tamang, S. Synthesis of Semiconductor Nanocrystals, Focusing on Nontoxic and Earth-Abundant Materials. *Chem. Rev*. **2016**, *116*, 10731–10819.
[36] Jing, L.; Kershaw, S. V.; Li, Y.; Huang, X.; Li, Y.; Rogach, A. L.; Gao, M. Aqueous Based Semiconductor Nanocrystals. *Chem. Rev.* **2016**, *116*, 10623–10730.
[37] Cossairt, B. M. Shining Light on Indium Phosphide Quantum Dots: Understanding the Interplay among Precursor Conversion, Nucleation, and Growth. *Chem. Mater*. **2016**, *28*, 7181–7189.
[38] Lu, H.; Brutchey, R. L. Tunable Room-Temperature Synthesis of Coinage Metal Chalcogenide Nanocrystals from *N*-Heterocyclic Carbene Synthons. *Chem. Mater*. **2017**, *29*, 1396−1403.
[39] Saldanha, P. L.; Lesnyak, V.; Manna, L. Large scale syntheses of colloidal nanomaterials. *Nano Today* **2017**, *12*, 46–63.
[40] Li, Y.; Pu, C.; Peng, X. Surface activation of colloidal indium phosphide nanocrystals. *Nano Res.* **2017**, *10*, 941–958.
[41] Lai, R. Pu, C.; Peng, X. On-Surface Reactions in the Growth of High-Quality CdSe

Nanocrystals in Nonpolar Solutions. *J. Am. Chem. Soc.* **2018**, *140*, 9174–9183.
[42] Zhao, X.; Liu, T.; Cui, Y.; Hou, X.; Liu, Z.; Dai, X.; Kong, J.; Shi, W.; Dennis, T. J. S. Antisolvent-assisted controllable growth of fullerene single crystal microwires for organic field effect transistors and photodetectors. *Nanoscale* **2018**, *10*, 8170–8179.
[43] Abécassis, B.; Bouet, C.; Garnero, C.; Constantin, D.; Lequeux, N.; Ithurria, S.; Dubertret, B.; Pauw, B. R.; Pontoni, D. Real-Time in Situ Probing of High-Temperature Quantum Dots Solution Synthesis. *Nano Lett.* **2015**, *15*, 2620–2626.
[44] Faraday, M. The Bakerian Lecture: Experimental Relations of Gold (and Other Metals) to Light. *Philos. Trans. R. Soc. London* **1857**, *147*, 145–181.
[45] Turkevich, J.; Stevenson, P. C.; Hillier, J. The Formation of Colloid Gold. *J. Phys. Chem.* **1953**, *57*, 670–673.
[46] Turkevich, J. Colloidal gold. Part I. *Gold Bull.* **1985**, *18*, 86–91.
[47] Chow, M. K.; Zukoski, C. F. Gold Sol Formation Mechanisms: Role of Colloidal Stability. *J. Colloid Interface Sci.* **1994**, *165*, 97–109.
[48] Watzky, M. A.; Finke, R. G. Transition Metal Nanocluster Formation Kinetic and Mechanistic Studies. A New Mechanism When Hydrogen Is the Reductant: Slow, Continuous Nucleation and Fast Autocatalytic Surface Growth. *J. Am. Chem. Soc.* **1997**, *119*, 10382–10400.
[49] Watzky, M. A.; Finke, R. G. Nanocluster Size-Control and "Magic Number" Investigations. Experimental Tests of the "Living-Metal Polymer" Concept and of Mechanism-Based Size-Control Predictions Leading to the Syntheses of Iridium(0) Nanoclusters Centering about Four Sequential Magic Numbers. *Chem. Mater.* **1997**, *9*, 3083–3095.
[50] Aiken, J. D., III; Finke, R. G. Nanocluster Formation Synthetic, Kinetic, and Mechanistic Studies. The Detection of, and then Methods to Avoid, Hydrogen Mass-Transfer Limitations in the Synthesis of Polyoxoanion- and Tetrabutylammonium-Stabilized, Near-Monodisperse 40 ± 6 Å Rh(0) Nanoclusters. *J. Am. Chem. Soc.* **1998**, *120*, 9545–9554.
[51] Privman, V.; Goia, D. V.; Park, J.; Matijević, E. Mechanism of Formation of Monodispersed Colloids by Aggregation of Nanosize Precursors. *J. Colloid Interface Sci*. **1999**, *213*, 36–45.
[52] Van Hyning, D. L.; Klemperer, W. G.; Zukoski, C. F. Silver Nanoparticle Formation: Predictions and Verification of the Aggregative Growth Model. *Langmuir* **2001**, *17*, 3128–3135.
[53] Widegren, J. A.; Bennett, M. A.; Finke, R. G. Is It Homogeneous or Heterogeneous Catalysis? Identification of Bulk Ruthenium Metal as the True Catalyst in Benzene Hydrogenations Starting with the Monometallic Precursor, Ru(II)(η^6-C_6Me_6)$(OAc)_2$, Plus Kinetic Characterization of the Heterogeneous Nucleation, Then Autocatalytic Surface-Growth Mechanism of Metal Film Formation. *J. Am. Chem. Soc.* **2003**, *125*, 10301–10310.
[54] Wang, J.; Boelens, H. F. M.; Thathagar, M. B.; Rothenberg, G. In Situ Spectroscopic Analysis of Nanocluster Formation. *ChemPhysChem* **2004**, *5*, 93–98.
[55] Hornstein, B. J.; Finke, R. G. Transition-Metal Nanocluster Kinetic and Mechanistic Studies Emphasizing Nanocluster Agglomeration: Demonstration of a Kinetic Method That Allows Monitoring of All Three Phases of Nanocluster Formation and Aging. *Chem. Mater.* **2004**, *16*, 139–150. (Please also the correction: *Chem. Mater.* **2004**, *16*, 3972.)
[56] Besson, C.; Finney, E. E.; Finke, R. G. A Mechanism for Transition-Metal Nanoparticle Self-Assembly. *J. Am. Chem. Soc.* **2005**, *127*, 8179–8184.
[57] Besson, C.; Finney, E. E.; Finke, R. G. Nanocluster Nucleation, Growth, and Then Agglomeration Kinetic and Mechanistic Studies: A More General, Four-Step Mechanism Involving Double Autocatalysis. *Chem. Mater.* **2005**, *17*, 4925–4938.

[58] Pong, B.–K.; Elim, H. I.; Chong, J.–X.; Ji, W.; Trout, B. L.; Lee, J.–Y. New Insights on the Nanoparticle Growth Mechanism in the Citrate Reduction of Gold(III) Salt: Formation of the Au Nanowire Intermediate and Its Nonlinear Optical Properties. *J. Phys. Chem. C* **2007**, *111*, 6281–6287.
[59] Ji, X.; Song, X.; Li, J.; Bai, Y.; Yang, W.; Peng, X. Size Control of Gold Nanocrystals in Citrate Reduction: The Third Role of Citrate. *J. Am. Chem. Soc.* **2007**, *129*, 13939–13948.
[60] Ott, L. S.; Finke, R. G. Transition-Metal Nanocluster Stabilization versus Agglomeration Fundamental Studies: Measurement of the Two Types of Rate Constants for Agglomeration Plus Their Activation Parameters under Catalytic Conditions. *Chem. Mater.* **2008**, *20*, 2592–2601.
[61] Finney, E. E.; Finke, R. G. The Four-Step, Double-Autocatalytic Mechanism for Transition-Metal Nanocluster Nucleation, Growth, and Then Agglomeration: Metal, Ligand, Concentration, Temperature, and Solvent Dependency Studies. *Chem. Mater.* **2008**, *20*, 1956–1970.
[62] Morris, A. M.; Watzky, M. A.; Agar, J. N.; Finke, R. G. Fitting Neurological Protein Aggregation Kinetic Data via a 2-Step, Minimal/"Ockham's Razor" Model: The Finke−Watzky Mechanism of Nucleation Followed by Autocatalytic Surface Growth. *Biochemistry* **2008**, *47*, 2413–2427.
[63] Watzky, M. A.; Morris, A. M.; Ross, E. D.; Finke, R. G. Fitting Yeast and Mammalian Prion Aggregation Kinetic Data with the Finke−Watzky Two-Step Model of Nucleation and Autocatalytic Growth. *Biochemistry* **2008**, *47*, 10790–10800.
[64] Finney, E. E.; Finke, R. G. Nanocluster nucleation and growth kinetic and mechanistic studies: A review emphasizing transition-metal Nanoclusters. *J. Colloid Interface Sci.* **2008**, *317*, 351−374.
[65] Finney, E. E.; Finke, R. G. Is There a Minimal Chemical Mechanism Underlying Classical Avrami-Erofe'ev Treatments of Phase-Transformation Kinetic Data? *Chem. Mater.* **2009**, *21*, 4692–4705.
[66] Harada, M.; Inada, Y. In Situ Time-Resolved XAFS Studies of Metal Particle Formation by Photoreduction in Polymer Solutions. *Langmuir* **2009**, *25*, 6049–6061.
[67] Mondloch, J. E.; Yan, X.; Finke, R. G. Monitoring Supported-Nanocluster Heterogeneous Catalyst Formation: Product and Kinetic Evidence for a 2-Step, Nucleation and Autocatalytic Growth Mechanism of $Pt(0)_n$ Formation from H_2PtCl_6 on Al_2O_3 or TiO_2. *J. Am. Chem. Soc.* **2009**, *131*, 6389–6396.
[68] Mondloch, J. E.; Wang, Q.; Frenkel, A. I.; Finke, R. G. Development Plus Kinetic and Mechanistic Studies of a Prototype Supported-Nanoparticle Heterogeneous Catalyst Formation System in Contact with Solution: Ir(1,5-COD)Cl/γ-Al_2O_3 and Its Reduction by H_2 to $Ir(0)_n$/γ-Al_2O_3. *J. Am. Chem. Soc.* **2010**, *132*, 9701–9714.
[69] Polte, J.; Ahner, T. T.; Delissen, F.; Sokolov, S.; Emmerling, F.; Thünemann, A. F.; Kraehnert, R. Mechanism of Gold Nanoparticle Formation in the Classical Citrate Synthesis Method Derived from Coupled In Situ XANES and SAXS Evaluation. *J. Am. Chem. Soc.* **2010**, *132*, 1296–1301.
[70] Polte, J.; Herder, M.; Erler, R.; Rolf, S.; Fischer, A.; Würth, C.; Thünemann, A. F.; Kraehnert, R.; Emmerling, F. Mechanistic insights into seeded growth processes of gold nanoparticles. *Nanoscale* **2010**, *2*, 2463–2469.
[71] Polte, J.; Erler, R.; Thünemann, A. F.; Sokolov, S.; Ahner, T. T.; Rademann, K.; Emmerling, F.; Kraehnert, R. Nucleation and Growth of Gold Nanoparticles Studied *via in situ* Small Angle X-ray Scattering at Millisecond Time Resolution. *ACS Nano* **2010**, *4*, 1076–1082.
[72] Richards, V. N.; Rath, N. P.; Buhro, W. E. Pathway from a Molecular Precursor to Silver

Nanoparticles: The Prominent Role of Aggregative Growth. *Chem. Mater.* **2010**, *22*, 3556–3567.
[73] Yao, T.; Sun, Z.; Li, Y.; Pan, Z.; Wei, H.; Xie, Y.; Nomura, M.; Niwa, Y.; Yan, W.; Wu, Z.; Jiang, Y.; Liu, Q.; Wei, S. Insights into Initial Kinetic Nucleation of Gold Nanocrystals. *J. Am. Chem. Soc.* **2010**, *132*, 7696–770158.
[74] Richards, V. N.; Shields, S. P.; Buhro, W. E. Nucleation Control in the Aggregative Growth of Bismuth Nanocrystals. *Chem. Mater.* **2011**, *23*, 137–144.
[75] Mondloch, J. E.; Bayram, E.; Finke, R. G. A review of the kinetics and mechanisms of formation of supported-nanoparticle heterogeneous catalysts. *J. Mol. Catal. A.* **2012**, *355*, 1–38.
[76] Harada, M.; Kamigaito, Y. Nucleation and Aggregative Growth Process of Platinum Nanoparticles Studied by in Situ Quick XAFS Spectroscopy. *Langmuir* **2012**, *28*, 2415–2428.
[77] LaGrow, A. P.; Ingham, B.; Toney, M. F.; Tilley, R. D. Effect of Surfactant Concentration and Aggregation on the Growth Kinetics of Nickel Nanoparticles. *J. Phys. Chem. C* **2013**, *117*, 16709–16718.
[78] An, K.; Alayoglu, S.; Ewers, T.; Somorjai, G. A. Colloid chemistry of nanocatalysts: A Molecular View. *J. Colloid Interface Sci.* **2012**, *373*, 1–13.
[79] Georgiev, P.; Bojinova, A.; Kostova, B.; Momekova, D.; Bjornholm, T.; Balashev, K. Implementing atomic force microscopy (AFM) for studying kinetics of gold nanoparticle's growth. *Colloids and Surfaces A: Physiochem. Eng. Aspects* **2013**, *434*, 154–163.
[80] Tatarchuk, V. V.; Sergievskaya, A. P.; Korda, T. M.; Druzhinina, I. A.; Zaikovsky, V. I. Kinetic Factors in the Synthesis of Silver Nanoparticles by Reduction of Ag^+ with Hydrazine in Reverse Micelles of Triton N–42. *Chem. Mater.* **2013**, *25*, 3570–3579.
[81] Handwerk, D. R.; Shipman, P. D.; Whitehead, C. B.; Özkar, S.; Finke, R. G. Mechanism-Enabled Population Balance Modeling of Particle Formation en Route to Particle Average Size and Size Distribution Understanding and Control. *J. Am. Chem. Soc.* **2019**, *141*, 15827–15839.
[82] Perala, S. R. K.; Kumar, S. On the Mechanism of Metal Nanoparticle Synthesis in the Brust−Schiffrin Method. *Langmuir* **2013**, *29*, 9863–9873.
[83] Yan, S.; Wu, Z.; Yu, H.; Gong, Y.; Tan, Y.; Du, R.; Chen, W.; Xing, X.; Mo, G.; Chen, Z.; Cai, Q.; Sun, D. Time-Resolved Small-Angle X-ray Scattering Study on the Growth Behavior of Silver Nanoparticles. *J. Phys. Chem. C* **2014**, *118*, 11454–11463.
[84] Kent, P. D.; Mondloch, J. E.; Finke, R. G. A Four-Step Mechanism for the Formation of Supported-Nanoparticle Heterogeneous Catalysts in Contact with Solution: The Conversion of Ir(1,5-COD)Cl/γ-Al_2O_3 to $Ir(0)_{\sim 170}$/γ-Al_2O_3. *J. Am. Chem. Soc.* **2014**, *136*, 1930–1941.
[85] Laxson, W. W.; Finke, R. G. Nucleation is Second Order: An Apparent Kinetically Effective Nucleus of Two for $Ir(0)_n$ Nanoparticle Formation from [(1,5-COD)Ir^{I}•$P_2W_{15}Nb_3O_{62}$]$^{8-}$ Plus Hydrogen. *J. Am. Chem. Soc.* **2014**, *136*, 17601–17615.
[86] Thanh, N. T. K.; Maclean, N.; Mahiddine, S. Mechanisms of Nucleation and Growth of Nanoparticles in Solution. *Chem. Rev.* **2014**, *114*, 7610−7630.
[87] Watzky, M. A.; Finney, E. E.; Finke, R. G. Transition-Metal Nanocluster Size vs Formation Time and the Catalytically Effective Nucleus Number: A Mechanism-Based Treatment. *J. Am. Chem. Soc.* **2008**, *130*, 11959–11969.
[88] Perala, S. R. K.; Kumar, S. On the Two-Step Mechanism for Synthesis of Transition-Metal Nanoparticles. *Langmuir* **2014**, *30*, 12703–12711.
[89] Wuithschick, M.; Birnbaum, A.; Witte, S.; Sztucki, M.; Vainio, U.; Pinna, N.; Rademann, K.; Emmerling, F.; Kraehnert, R.; Polte, J. Turkevich in New Robes: Key Questions Answered for the Most Common Gold Nanoparticle Synthesis. *ACS Nano* **2015**, *9*, 7052–7071.

[90] Polte, J. Fundamental growth principles of colloidal metal nanoparticles – a new perspective. *CrystEngComm* **2015**, *17*, 6809–6830.
[91] Dzido, G.; Markowski, P.; Malachowska-Jutsz, A.; Prusik, K.; Jarzębski, A. B. Rapid continuous microwave-assisted synthesis of silver nanoparticles to achieve very high productivity and full yield: from mechanistic study to optimal fabrication strategy. *J. Nanopart. Res.* **2015**, *17*, 1–15.
[92] Kytsya, A.; Bazylyak, L.; Hrynda, Y.; Horechyy, A.; Medvedevdkikh, Y. The Kinetic Rate Law for the Autocatalytic Growth of Citrate-Stabilized Silver Nanoparticles. *Int. J. Chemical Kinetics* **2015**, *47*, 351–360.
[93] Sergievskaya, A. P.; Tatarchuk, V. V.; Makotchenko, E. V.; Mironov, I. V. Formation of gold nanoparticles during the reduction of $HAuBr_4$ in reverse micelles of oxyethylated surfactant: Influence of gold precursor on the growth kinetics and properties of the particles. *J. Mater. Res.* **2015**, *30*, 1925–1933.
[94] Karim, A. M.; Al Hasan, N.; Ivanov, S.; Siefert, S.; Kelly, R. T.; Hallfors, N. G.; Benavidez, A.; Kovarik, L.; Jenkins, A.; Winans, R. E.; Datye, A. K. Synthesis of 1 nm Pd Nanoparticles in a Microfluidic Reactor: Insights from in Situ X-ray Absorption Fine Structure Spectroscopy and Small-Angle X-ray Scattering. *J. Phys. Chem. C* **2015**, *119*, 13257−13267.
[95] Harada, M.; Kizaki, S. Formation Mechanism of Gold Nanoparticles Synthesized by Photoreduction in Aqueous Ethanol Solution of Polymers Using In Situ Quick Scanning X-ray Absorption Fine Structure and Small-Angle X-ray Scattering. *Cryst. Growth Des.* **2016**, *16*, 1200–1212.
[96] Meshgi, M. A.; Kriechbaum, M.; Biswas, S.; Holmes, J. D.; Marschner, C. Synthesis of indium nanoparticles at ambient temperature; simultaneous phase transfer and ripening. *J. Nanopart. Res.* **2016**, *18*, 363–372.
[97] Wojnicki, M.; Fitzner, K.; Luty-Błocho, M. Kinetic studies of nucleation and growth of palladium nanoparticles. *J. Colloid Interface Sci.* **2016**, *465*, 190–199.
[98] Özkar, S.; Finke, R. G. Palladium(0) Nanoparticle Formation, Stabilization, and Mechanistic Studies: $Pd(acac)_2$ as a Preferred Precursor, $[Bu_4N]_2HPO_4$ Stabilizer, plus the Stoichiometry, Kinetics, and Minimal, Four-Step Mechanism of the Palladium Nanoparticle Formation and Subsequent Agglomeration Reactions. *Langmuir* **2016**, *32*, 3699–3716.
[99] Abellan, P.; Parent, L. R.; Al Hasan, N.; Park, C.; Arslan, I.; Karim, A. M.; Evans, J. E.; Browning, N. D. Gaining Control over Radiolytic Synthesis of Uniform Sub-3-nanometer Palladium Nanoparticles: Use of Aromatic Liquids in the Electron Microscope. *Langmuir* **2016**, *32*, 1468−1477.
[100] Zacharaki, E.; Kalyva, M.; Fjellvåg, H.; Sjåstad, A. O. Burst nucleation by hot injection for size controlled synthesis of ε-cobalt nanoparticles. *Chem. Cent. J.* **2016**, *10*, 10.
[101] Xia, H.; Xiahou, Y.; Zhang, P.; Ding, W.; Wang, D. Revitalizing the Frens Method To Synthesize Uniform, Quasi-Spherical Gold Nanoparticles with Deliberately Regulated Sizes from 2 to 330 nm. *Langmuir* **2016**, *32*, 5870−5880.
[102] Yin, X.; Shi, M.; Wu, J.; Pan, Y.–T.; Gray, D. L.; Bertke, J. A.; Yang, H. Quantitative Analysis of Different Formation Modes of Platinum Nanocrystals Controlled by Ligand Chemistry. *Nano Lett*. **2017**, *17*, 6146–6150.
[103] Özkar, S.; Finke, R. G. Nanoparticle Nucleation is Termolecular in Metal and Involves Hydrogen: Evidence for a Kinetically Effective Nucleus of Three, $\{Ir_3H_{2x}•P_2W_{15}Nb_3O_{62}\}^{6-}$ in $Ir(0)_n$ Nanopaticle Formation From $[(1,5\text{-COD})Ir^{I}•P_2W_{15}Nb_3O_{62}]^{8-}$ Plus Dihydrogen. *J. Am. Chem. Soc.* **2017**, *139*, 5444–5457.
[104] Yang, T.–H.; Peng, H.–C.; Zhou, S.; Lee, C.–T.; Bao, S.; Lee, Y.–H.; Wu, J.–M.; Xia, Y. Toward a Quantitative Understanding of the Reduction Pathways of a Salt Precursor in the

Synthesis of Metal Nanocrystals. *Nano Lett.* **2017**, *17*, 334–340.
[105] Shiraishi, Y.; Tanaka, H.; Sakamoto, H.; Hayashi, N.; Kofuji, Y.; Ichikawa, S.; Hirai, T. Synthesis of Au Nanoparticles with Benzoic Acid as Reductant and Surface Stabilizer Promoted Solely by UV Light. *Langmuir* **2017**, *33*, 13797–13804.
[106] Mozaffari, S.; Li, W.; Thompson, C.; Ivanov, S.; Seifert, S.; Lee, B.; Kovarik, L.; Karim, A. M. Colloidal nanoparticle size control: experimental and kinetic modeling investigation of the ligand–metal binding role in controlling the nucleation and growth kinetics. *Nanoscale* **2017**, *9*, 13772–13785.
[107] Wu, L.; Lian, H.; Willis, J. J.; Goodman, E. D.; McKay, I. S.; Qin, J.; Tassone, C. J.; Cargnello, M. Tuning Precursor Reactivity toward Nanometer-Size Control in Palladium Nanoparticles Studied by in Situ Small Angle X-ray Scattering. *Chem. Mater.* **2018**, *30*, 1127–1135.
[108] Togashi, T.; Nakayama, M.; Hashimoto, A.; Ishizaki, M.; Kanaizuka, K.; Kurihara, M. Solvent-free synthesis of monodisperse Cu nanoparticles by thermal decomposition of an oleylamine-coordinated Cu oxalate complex. *Dalton Trans.* **2018**, *47*, 5342–5347.
[109] Lindley, S. A.; Cooper, J. K.; Rojas-Andrade, M. D.; Fung, V.; Leahy, C. J.; Chen, S.; Zhang, J. Z. Highly Tunable Hollow Gold Nanospheres: Gaining Size Control and Uniform Galvanic Exchange of Sacrificial Cobalt Boride Scaffolds. *ACS Appl. Mater. Interfaces* **2018**, *10*, 12992−13001.
[110] Desireddy, A.; Conn, B. E.; Guo, J.; Yoon, B.; Barnett, R. N.; Monahan, B. M.; Kirschbaum, K.; Griffith, W. P.; Whetten, R. L.; Landman, U.; Bigioni, T. P. Ultrastable Silver Nanoparticles. *Nature* **2013**, *501*, 399−402.
[111] Bhattarai, B.; Zaker, Y.; Atnagulov, A.; Yoon, B.; Landman, U.; Bigioni, T. P. Chemistry and Structure of Silver Molecular Nanoparticles. *Acc. Chem. Res.* **2018**, *51*, 3104−3113.
[112] Wu, J.; Qian, H.; Lu, L.; Fan, J.; Guo, Y.; Fang, W. Influence of Reduction Kinetics on the Preparation of Well-Defined Cubic Palladium Nanocrystals. *Inorg. Chem.* **2018**, *57*, 8128−8136.
[113] Zhang, J.; Li, H.; Kuang, Q.; Xie, Z. Toward Rationally Designing Surface Structures of Micro- and Nanocrystallites: Role of Supersaturation. *Acc. Chem. Res.* **2018**, *51*, 2880−2887.
[114] Saeki, M.; Matsumura, D.; Yomogida, T.; Taguchi, T.; Tsuji, T.; Saitoh, H.; Ohba, H. In Situ Time-Resolved XAFS Studies on Laser-Induced Particle Formation of Palladium Metal in an Aqueous/EtOH Solution. *J. Phys. Chem. C* **2019**, *123*, 817−824.
[115] Stöber, W.; Fink, A.; Bohn, E. Controlled Growth of Monodisperse Silica Spheres in the Micron Size Range. *J. Colloid Interface Sci.* **1968**, *26*, 62–69.
[116] Matijević, E.; Scheiner, P. Ferric Hydrous Oxide Sols: III. Preparation of Uniform Particles by Hydrolysis of Fe(III)-Chloride, -Nitrate, and -Perchlorate Solutions. *J. Colloid Interface Sci*. **1978**, *63*, 509–524.
[117] Beattie, J. K. Monodisperse colloids of transition metal and lanthanide compounds. *Pure Appl. Chem.* **1989**, *61*, 937–941.
[118] Look, J.–L.; Bogush, G. H.; Zukoski, C. F. Colloidal Interactions during the Precipitation of Uniform Submicrometre Particles. *Faraday Discuss. Chem. Soc*. **1990**, *90*, 345–357.
[119] Zukoski, C. F.; Chow, M. K.; Bogush, G. H.; Look, J.-L. Precipitation of Uniform Particles: The Role of Aggregation. *Mater. Res. Soc. Symp. P.* **1990**, *180*, 131–140.
[120] Bailey, J. K.; Mecartney, M. L. Mechanisms of Silica and Titania Colloidal Particle Formation from Metal Alkoxides. *Mater. Res. Soc. Symp. P*. **1990**, *180*, 153–158.
[121] Bogush, G. H.; Zukoski, C. F. Studies of the Kinetics of the Precipitation of Uniform Silica Particles through the Hydrolysis and Condensation of Silicon Alkoxides. *J. Colloid Interface Sci*. **1991**, *142*, 1–18
[122] Feeney, P. J.; Napper, D. H.; Gilbert, R. G. Coagulative Nucleation and Particle Size

Distributions in Emulsion Polymerization. *Macromolecules* **1984**, *17*, 2520–2529.
[123] Murphy, P. J.; Posner, A. M.; Quirk, J. P. *J. Colloid Interface Sci.* **1976**, *56*, 270–283.
[124] Bogush, G. H.; Zukoski, C. F. Uniform Silica Particle Precipitation: An Aggregative Growth Model. *J. Colloid Interface Sci*. **1991**, *142*, 19–34.
[125] van Blaaderen, A.; van Geest, J.; Vrij, A. Monodisperse Colloidal Silica Spheres from Tetraalkoxysilanes: Particle Formation and Growth Mechanism. *J. Colloid Interface Sci.* **1992**, *154*, 481–501.
[126] Matijević, E. Preparation and Properties of Uniform Size Colloids. *Chem. Mater.* **1993**, *5*, 412–426.
[127] Bailey, J. K.; Brinker, C. J.; Mecartney, M. L. Growth Mechanisms of Iron Oxide Particles of Differing Morphologies from the Forced Hydrolysis of Ferric Chloride Solutions. *J. Colloid Interface Sci.* **1993**, *157*, 1–13.
[128] Zukoski, C. F.; Look, J.–L.; Bogush, G. H. Formation of Uniform Precipitates from Alkoxides. In *The Colloid Chemistry of Silica*; Bergna, H. E., Ed.; Advances in Chemistry; American Chemical Society: Washington, DC, 1994; pp 451–465.
[129] Giesche, H. Synthesis of Monodispersed Silica Powders I. Particle Properties and Reaction Kinetics. *J. Eur. Ceram. Soc*. **1994**, *14*, 189–204.
[130] Okubo, T.; Kobayashi, K.; Kuno, A.; Tsuchida, A. Kinetic study of the formation reaction of colloidal silica spheres by transmitted-light-intensity and dynamic light-scattering measurements. *Colloid. Polym. Sci*. **1999**, *277*, 483–487.
[131] Penn, R. L.; Banfield, J. F. Morphology development and crystal growth in nanocrystalline aggregates under hydrothermal conditions: Insights from titania. *Geochim. Cosmochim. Acta* **1999**, *63*, 1549–1557.
[132] He, T.; Chen, D.; Jiao, X.; Wang, Y.; Duan, Y. Solubility-Controlled Synthesis of High-Quality Co_3O_4 Nanocrystals. *Chem. Mater.* **2005**, *17*, 4023–4030.
[133] Kumar, S.; Davis, T. M.; Ramanan, H.; Penn, R. L.; Tsapatsis, M. Aggregative Growth of Silicalite–1. *J. Phys. Chem. B* **2007**, *111*, 3398–3403.
[134] Drofenik, M.; Kristl, M.; Žnidaršič, A.; Hanžel, D.; Lisjak, D. Hydrothermal Synthesis of Ba-Hexaferrite Nanoparticles. *J. Am. Ceram. Soc.* **2007**, *90*, 2057–2061.
[135] Kwon, S. G.; Piao, Y.; Park, J.; Angappane, S.; Jo, Y.; Hwang, N.–M.; Park, J.–G.; Hyeon, T. Kinetics of Monodisperse Iron Oxide Nanocrystal Formation by "Heating-Up" Process. *J. Am. Chem. Soc.* **2007**, *129*, 12571–12584.
[136] Kwon, S. G.; Hyeon, T. Colloidal Chemical Synthesis and Formation Kinetics of Uniformly Sized Nanocrystals of Metals, Oxides, and Chalcogenides. *Acc. Chem. Res*. **2008**, *41*, 1696–1709.
[137] Yokoi, T.; Wakabayashi, J.; Otsuka, Y.; Fan, W.; Iwama, M.; Watanabe, R.; Aramaki, K.; Shimojima, A.; Tatsumi, T.; Okubo, T. Mechanism of Formation of Uniform-Sized Silica Nanospheres Catalyzed by Basic Amino Acids. *Chem. Mater.* **2009**, *21*, 3719–3729.
[138] Ng, J.; Xu, S.; Zhang, X.; Yang, H. Y.; Sun, D. D. Hybridized Nanowires and Cubes: A Novel Architecture of a Heterojunctioned $TiO_2/SrTiO_3$ Thin Film for Efficient Water Splitting. *Adv. Funct. Mater.* **2010**, *20*, 4287–4294.
[139] Robb, D. T.; Privman, V. Model of Nanocrystal Formation in Solution by Burst Nucleation and Diffusional Growth. *Langmuir* **2008**, *24*, 26–35.
[140] Privman, V. Mechanisms of Diffusional Nucleation of Nanocrystals and Their Self-Assembly into Uniform Colloids. *Ann. N. Y. Acad. Sci.* **2009**, *1161*, 508–525.
[141] Huang, Y.; Pemberton, J. E. Synthesis of uniform, spherical sub–100 nm silica particles using a conceptual modification of the classic LaMer model. *Colloids and Surfaces A: Physiochem. Eng. Aspects* **2010**, *360*, 175–183.
[142] Zhao, S.; Xu, D.; Ma, H.; Sun, Z.; Guan, J. Controllable preparation and formation

mechanism of monodispersed silica particles with binary sizes. *J. Colloid Interface Sci.* **2012**, *388*, 40–46.
[143] Baaziz, W.; Pichon, B. P.; Fleutot, S.; Liu, Y.; Lefevre, C.; Greneche, J.–M.; Toumi, M.; Mhiri, T.; Begin-Colin, S. Magnetic Iron Oxide Nanoparticles: Reproducible Tuning of the Size and Nanosized-Dependent Composition, Defects, and Spin Canting. *J. Phys. Chem. C* **2014**, *118*, 3795–3810.
[144] Platt, J. R. Strong Inference. *Science* **1964**, *146*, 347–353.
[145] Arshadi, S.; Moghaddam, J.; Eskandarian, M. LaMer diagram approach to study the nucleation and growth of Cu_2O nanoparticles using supersaturation theory. *Korean J. Chem. Eng.* **2014**, *31*, 2020–2026.
[146] Wang, C.; Shpaisman, H.; Hollingsworth, A. D.; Grier, D. G. Celebrating *Soft Matter's* 10th Anniversary: Monitoring colloidal growth with holographic microscopy. *Soft Matter* **2015**, *11*, 1062–1066.
[147] Vreeland, E. C.; Watt, J.; Schober, G. B.; Hance, B. G.; Austin, M. J.; Price, A. D.; Fellows, B. D.; Monson, T. C.; Hudak, N. S.; Maldonado-Camargo, L.; Bohorquez, A. C.; Rinaldi, C.; Huber, D. L. Enhanced Nanoparticle Size Control by Extending LaMer's Mechanism. *Chem. Mater.* **2015**, *27*, 6059–6066.
[148] Sugimoto, T. Underlying mechanisms in size control of uniform nanoparticles. *J. Colloid Interface Sci.* **2007**, *309*, 106–118.
[149] Yang, S.; Liu, Q. Formation mechanism of apex-truncated octahedral Cu_2O microcrystal. *CrystEngComm* **2016**, *18*, 8229–8236.
[150] Stolzenburg, P.; Garnweitner, G. Experimental and numerical insights into the formation of zirconia nanoparticles: a population balance model for the nonaqueous synthesis. *React. Chem. Eng.* **2017**, *2*, 337–348.
[151] Luo, L.; Liang, Y.; Erichsen, E. S.; Anwander, R. Monodisperse mesoporous silica nanoparticles of distinct topology. *J. Colloid Interface Sci.* **2017**, *495*, 84–93.
[152] Lassenberger, A.; Grünewald, T. A.; van Oostrum, P. D. J.; Rennhofer, H.; Amenitsch, H.; Zirbs, R.; Lichteneggar, H. C.; Reimhult, E. Monodisperse Iron Oxide Nanoparticles by Thermal Decomposition: Elucidating Particle Formation by Second-Resolved in Situ Small-Angle X-ray Scattering. *Chem. Mater.* **2017**, *29*, 4511–4522.
[153] Han, Y.; Lu, Z.; Teng, Z.; Liang, J.; Guo, Z.; Wang, D.; Han, M.–Y.; Yang, W. Unraveling the Growth Mechanism of Silica Particles in the Stöber Method: In Situ Seeded Growth Model. *Langmuir* **2017**, *33*, 5879–5890.
[154] Dehsari, H. S.; Harris, R. A.; Ribeiro, A. H.; Tremel, W.; Asadi, K. Optimizing the Binding Energy of the Surfactant to Iron Oxide Yields Truly Monodisperse Nanoparticles. *Langmuir* **2018**, *34*, 6582–6590.
[155] Uskoković, V.; Tang, S.; Wu, V. M. On Grounds of the Memory Effect in Amorphous and Crystalline Apatite: Kinetics of Crystallization and Biological Response. *ACS Appl. Mater. Interfaces* **2018**, *10*, 14491–14508.
[156] Belaïd, S.; Stanicki, D.; Vander Elst, L.; Muller, R. N.; Laurent, S. Influence of experimental parameters on iron oxide nanoparticle properties synthesized by thermal decomposition: size and nuclear magnetic resonance studies. *Nanotechnology* **2018**, *29*, 165603, 1–12.
[157] Famiani, S.; LaGrow, A. P.; Besenhard, M. O.; Maenosono, S.; Thanh, N. T. K. Synthesis of Fine-Tuning Highly Magnetic $Fe@Fe_xO_y$ Nanoparticles through Continuous Injection and a Study of Magnetic Hyperthermia. *Chem. Mater.* **2018**, *30*, 8897–8904.
[158] Lifshitz, I. M.; Slyozov, V. V. The kinetics of precipitation from supersaturated solid solutions. *J. Phys. Chem. Solids* **1961**, *19*, 35–50.
[159] Penn, R. L.; Banfield, J. F. Imperfect Oriented Attachment: Dislocation Generation in

Defect-Free Nanocrystals. *Science* **1998**, *281*, 969–971.
[160] Auer, S.; Frenkel, D. Prediction of absolute crystal-nucleation rate in hard-sphere colloids. *Nature* **2001**, *409*, 1020–1023.
[161] Sugimoto, T. Formation of Monodispersed Nano- and Micro-Particles Controlled in Size, Shape, and Internal Structure. *Chem. Eng. Technol.* **2003**, *26*, 313–321.
[162] Penn, R. L. Kinetics of Oriented Aggregation. *J. Phys. Chem. B* **2004**, *108*, 12707–12712.
[163] Drews, T. O.; Katsoulakis, M. A.; Tsapatsis, M. A Mathematical Model for Crystal Growth by Aggregation of Precursor Metastable Nanoparticles. *J. Phys. Chem. B* **2005**, *109*, 23879–23887.
[164] Wilhelmy, D. M.; Matijević, E. Preparation and properties of monodispersed spherical-colloid particles of zinc sulphide. *J. Chem. Soc., Faraday Trans. I* **1984**, *80*, 563–570.
[165] Matijević, E.; Goia, D. Formation Mechanisms of Uniform Colloid Particles. *Croat. Chem. Acta* **2007**, *80*, 485–491.
[166] Drews, T. O.; Tsapatsis, M. Model of the evolution of nanoparticles to crystals via an aggregative growth mechanism. *Micropor. Mesopor. Mat.* **2007**, *101*, 97–107.
[167] Sharaf, M. A.; Dobbins, R. A. A Comparison of Measured Nucleation Rates with the Predictions of Several Theories of Homogeneous Nucleation. *J. Chem. Phys.* **1982**, *77*, 1517–1526.
[168] Strey, R.; Wagner, P. E.; Schmeling, T. Homogeneous Nucleation Rates for n-Alcohol Vapors Measured in a Two-Piston Expansion Chamber. *J. Chem. Phys.* **1986**, *84*, 2325–2335.
[169] Knezic, D.; Zaccaro, J.; Myerson, A. S. Nucleation Induction Time in Levitated Droplets, *J. Phys. Chem. B* **2004**, *108*, 10672–10677.
[170] Oxtoby, D. W. Nucleation of First-Order Phase Transitions. *Acc. Chem. Res.* **1998**, *31*, 91–97.
[171] Schuth, F. Nucleation and Crystallization of Solids from Solution. *Curr. Opin. Solid State Mater. Sci.* **2001**, *5*, 389–395.
[172] Erdemir, D.; Lee, A. Y.; Myerson, A. S. Nucleation of Crystals from Solution: Classical and Two-Step Models. *Acc. Chem. Res.* **2009**, *42*, 621–629.
[173] Pan, D.; Wang, Q.; An, L. Controlled synthesis of monodisperse nanocrystals by a two-phase approach without the separation of nucleation and growth processes. *J. Mater. Chem*. **2009***, 19*, 1063–1073.
[174] Hung, C.–H.; Krasnopoler, M. J.; Katz, J. L. Condensation of a supersaturated vapor. VIII. The homogeneous nucleation of *n*-nonane. *J. Chem. Phys.* **1989**, *90*, 1856–1865.
[175] Agarwal, G.; Heist, R. H. Homogeneous nucleation in associated vapors. III. Heptanoic, decanoic, and myristic acids. *J. Chem. Phys.* **1980**, *73*, 902–907.
[176] Whitehead, C. B.; Özkar, S.; Finke, R. G. LaMer's 1950 Model for Particle Formation of Instantaneous Nucleation and Diffusion-Controlled Growth: A Historical Look at the Model's Origins, Assumptions, Equations, and Underlying Sulfur Sol Formation Kinetics Data. *Chem. Mater.* **2019**, *31*, 7116–7132.
[177] Zhang, R.; Khalizov, A.; Wang, L.; Hu, M.; Xu, W. Nucleation and Growth of Nanoparticles in the Atmosphere. *Chem. Rev*. **2012**, *112*, 1957–2011.
[178] Skrdla, P. J. Use of Dispersive Kinetic Models for Nucleation and Denucleation to Predict Steady-State Nanoparticle Size Distributions and the Role of Ostwald Ripening. *J. Phys. Chem. C* **2012**, *116*, 214–225.
[179] St. John, S.; Nan, Z.; Hu, N.; Schaefer, D. W.; Angelopoulos, A. P. A nanoscale-modified LaMer model for particle synthesis from inorganic tin-platinum complexes. *J. Mater. Chem. A* **2013**, *1*, 8903–8916.
[180] Wang, F.; Richards, V. N.; Shields, S. P.; Buhro, W. E. Kinetics and Mechanisms of Aggregative Nanocrystal Growth. *Chem. Mater.* **2014**, *26*, 5–21.

[181] Tong, F.; Hanson, M. P.; Bardeen, C. J. Analysis of reaction kinetics in the photomechanical molecular crystal 9-methylanthracene using an extended Finke-Watzky model. *Phys. Chem. Chem. Phys.* **2016**, *18*, 31936–31945.